# Translational Design Computation

Christoph Bader

Bachelor of Science in Applied Computer Science,
University of Applied Sciences Ravensburg-Weingarten, 2014

Submitted to the Program in Media Arts and Sciences, School of Architecture and Planning, in partial fulfilment of the requirements for the degree of Master of Science in Media Arts and Sciences at the

MASSACHUSETTS INSTITUTE OF TECHNOLOGY

June 2017



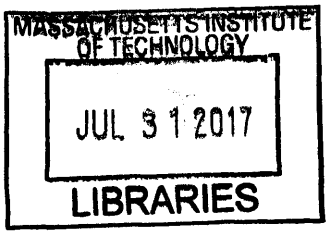


ARCHIVES

Signature redacted

Author, *Christoph Bader*,
Program in Media Arts and Sciences,
May 9, 2017

Signature redacted

Certified by *Neri Oxman*,
Associate Professor of Media Arts and Sciences,
Thesis Advisor

Signature redacted

Accepted by *Pattie Maes*,
Academic Head, Program in Media Arts and Sciences.

# Translational Design Computation

Christoph Bader

Submitted to the Program in Media Arts and Sciences,
School of Architecture and Planning,
in partial fulfilment of the requirements for the degree of
Master of Science in Media Arts and Sciences

## Abstract

This thesis introduces, demonstrates and implements *translational design computation*: a theoretical approach and technical framework for mediating living and nonliving matter through design computation. I propose that computational design can act as a "language" for the enablement of design at the intersection of the material and the biological domains. I support and validate this proposition by formulating, deploying and evaluating a triad of strategies as follows: (1) *Programmable Matter*—utilizing computational design in combination with synthetic material systems to enable biologically inspired and informed design; (2) *Programmable Templating*—utilizing computational design in combination with, and at the intersection of, synthetic and biological systems in order to facilitate their synergetic relationships; and (3) *Programmable Growth*—utilizing computational design in combination with biological systems to grow material architectures. Each of these design strategies is demonstrated through specific design challenges. For *Programmable Matter;* a data-driven material modeling method that allows to reinterpret visual complexities found in nature is presented and subsequently extended to a design framework for the 3D printing of functionally graded structures. For *Programmable Templating;* a design approach for creating a macrofluidic habitat, exploring phototrophic and heterotrophic bacterial augmentation templated by continuous opacity gradients, is presented. Following, spatio-temporal templating of engineered microorganisms via 3D printed diffusion gradients is investigated. Finally, for *Programmable Growth;* a framework is proposed with the objective of importing computer-aided design capabilities to biology. Enforcing the design-centric approach, a design collection called *Vespers*—a reinterpretation of the practice of the ancient death mask—is presented and discussed in the context of the introduced concepts. Thesis contributions are not limited to innovations in computational design and digital fabrication but also to materials engineering and biology by proposing new ecological perspectives on and for design.

Thesis Supervisor: Neri Oxman
Title: Associate Professor of Media Arts and Sciences, Program in Media Arts and Sciences.

# Translational Design Computation

Christoph Bader

Submitted to the Program in Media Arts and Sciences,
School of Architecture and Planning,
in partial fulfilment of the requirements for the degree of
Master of Science in Media Arts and Sciences

Signature redacted

Thesis Reader, *Peter Fratzl*,
Director,
Max Planck Institute of Colloids and Interfaces

# Translational Design Computation

Christoph Bader

Submitted to the Program in Media Arts and Sciences,
School of Architecture and Planning,
in partial fulfilment of the requirements for the degree of
Master of Science in Media Arts and Sciences

Signature redacted

Thesis Reader, *James Weaver*,
Senior Research Scientist,
Wyss Institute for Biologically Inspired Engineering

# Acknowledgements

I thank my family — my mother Erika, my father Erich, my brother Tobias and his young family. I thank my advisor, mentor and friend Neri Oxman. I thank James Weaver for being a constant source of motivation, ideas and general awesomeness. I thank the whole Mediated Matter Group who provided me a home. Especially, Sunanda Sharma, Rachel Smith and Kelly Donovan for their incredible work, teamwork and care. I thank all the team members at Stratasys who I had the privilege to interact with. Boris Belocon, Gal Begun, Naomi Kaempfer, Yoav Bressler, Ori Moalem and Tal Ely who provided insights and dedication. Lastly, I would like to thank my friend and colleague Dominik Kolb for sharing a path with me for almost ten years. I hope our ways cross again in the future.

# Contents


Introduction 21

Vespers – Series 1 27

Recursive Symmetries for Geometrically Complex and Materially Heterogeneous Additive Manufacturing 37
- Abstract 37
- Introduction 38
- Method 39
  - Description 39
  - Parameters, Modification & Evaluation 41
- Production 48
- Conclusion 51
- Acknowledgments 52

Programmable Matter 55

Data-driven Material Modeling with Functional Advection for 3D printing of Materially Heterogeneous Objects 57
- Abstract 57
- Introduction 58
- Data-driven Material Modeling (DdMM) 59
  - Computational Framework 59
- Data Driven Design 63
- Conclusion 68
- Acknowledgments 69

Design of 3D Printable Functionally Graded Material Systems 71
- Abstract 71
- Introduction 72
- Extensions to the Data-Driven Design Framework 72
- Applications – Exploring the Design Space 76
  - 3D printable opacity gradients 76
  - 3D printable modulus gradients 80
  - 3D printable shape memory gradients 81
  - 3D printable expansion gradients 82
  - 3D printable hydrophilicity gradients 84
  - 3D printable refractive index gradients 85
- Rottlace, a Mask for Björk 87
- Conclusion 89

Vespers – Series 2 91

Programmable Templating 103

Grown, Printed, and Biologically Augmented: An Additively Manufactured Microfluidic Wearable, Functionally Templated for Synthetic Microbes 105
Abstract 105
Introduction 106
Vision 106
Approach 106
Organization 107
Growing Mushtari 108
General Framework 109
Growth of Polygonal Lines 110
Functional Templating 112
Printing Mushtari 113
3D printing a Materially Heterogeneous Tract 113
Multi-Material Voxel-Printing of Fluidic Channels 114
Printing a Hollow Channel 116
Characterization and Evaluation of Support Methods 117
Visualizing Mushtari's inner channels 119
Augmenting Mushtari 120
Cytotoxicity Studies 121
Conclusion and Future Work 123
Acknowledgements 125

Heterogeneous Hybrid Living Materials 127
Abstract 127
Introduction 128
Results 129
Fabricating heterogeneous hybrid living materials 129
Controlled Templating through Material Heterogeneity 133
Designing Materially Heterogeneous Templates 135
3d Printable Bio Signaling Resins 140
Modeling 141
Modeling of Living Hybrid Material Systems 141
Materials & Methods 144
Template fabrication 144
Bacterial Strain and Plasmids 144
Cell Viability Assay 144
Template Diffusion Characterization 145
Preparation and Testing of 3D Printable Bio Signaling Resins 145
Characterization of Material Expansion and Weight Gain 146
Conclusion 147

Vespers – Series 3 149

Programmable Growth 157

Engineering Living Materials – Programming seed cells to grow and differentiate into defined patterns 159
Introduction 159
Background 160
Methods 161
Permanent differentiation of a seed cell into multiple cell types during growth 162
Synthetic developmental circuits for the formation of "embryonic" patterns. 163
Flexible platform for high-throughput imaging of patterns. 166
Development of a computer-aided design platform to simulate and design the growth of a seed cell into a final structure. 166

Conclusions 171

Review 171

Future Work 171
Growth 171
Dynamics 172
Unification 173
Applications 173

Conclusion 174

References 175

# List of Figures

Figure 1 – Applying computational design in the transition between the biological and the material domain. 22
Figure 2 – The Structure of the Thesis. 25
Figure 3 – Vespers. Series 1 Mask 5. Back view. 29
Figure 4 – Vespers. Series 1 Mask 4. 30
Figure 5 – Vespers. Series 1 Mask 2. Front and side view. 30
Figure 6 – Vespers. Series 1 Mask 1. Side view. 31
Figure 7 – Vespers. Series 1 Mask 3. Close up. 32
Figure 8 – Vespers. Series 1 Mask 4. Side view. 33
Figure 9 – Vespers. Series 1 Mask 4. Side view. 34
Figure 10 – Vespers. Series 1 Mask 1. Top view. 34
Figure 11 – Vespers. Series 1 Mask 3. Back view. 35
Figure 12 – A visual representation of the generative method. 40
Figure 13 – Different input shapes and their results. 42
Figure 14 – Exploration of the emergent design space. 43
Figure 15 – Modifications to the design space. 44
Figure 16 – Characterization of the generative method. 47
Figure 17 – Adapting a generated shape to a given target geometry. 48
Figure 18 – The slicing process. 49
Figure 19 – Parts printed on a multi-material Stratasys J750 printer using seven base resins showcasing the geometric and material complexity that can be achieved. 51
Figure 20 – The programmable matter approach. 55
Figure 21 – A data-driven computational framework for the production of bitmap-printable parts: 59
Figure 22 – An example of data-driven priority sorting for the production of large and structurally complex objects[48] 61
Figure 23 – Object cross section illustrating variations in material composition of an object 3D printed with 3 different materials. 62
Figure 24 – A collection of three general examples of the DdMM approach, illustrating an array of internal material compositions achieved through the implementation of the described methods to achieve visually complex patterns. 63
Figure 25 – Visualization of the design approach for Lazarus. 66
Figure 26 – Volumetric visualization of the contribution of each original data-source for the generation of internal material distributions. 67

Figure 27 – Lazarus, 2016. Designed by Neri Oxman and The Mediated Matter Group in collaboration with Stratasys. 68
Figure 28 – Proposed design framework. 74
Figure 29 – Examples of opacity gradients. 76
Figure 30 – Example of 3D printing volumetric datasets. 78
Figure 31 – Example of a biological tissue datasets directly fabricated through the voxel printing process. 79
Figure 32 – Examples of objects with gradients in elastic modulus. 80
Figure 33 – Graded shape memory objects. 82
Figure 34 – Designing objects with spatially tunable expansion. 84
Figure 35 – Wettability gradients. 84
Figure 36 – Examples of objects with refractive index gradients. 85
Figure 37 – Rottlace, 2016. 88
Figure 38 – Vespers. Series 2 Mask 5. Bottom view. 93
Figure 39 – Vespers. Series 2 Mask 2. Side view. 94
Figure 40 – Vespers. Series 2 Mask 2. Top and bottom view. 94
Figure 41 – Vespers. Series 2 Mask 3. Side view. 95
Figure 42 – Vespers. Series 2 Mask 3. Side view. 96
Figure 43 – Vespers. Series 2 Mask 5. Bottom view. 97
Figure 44 – Vespers. Series 2 Mask 2. Back and front view. 98
Figure 45 – Vespers. Series 2 Mask 2. Top and bottom view. 98
Figure 46 – Vespers. Series 2 Mask 3. Front view. 99
Figure 47 – The programmable templating approach. 103
Figure 48 – Side-view of Mushtari. 108
Figure 49 – Visualization of 100 iteration steps from three different growth variations used to generate the fluidic wearable, Mushtari 109
Figure 50 – Schematic overview of the general framework used for the generation of computationally grown structures. 110
Figure 51 – (a) Example of the general framework applied to a polygonal line. 112
Figure 52 – (a) The desired effect of material transparency on microbial activity. 113
Figure 53 – Fabrication of internal channels. 116
Figure 54 – Representative optical images of test piece cross-sections 118
Table1: Mean and standard deviation of diameters A-G (mm) of the test pieces with various support materials. 119
Figure 55 – Visualization of smaller scale test-piece used. 119
Figure 56 – (a) Comparison of growth rates (doublings per hour) of Escherichia coli and Bacillus subtilis in various tube materials. 123

Figure 57 – Process of fabricating heterogeneous hybrid living materials. 130
Figure 58 – Close up of diffusion gradients visualized through CPRG (yellow) and bacterial response (green). 132
Figure 59 – Templating of biological activity through material ratios. 133
Figure 60 – Rational design method through bacterial response characterization. 135
Figure 61 – Part augmented with small molecules to allow multiple substrate outputs. 137
Figure 62 – Heterogeneous additively manufactured part made out of flexible inactive, rigid inactive and active materials. 137
Figure 63 Close up of the multiple output substrate mixing and bacterial response. 138
Figure 64 – Multi-material fabricated part showcasing temporal control over bacterial activity. 139
Figure 65 – Inverted (to aid in visualization) transillumination photographs of GFP expression response to biosignaling resin test pieces. 140
Figure 66 – Modeling of IPTG diffusion and bacterial response. 143
Figure 67 – Vespers. Series 3 Mask 2. Front view after incubation. 151
Figure 68 – Vespers. Series 3 Mask 2. Material induced pattern formation over time filmed during incubation. 152
Figure 69 – Vespers. Series 3 Mask 2. Side view after post processing. 153
Figure 70 – Vespers. Series 3 Mask 2. Front view after post processing. 153
Figure 71 – Vespers. Series 3 Mask 1. Close up view. 154
Figure 72 – Vespers. Series 3 Mask 1. Close up view. 154
Figure 73 – The programmable growth approach. 157
Figure 74 – Design flow to create a single DNA sequence that controls the differentiation of a seed cell into a material. 159
Figure 75 – Exemplary target patterns to be produced. 162
Figure 76 – Programmable biological primitives. 163
Figure 77 – Bottom-up approach to simulation and design of cellular development and pattern formation. 168

# Introduction

The complex relationship between the physical and the digital domain has—at least since the dawn of digital manufacturing—been expressed through tools, techniques and technologies associated with their development and deployment. This relationship is less complementary than it is co-dependent: new capabilities in digital fabrication enable the realization of sophisticated tools of design computation, while—in turn—new affordances in design computation inspire innovation in digital fabrication. The level and quality of co-dependency—whereby design computation enables control and manipulation over the *digital* domain, as digital fabrication affords control and manipulation over the domain of the *physical*—determines their level of progress as synergetic design domains. Moreover, the ability to reduce, and even eliminate, the mismatch between digital and physical design tools will ultimately result in fully integrated platforms for design and designers with little to none 'acts of translation' thereby bridging the gap between the physical and the digital. But—for designers leading the transition from the digital age to the biological age—the challenge to author a cross-domain auxiliary language does not cease here, nor do its associated acts of translation. As we face the challenge to shift between and across fields—their associated units and modes of expression—we must find ways by which to mediate between the physical, the digital *and* the biological, enabling new ecological perspectives [1].

While the first two domains operate from the top-down, the biological domain operates—through growth—from the bottom up. This dichotomy therefore expands the mismatch but increases the design space. In order to 'solve the riddle' of how designers can operate across domains as well as across spatio-temporal scales, we must define a new research territory that lies at the intersection of Computational Design, Digital Fabrication, Materials Engineering and Synthetic Biology. At the heart of this thesis is the proposition that the mismatch across physical, digital and biological design domains can be overcome through *translational design computation*: a framework enabling design computation to be a necessary language to mediate between the units of physical, digital and biological matter. This is shown by a set of strategies forming a triad, which shift across domains as we progress from the 'biology-inspired' to an 'inspired-biology' (Figure 1). Further, as these strategies apply computational design at different points in the transition from the biological to the material, this thesis aims to identify computationally enabled synergies between biology, computational design, and fabrication.

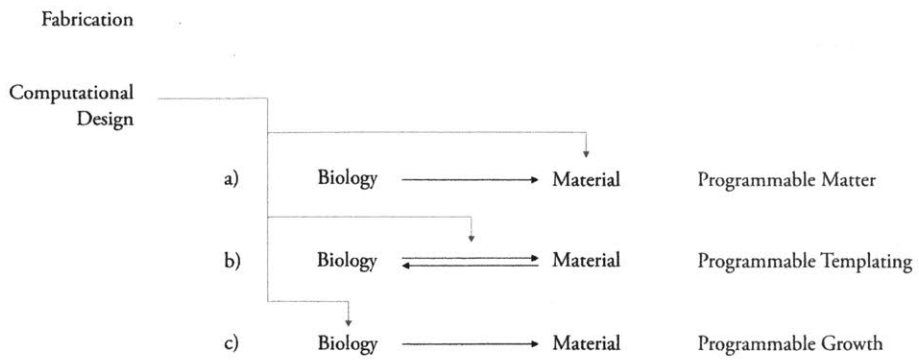


*Figure 1 – Applying computational design in the transition between the biological and the material domain.* a) Represents the nature-inspired 'programmable matter' approach, which through computational methods translates biological principles to physical objects. b) Shows the 'programmable templating' approach where a material system can be utilized to influence a biological system and vice-versa; here computational design can mediate between both through modelling and simulation. c) Characterizes the programmable growth approach, applying computational design to biological primitives (such as differentiation, quorum signaling, sensing and response) to infer material formation processes through engineered living systems.

The three strategies are outlined in the following. Briefly, *Programmable Matter* utilizes computational design on synthetic material systems to enable biologically inspired design strategies; *Programmable Templating* utilizes computational design at the intersection of synthetic and biological systems facilitating synergetic relationships, and *Programmable Growth* applies computational design to biological systems to give rise to material architectures.

Part 1, Programmable Matter:

---

Functionally graded structures in nature are known to be the source of elaborate behaviours such as the alleviation of stress concentrations in tendon-to-bone attachments by stiffness gradients, improved vision of aquatic animals by refractive index gradients, and self-shaping behaviour of plant systems through hygroscopic swellability of their hemicellulose matrix. Therefore, mirroring the biological in the fabricated requires to move computational design capabilities from the purely geometrical to the material. Yet, the application of, and the computational design with, continuous material property gradients is largely limited due to technical challenges associated with computational design, material characterisation and evaluation, and fabrication of heterogeneous material objects. Here we will introduce a computational framework, combining parametric geometric modeling and parametric material modeling, material-function evaluation, and high-resolution on-slice time composite creation to enable the digital fabrication of materially heterogeneous objects through multi-material 3D printing. This enables the modeling and

fabrication of programmable material properties within an objects volume and allows decoupling material behavior from geometry. This framework will be utilized and showcased in two instances,

1) Spatial control through high-resolution data-driven material-modeling of complex material structures to visually mimicking complexities found in nature, and
2) Extending the framework for the design of functionally gradable multi-material structures to mimic natural hybrid systems.

Part 2, Programmable Templating:

---

While programming matter allows to mimic material behaviors found in nature and further allows to leverage design strategies having evolved over centuries, it is due to nature's bottom-up processes that design in the biological domain will resort to more controllable top-down strategies. However, one strategy to enable synergies at the intersection of fabrication, material science and biology is to go beyond using biology as a template for the material and to design a relationship between both. Here, we will introduce *computational design as a mediator* between programmable matter and programmable life. By using the programmable matter approach in conjunction with synthetically engineered microorganisms, a synthetic ecology between the material domain and the biological domain can be established. In part 2, we showcase this using two different approaches.

1) Geometrically designing a macrofluidic wearable habitat made out of a single long channel. Utilizing 3D printing in combination with a liquid support material the wearable habitat is digitally fabricated potentially hosting a co-culture of phototrophic and heterotrophic bacteria templated by continuous opacity gradients.
2) Materially designing spatially controllable bacterial response on heterogeneous templates. Utilizing materials which allow to embed and release small molecule inducers, biosynthesis of cells can be controllably designed by a materially tunable signaling processes.

Part 3, Programmable Growth:

---

Purely biological 'fabrication' in the form of growth can be self-sufficient. Starting from a single cell, through an interplay of growth and endogenous gradients, simple rules encoded in DNA drive the formation of matter from the embryonic to almost arbitrary complexity. Recent advances in synthetic biology allow to encode rules for stochastic cell differentiation, endogenous establishment of quorum signals and the response to these chemical gradients by activation and repression of cellular behavior. Here—as an outlook—we will investigate how these 'biological primitives' can give rise to embryonic

patterns that could lead to larger 2D skins of a living material or complex 3D structures. By building a computational design framework allowing to design with these primitives, and inferring high-level descriptions for implementable regulatory networks, this work paves the way towards computationally designing autonomously forming living material entities.

Part 4, Vespers

---

In a design context, methodologies can only be as strong as their application to an embodiment. Hence, as guiding project interwoven within the chapters of the thesis, we introduce the *Vespers* Series. *Vespers*, revisits the concept of the death mask. The series explores the idea of an ancient 'product', and thereby giving it new meaning through the lens of design, science and technology. The series is composed of three subseries:

1) *Vespers* – Series 1. The first series employs an algorithmic approach to mimic the super symmetrical and colourful ornamental structures we can find in cultural artefacts. Here, novel seven material 3D printing is utilized to recreate the variety and nuance of ancient crafts.
2) *Vespers* – Series 2. The second series presents a transition from the external to the internal, and a move away from the pure design of surfaces to the design of material distributions in an objects volume that mimic and reinterpret natural phenomena.
3) *Vespers* – Series 3. The third series represents the duality between decay and birth. Here, in an attempt to bridge the gap between a programmable material system and programmable life, patterns and colours form the first series are reinterpreted through a spatially templated living system.

At the same time, *Vespers* carries the concept of transition. Transitions from culture to nature, from life to death, from the conservation to recreation, from extrinsic features to intrinsic design, be as it may in the eye of the beholder. The subseries show the application of the concepts introduced in Part 1 and Part 2 in a design context and have been exhibited at the London Design Museum in the *Fear and Love* exhibit. The outline of the thesis is shown in Figure 2.

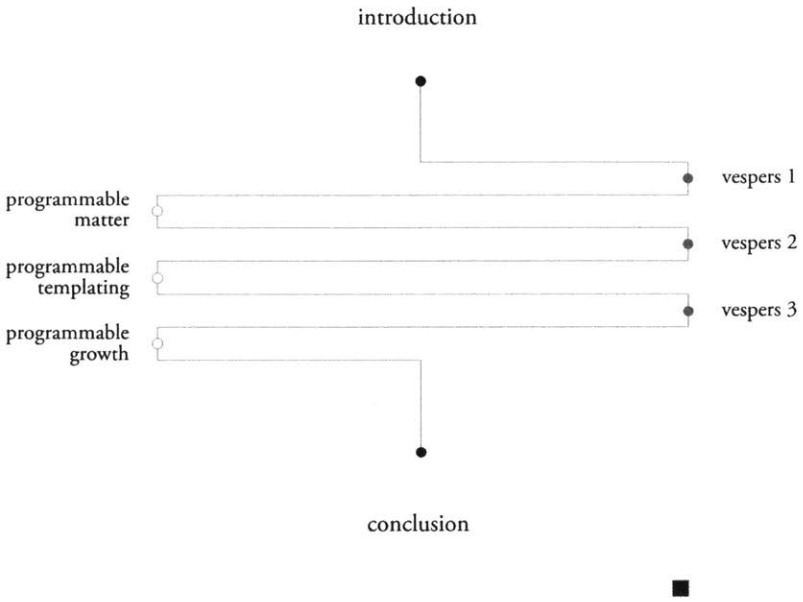


*Figure 2 – The Structure of the Thesis.* First the *Vespers* series is introduced with *Vespers – Series 1* as a starting point. Here, the approach behind this series is presented as a geometry centric view on design computation and as a review of the practice. Then—and in contrast—the *programmable matter* approach is introduced and its counterpart *Vespers – Series2* is presented. Moving from the material domain to biological domain, the intersection is investigated and computational design strategies within the *programmable templating* approach are identified. As an embodiment, *Vespers – Series3* is given. Lastly, the *programmable growth* approach is presented in form of a proposal and a prototypical implementation. No embodiment is given for this approach (yet), as it is left for future exploration.

# Vespers – Series 1

*"The most iconic death masks—like those of Agamemnon and King Tutankhamun—were made entirely of, or inlaid with, precious stones and minerals. The use of color often expressed the cultural attributes of the deceased associated with their spiritual powers, or religious affiliation.*

*The first series explores life through the lens of death. Inspired by ancient masks, it uses five color combinations commonly found in religious practices across regions and eras, and is embedded with natural minerals, such as bismuth, silver, and gold.*

*The masks' colors are correlated with underlying geometries which are, in combination, driven by a parametric grammar. Compared to their crafted counterparts the masks are purely algorithmically created, where the algorithmic approach mimics the super symmetrical and colourful ornamental structures we can find in cultural artefacts*

*In this series, polyhedral meshes are 'evolved' into subdivided surfaces using an algorithm, which—like the formation of life itself—emulates cellular subdivision. Using a minimal set of rules, the series generates a plethora of color/shape schemes. The implementation of the Stratasys full-color-multi-material 3D printing technology enables the creation of objects—for the first time in the history of additive manufacturing—that match the variety and nuance of ancient crafts."* [2]

*Figure 3* – Vespers. *Series 1 Mask 5. Back view.* Designed by Neri Oxman and members of The Mediated Matter Group for The New Ancient Collection curated and 3D printed by Stratasys, 2016. Photo: Yoram Reshef.

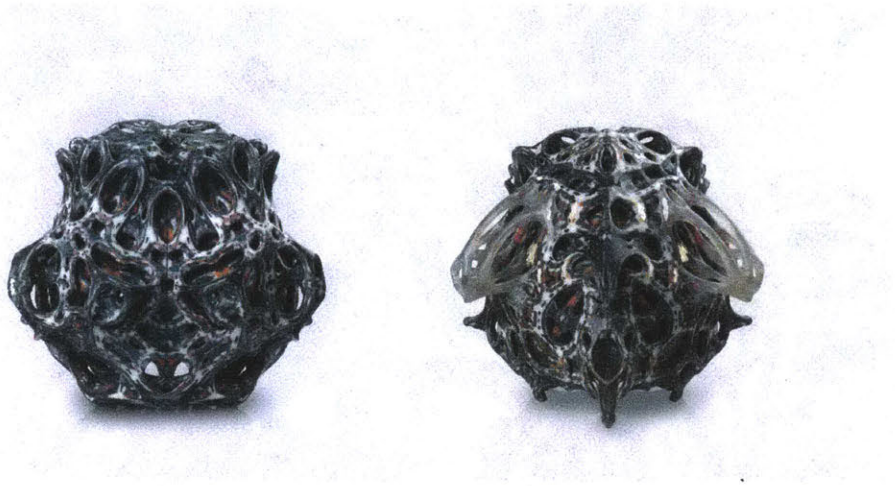

*Figure 4* – Vespers. *Series 1 Mask 4.* Top and bottom view. Designed by Neri Oxman and members of The Mediated Matter Group for The New Ancient Collection curated and 3D printed by Stratasys, 2016. Photo: Yoram Reshef.

*Figure 5* – Vespers. *Series 1 Mask 2. Front and side view.* Designed by Neri Oxman and members of The Mediated Matter Group for The New Ancient Collection curated and 3D printed by Stratasys, 2016. Photo: Yoram Reshef.

*Figure 6* – Vespers. *Series 1 Mask 1. Side view.* Designed by Neri Oxman and members of The Mediated Matter Group for The New Ancient Collection curated and 3D printed by Stratasys, 2016. Photo: Yoram Reshef.

*Figure 7* – Vespers. *Series 1 Mask 3. Close up.* Designed by Neri Oxman and members of The Mediated Matter Group for The New Ancient Collection curated and 3D printed by Stratasys, 2016. Photo: Yoram Reshef.

*Figure 8* – Vespers. *Series 1 Mask 4. Side view.* Designed by Neri Oxman and members of The Mediated Matter Group for The New Ancient Collection curated and 3D printed by Stratasys, 2016. Photo: Yoram Reshef.

*Figure 9* – Vespers. *Series 1 Mask 4. Side view.* Designed by Neri Oxman and members of The Mediated Matter Group for The New Ancient Collection curated and 3D printed by Stratasys, 2016. Photo: Yoram Reshef.

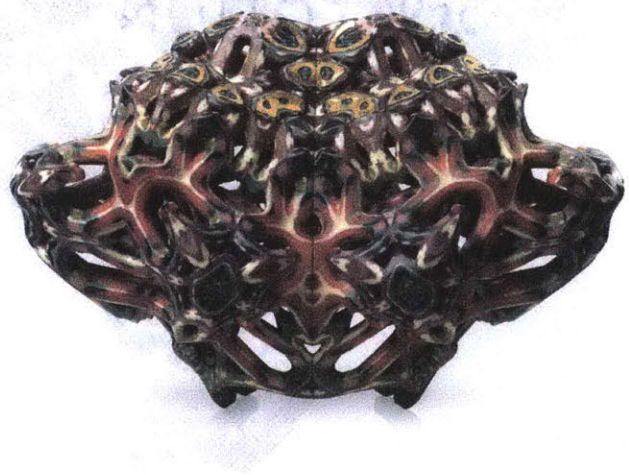

*Figure 10* – Vespers. *Series 1 Mask 1. Top view.* Designed by Neri Oxman and members of The Mediated Matter Group for The New Ancient Collection curated and 3D printed by Stratasys, 2016. Photo: Yoram Reshef.

*Figure 11* – Vespers. *Series 1 Mask 3. Back view.* Designed by Neri Oxman and members of The Mediated Matter Group for The New Ancient Collection curated and 3D printed by Stratasys, 2016. Photo: Yoram Reshef.

# Recursive Symmetries for Geometrically Complex and Materially Heterogeneous Additive Manufacturing

Christoph Bader[1] and Neri Oxman[1].

*(as published in Computer-Aided Design, Issue 81, September 2016 – with minor edits)*

[1] Mediated Matter Group, Media Lab, Massachusetts Institute of Technology, Cambridge, MA 02139, USA

## Abstract

We present a generative method for the creation of geometrically complex and materially heterogeneous objects. By combining generative design and additive manufacturing, we demonstrate a unique form-finding approach and method for multi-material 3D printing. The method offers a fast, automated and controllable way to explore an expressive set of symmetrical, complex and colored objects, which makes it a useful tool for design exploration and prototyping. We describe a recursive grammar for the generation of solid boundary surface models suitable for a variety of design domains. We demonstrate the generation and digital fabrication of watertight 2-manifold polygonal meshes, with feature aligned topology that can be produced on a wide variety of 3D printers, as well as post-processed with traditional 3D modeling tools. To date, objects with intricate spatial patterns and complex heterogeneous material compositions generated by this method can only be produced through 3D printing.

# Introduction

Symmetries are abundant in the domains of mathematics, the sciences and the arts [3]. Throughout history, and across scales of material practice—within architecture, arts and crafts—symmetries can be found in combination with color, as can be observed in fabricated ornamental artifacts known to carry and express cultural identity and significance [4]. Within the natural world alone, a multitude of symmetrical forms are thought to have evolved as a consequence of the need to identify and to recognize objects [5]. Furthermore, symmetries are known to be associated with genetic quality [6] and, along with complexity, symmetries have long been associated with the perception of beauty [7].

While known to enable the creation of highly complex objects [8], the availability of generative design methods that enable the creation of objects that are *truly complex*—both in shape and in material composition—is limited. Furthermore, implemented rule-sets are often restricted to the generation of *specific* types of artefacts. As such, the resulting objects are generally not diverse. And, even when they do enable geometrical diversity, such generative methods often generate descriptions that are not directly suitable for 3D printing or yet do not produce material distributions alongside geometry. Thus, generative design methods are typically not used in combination with streamlined workflows supporting the generation of physical material distributions for multi-material 3D printing. Driven by the motivation to overcome such limits, and by design opportunities associated with them, we present a generative method that enables the creation of a diverse set of geometrically complex colored objects, driven by symmetry.

The presented method can generate a wide variety of 3D printable objects with geometry-associated material distributions, and—as a result—it can be utilized as a valuable tool for the customizable generation of geometrically and materially complex 3D printable artefacts for use in creative workflows, design-exploration and the generation of unique 3D printable objects.

Generative methods are well known in research areas associated with generative design [9]. They embody process descriptions and rule-based systems for the semiautonomous generation of artefacts such as images, sounds, animations, or 3 dimensional objects. These descriptions act in a similar way to the way in which DNA does, in the biological world. The generative method is either controlled by parameters or by making direct modifications to the algorithm itself. One usually distinguishes between the algorithm or process created by the generative designer, the parameter controlled instance of the process utilized by the method's designer (or a third person), and the artefacts generated by that instance. Recently, generative methods have been utilized as mass-customization

tools with 3D printing being a means for production to give users the opportunity to generate unique objects. Examples include Cell Cycle by Nervous Systems [10] and Autodesk's Shapeshifter [11]. As generative methods enable the generation of complex geometries by automation and customization by parameterization, 3D printing has become the only viable solution that enables the transformation of arbitrary generated output into physical form, without losing the benefits of the generative method [12].

Multi-material 3D printing [13] enables the additive fabrication of objects comprised of multiple materials within a single build, omitting the need for assemblies. This method also enables the digital fabrication of material compositions with heterogeneous property distributions within a single assembly. In this paper we present 3D models that have been digitally fabricated by depositing UV-curable resin droplets in an inkjet like fashion, layer-by-layer. Every new layer of jetted ink is cured through UV-light while nearby droplets diffuse and aggregate with the surrounding deposited droplets, and through successive repetition, to form a 3D volume. Recently, developed methods for heterogeneous material distributions have found their application as a tool for design expressions, most prominently featured in the work of Neri Oxman and The Mediated Matter Group [14].

In the following section we present a method for the generation of customizable and highly articulated objects; we showcase a diversity of outcomes, we evaluate the method's usefulness; and, finally, we describe the digital fabrication process of the generated objects through multi-material 3D printing.

# Method

### *Description*

The method implemented defines a recursive parametric grammar using polyhedral forms. Polyhedra are initially represented as polygonal meshes that, iteratively, 'evolve' into subdivision surfaces in a process resembling cellular division. This is achieved through the application of a recursive rule transforming the polygonal mesh, consisting of a collection of vertices, edges and faces, which will subsequently be used as the "control mesh" for the generation of a subdivision surface. This method, and its formalism, resembles shape-grammar formalisms [15]. Grammar-based formalisms have been successfully utilized in a wide variety of design settings [16], especially in the design of patterns mimicking cultural artefacts [17]. Similarly, our method defines a grammar in the vein of boundary solid grammars [18], using only a limited set of rules while offering a high level of diversity of shapes.

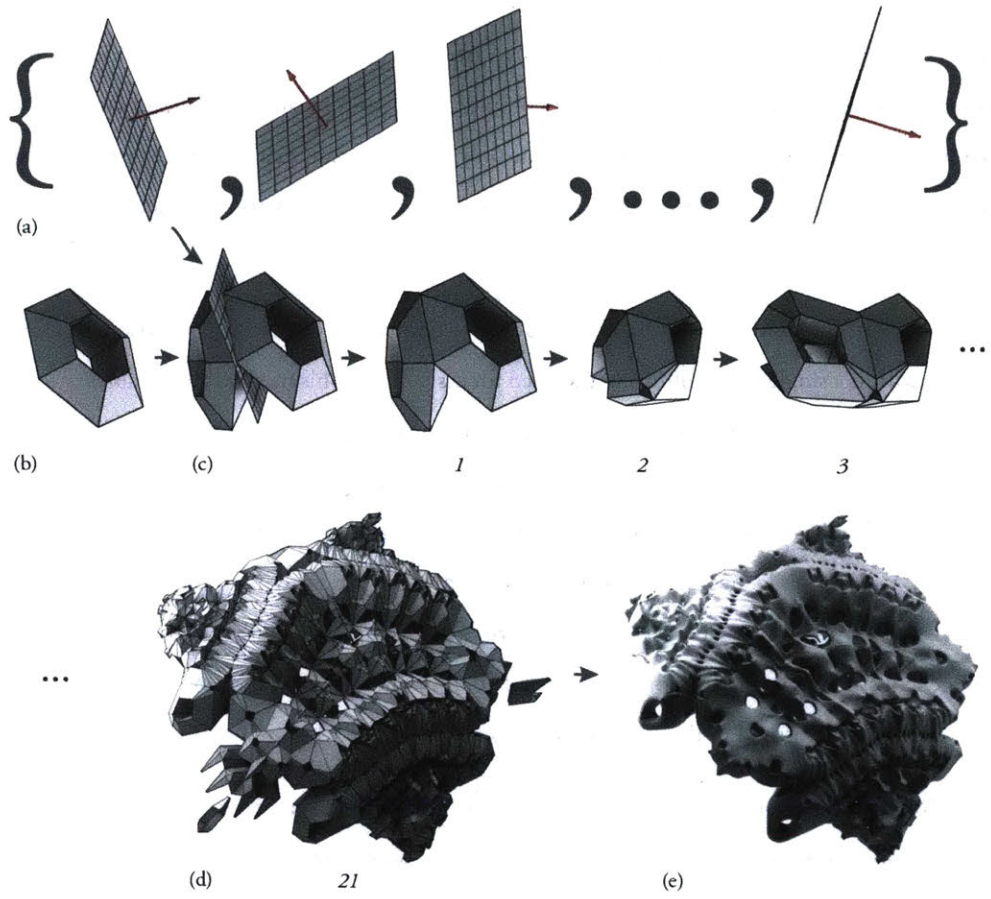


*Figure 12 – A visual representation of the generative method.* (a) a set of planes is generated as the base or underlying framework for all subsequent operations; (b) a user-guided input mesh is generated, upon which all operations are executed; (c) based on (b), a symmetrical mesh is generated; (d) the method is recursively re-applied and the result, following 21 iterations, is shown; (e) smaller sub-meshes are deleted and the subdivision surface is generated to produce the final artifact.

We define the $\Omega$ as the mirroring of a polygonal mesh along a given plane. Here mirroring refers to $\Omega$ cutting a polygonal mesh by a given plane, discarding regions in the negative half-space of the plane, subsequently reflecting the resulting mesh across this plane and obtaining a boolean union with the original non-reflected shape. Given a set $P$ of planes in $\mathbb{R}^3$, $P = \{p_1, \dots, p_n\}$, we denote the operator $\Omega$ as a function taking a coarse polygonal mesh $M^0$ with possible vertex or face properties. Here, $M^i$ is a mesh with vertices $V_M = \{v_1, \dots, v_n\}$ and faces $F_M = \{f_1, \dots, f_m\}, f_j \in V_M \times \dots \times V_M$ where a position $p(v_i)$ in $\mathbb{R}^3$ is associated with each vertex $v_i \in V_M$. Besides position we assume that there is an additional property $C$, carrying ratios of material-distribution information, associated with each vertex or face such that $C = \{c_1, \dots, c_n\}, c: V_M \to C, c_i = c(v_i)$ or $C = \{c_1, \dots, c_n\}, c: F_M \to C, c_i = c(f_i)$ respectively. $\Omega$ takes $M^0$ and transforms it into a symmetrical mesh $M^1$ by sequentially cutting and mirroring it as follows

$$M^1 = \Omega_{p_1}(M^0) = mirror(cut(M^0, p_1), p_1)$$

Here the $cut$ operation is the boolean intersection of $M^i$ with the positive positive-space defined by $p_{i-1}$ resulting in an open mesh. The mirroring procedure produces a symmetrical mesh along $p_1$ and the resulting mesh must be closed. This can be achieved by reflection of the original mesh and performing a boolean union with the original mesh. Finally we assume that $\Omega$ does not introduce degenerated non 2-manifold cases such as singular vertices or complex edges [19].

$$M^i = \Omega_{p_i}(M^{i-1})$$

The operator is repeated recursively for $n$ user-defined steps resulting in $M^n$. The resulting mesh may have unconnected parts $N = \{M^n{}_1, M^n{}_2, \dots, M^n{}_k\}$, where $M^n = \bigcup M^n{}_i$ and $\forall\, M^n{}_i, M^n{}_j \in N \text{ with } i \neq j \Rightarrow M^n{}_i \cap M^n{}_j = \emptyset$. From these, we find the largest surface area and find $M_{max} = argmax\ Area(N)$ where $Area$ is the usual $\sum_{f \in F} n \cdot \sum_{v_i \in f} \frac{p(v_i) \times p(v_{i-1})}{2}$. We keep the largest part in order to obtain a connected mesh. Finally, $M^{max}$ is used as control polyhedron and recursively refined by the Catmull-Clark subdivision scheme [20] to obtain the final output $M^f$. We use the Catmull-Clark scheme as it results in $M^f$ consisting of quadrilaterals; we use this subdivision method as it enables the alignment of quadrilaterals with symmetries of the resulting object [21]. The method is depicted in Figure 12, and exemplary outputs are shown in Figure 13, Figure 14 and Figure 15. We note that by adhering to the aforementioned conditions, $M^f$ will be a closed 2-manifold polygonal mesh and, as such, it would be suitable for 3D printing. This process can be described in a grammar formalism, where the formal grammar $G$ is given by $G = (\{M^i | 1 \leq i \leq n\}, M^f, \{\Omega_{p_i}, M^n \rightarrow M^{max}, M^{max} \rightarrow M^f\}, M^0, P)$.

*Parameters, Modification & Evaluation*

The appearance of the output $M^f$ is typically governed by the input Mesh $M^0$, and the number and configuration of the planes in the set $P$, given by plane normal $n_p(p_i)$ and distance $d_p(p_i)$ from the origin. Several generated examples are given in Figure 13, showcasing various levels of heterogeneity in material composition. Figure 14 illustrates the effect of different arrangements of planes on the outcomes. Planes must be defined such that they always pass through the currently largest object (given by the surface area). To achieve well-defined cutting, we precompute the largest part, before actually performing the cutting operation. Thus, planes which do not cut this largest part, can be adjusted accordingly during recursive execution of the process.

Interesting variations are achieved by incrementally increasing the distance from the origin for the planes in $P$ such that $d_p(p_i) < d_p(p_j), for\ i < j$. While random normal distributions for the planes $P$ work well, aligning the plane-normals, as shown in Figure 15 along a certain direction results in particular interesting examples.

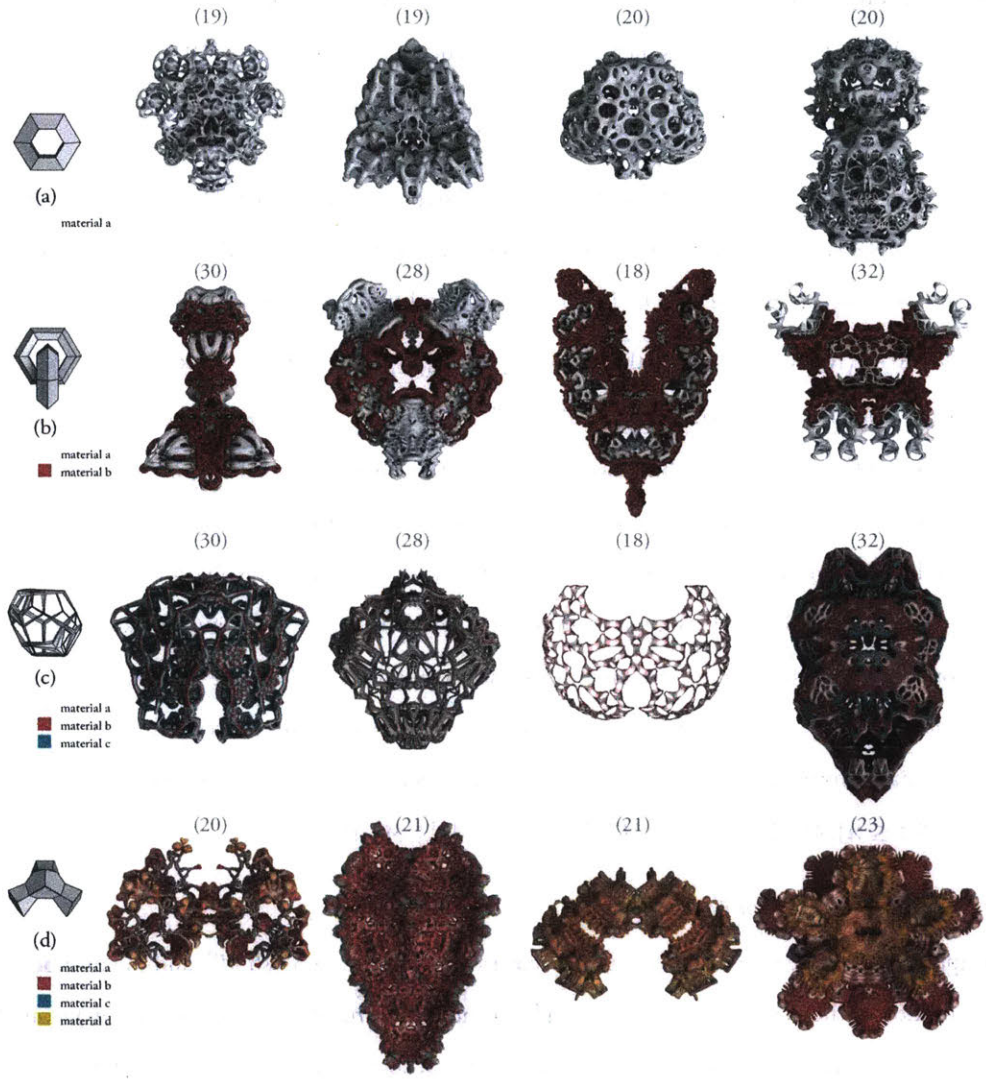


*Figure 13 – Different input shapes and their results.* Here the cardinality of the given plane-sets is shown in parentheses. In addition, we show different generated material distributions over the surface of the generated geometry with varying heterogeneity. (a) a single material, showcased by only one color; (b) two discretely disjoint geometries and materials; (c) geometrical discrete but materially heterogeneous material distributions; (d) geometrically heterogeneous and materially heterogeneous material distribution. Here we use color but as shown in Section 3 the colored material can encode for arbitrary printable materials and gradients between colors are visual indicators for intermediated mixed materials.

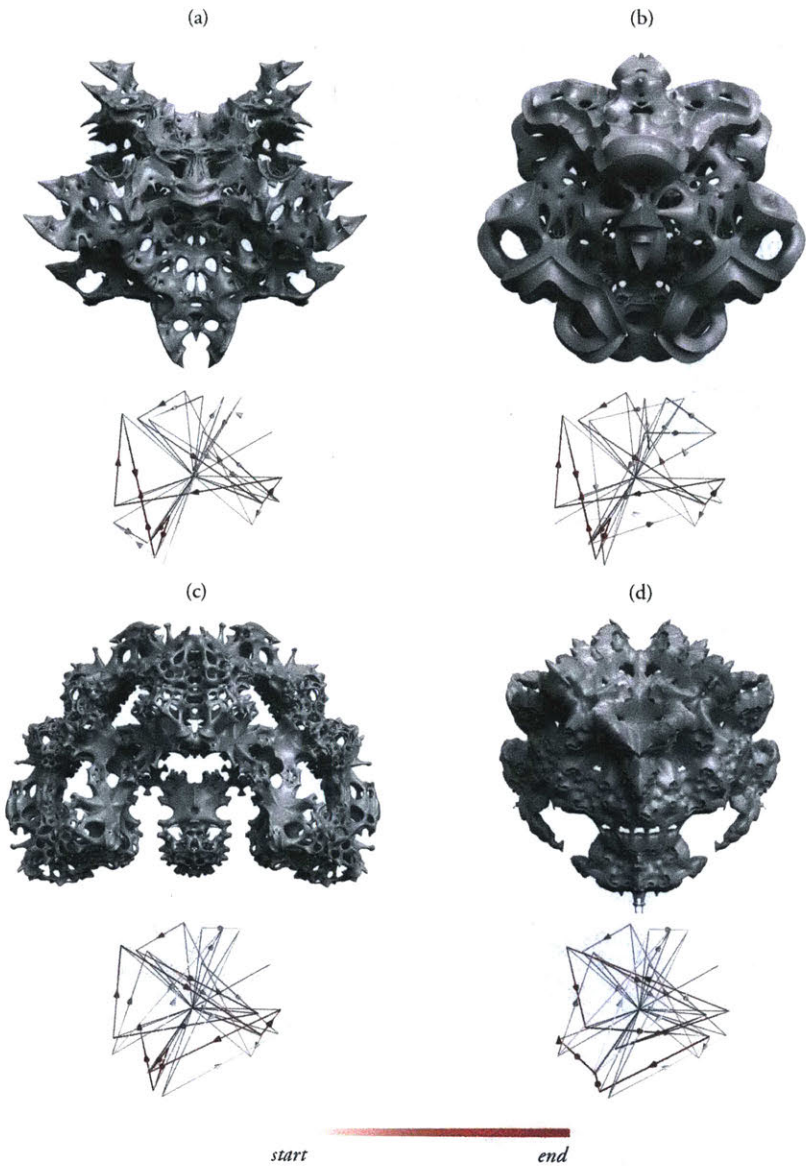


*Figure 14 – Exploration of the emergent design space.* All the generated objects utilize the same distribution of planes, but traverse them in different orders. Each section shows the generated object on top and the order in which the planes, depicted by their normal, are traversed below. (a) and (b) have different starting orders but the same order of planes in the end. (c) and (d) have the same starting order but diverge to different orders in the end.

Furthermore, we can increase the 'expressiveness' of the algorithm by modifying the *mirror* operation. By introducing deformations or geometric operations that are *distinct* for the two symmetrical sides generated, we can achieve an even greater diversity in the output. More generally reflections across arbitrary geometries are also possible as shown in Figure 15(d). However, 'manifoldness' in this case is harder to achieve or must be sacrificed. To achieve reflections, we use a

triangular mesh $T$ instead of a plane across which the $M$ should be reflected. To reflect we simply find the closest point $k_i$ for the vertex $v_i \in V_M$ on $T$ then compute the corresponding surface normal $n_i$ at $k_i$ and reflect across the plane defined by $k_i$ and $n_i$. This is shown in Figure 15. Manifoldness is sacrificed as this reflection mapping is no longer necessarily injective. If the reflection mapping can be given by a deformation mapping $F: \mathbb{R}^3 \rightarrow \mathbb{R}^3$ we must require that $\det(DF(p(v_i))) \neq 0$ for all $v_i \in V_M$ where $DF$ denotes the Jacobian of $F$.

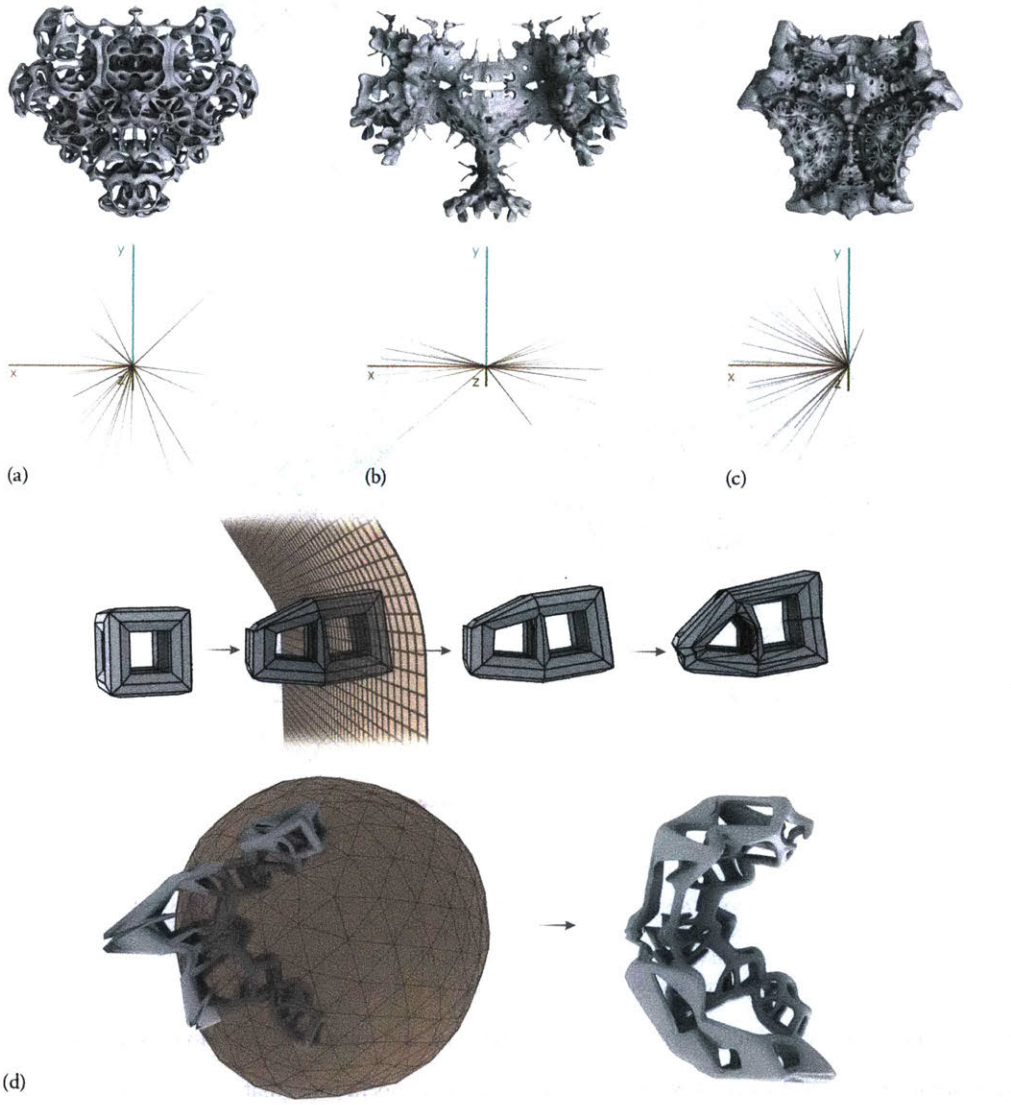


*Figure 15 – Modifications to the design space.* Upper: Sets of plane-normals and respective outcomes. (a) a uniform distribution of plane normals; (b) plane normal distribution aligned with x-axis; (c) plane normal distribution aligned with positive x-axis only. Lower: (d) Reflection across arbitrary shapes such as deformed planes or spheres enabling more general outcomes.

We note that, while the presented method appears simple, it produces outcomes that are otherwise challenging to reproduce, are sophisticated in detail and rich in complexity, and showcase a high level of diversity. We also highlight the similarity of some of the produced artefacts to the artistic work of Nick Ervinck [22] or Michael Hansmeyer [23], who use 3D printing as a fabrication method, thereby showcasing the usability of the method for creative practice. Furthermore, as argued in [7], complex symmetrical patterns—as produced by our method—show a high correlation with aesthetic 'judgments' of beauty. As such, given the high diversity produced, and the ability to create objects that are considered "aesthetically pleasing", the method is suitable for the exploration of artistic design possibilities and, thereby, can enhance or contribute to the creative process. Finally, the outcome's feature-aligned topology allows for straightforward and efficient editing of the generated meshes with common 3D modeling tools.

Similarly to [24], we evaluate our method by performance, stability, expressivity, control and applicability. We argue that, since the method is based upon operations with low computational complexity, and given that all operations are efficiently implementable using a half-edge data structure [25]; adequate performance can be achieved such that models with millions of vertices can be generated in seconds. This is experimentally verified as shown in Figure 16(a), where models up to one million polygons are generated within a single second. The method produces objects reliably as all sub-operations are well studied and do not produce degenerated cases easily. As such, the method can be qualified as stable. The expressivity of the method is shown in Figure 13, Figure 14 and Figure 15. We argue that the method can produce a wide variety of diverse and interesting shapes. To investigate this diversity further, we show that generated objects can be drastically dissimilar. To evaluate dissimilarity, we utilize weighted spectral distances [26], a shape distance measure similar to the distance obtained from to the well-known Shape-DNA [27]. For two given shapes $\Omega_\lambda, \Omega_\xi$ the weighted spectral distance (WESD) uses the spectra $\{\lambda\}_{n=1}^{\infty}, \{\xi\}_{n=1}^{\infty}$ of the laplace-beltrami operator to define the distance given by $\rho(\Omega_\lambda, \Omega_\xi) \triangleq \left[\sum_{n=1}^{\infty}(\frac{|\lambda_n - \xi_n|}{\lambda_n \xi_n})^p\right]^{1/p}$. For dissimilarity measurements we consider a set of 10 generated meshes shown in Figure 9, using the same input mesh throughout, and compute their mutual WESD. For each generated mesh we compute the discrete laplace-beltrami operator by its finite element approximation [28]. Using a spectra signature size of 100, we evaluate the WESD with $p = 2$ between each object and apply classical MDS to visualize the results as shown in Figure 16(b). The distribution of the generated samples in the MDS plot clearly shows dissimilarity of the exemplary generated objects. Furthermore, as Figure 16(c) shows dissimilarity can be achieved between generated objects by simply varying parameters of the method.

Control over generated outcomes is the method's single limiting factor. While the amount and configuration of planes, the input shape and additional modified mirror operations are possible, there is no target-specific control that allows a user to modify the shape of the resulting object locally without modifying the global shape. This, however, does not limit the explorative nature of the method. Choosing a fixed number of planes, and continuously varying plane normal, distance of each plane or other parameters (Figure 16(c)), while not performing the recursive subdivision step, heuristic design optimization methods [29] can be employed to fit the resulting object to a target envelop by minimizing the total Hausdorff distance between this target and the generated objects, as shown in Figure 17. We discuss the applicability, of our method for the generation of 3D printable shapes in the next section.

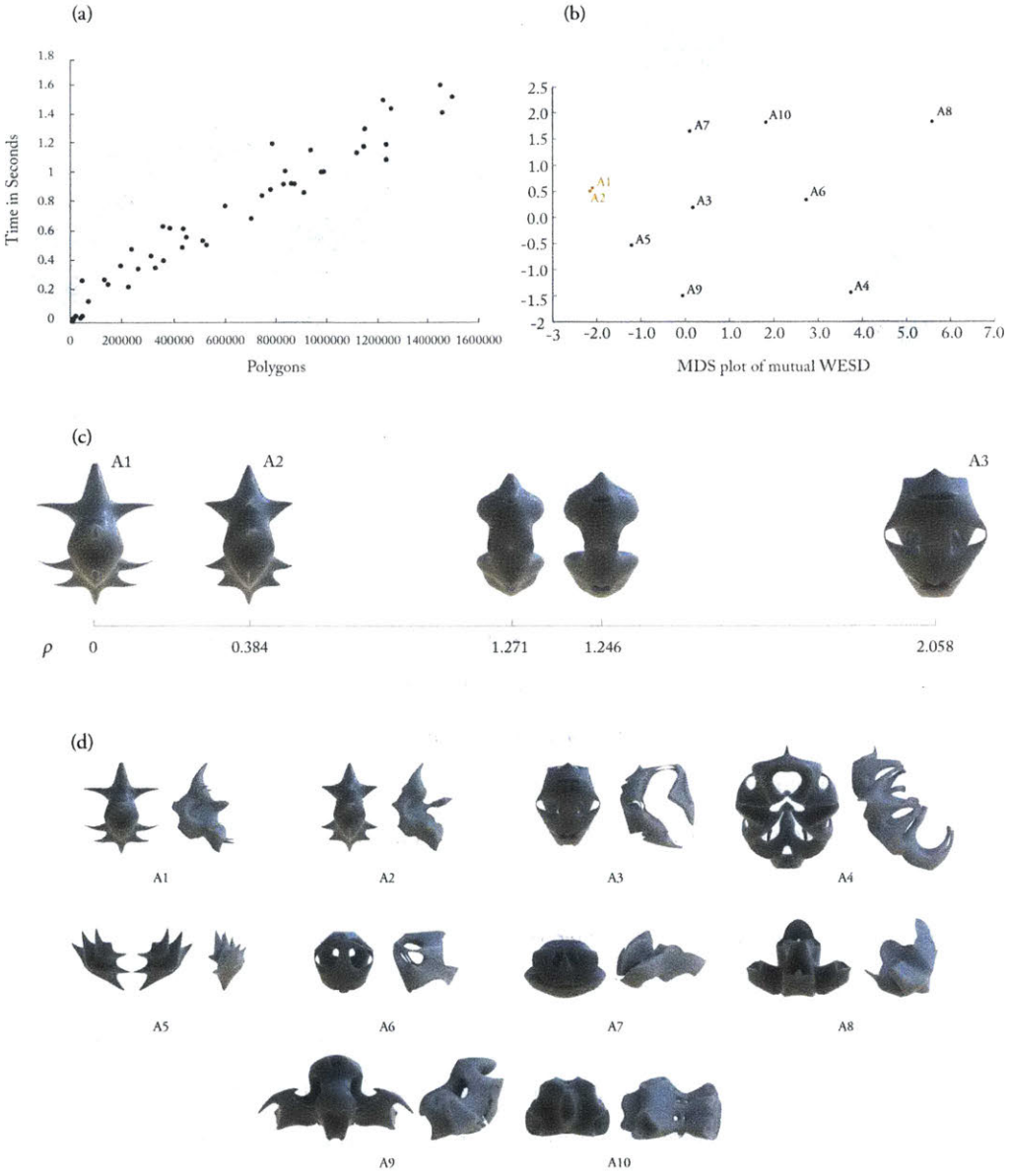


*Figure 16 – Characterization of the generative method.* (a) Performance measurements of the method for generated models with different polygon counts. All measurements were taken on an Intel Xeon E5-1650v3 with 3.50GhZ. (b) MDS-plot of weighted spectral distances. While the objects A1 and A2 were intentionally generated to be similar, objects A3 to A10 have been generated with arbitrary parameters but from the same input mesh. (c) By continuously modifying the alignment of the input geometry the generated geometry changes, which results in a monotonically increasing WESD. In the evaluated objects we were limited to objects with low complexity (Polygon counts below 10000) due to the high computational overhead for computing the spectra. All evaluate shapes are shown in (d).

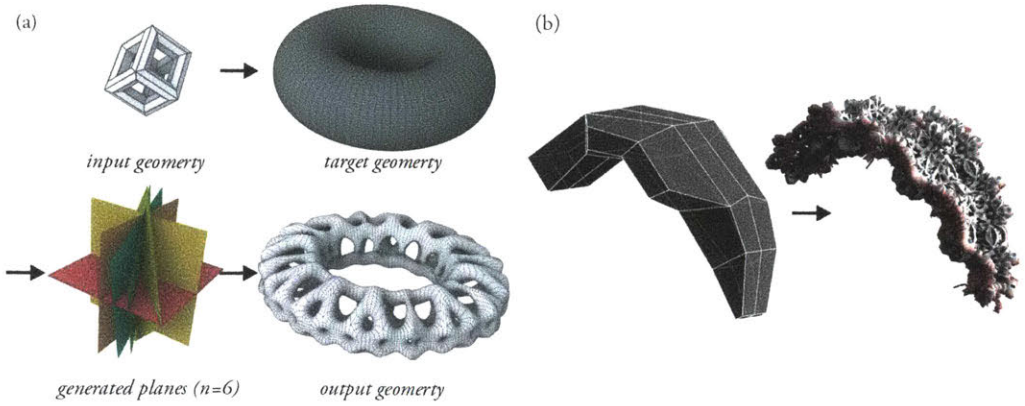


*Figure 17 – Adapting a generated shape to a given target geometry.* (a) The input geometry is to be transformed such that—following several applications of $\Omega$ —it fits to target geometry. To achieve this, the mirroring planes, must be determined as shown. Illustration (b) shows a more complex envelope shape with more complex internal shape.

## Production

Since objects are generated without the direct influence of a user, it is important to validate that generated geometries are suitable for 3D printing. As described above, the objects generated by our method are inherently suitable for 3D printing, as outcomes can be characterized, in most cases, as closed 2-manifold polygonal meshes separating an inner and outer domain. We assume that the input mesh $M_0$ is a closed piecewise linear (PL) 2-manifold embedded in $\mathbb{R}^3$. The cut operation removes regions of this surface which are in the negative half-plane given by $p_i$. Leaving a PL 2-manifold embedded in $\mathbb{R}^3$ with boundary. The generated boundary is required to be a set of closed 1-manifolds embedded in $\mathbb{R}^2$ (closed curves). This is achieved by picking or adjusting the cutting planes such that—if a violating case is detected—the plane is slightly offset along its normal direction. This cutted mesh is then reflected, and topologically connected, with its not reflected counterpart giving $M_{i+1}$. Thus, if the original shape $M_0$ is a closed 2-manifold, at no point self-intersections or non-manifold cases such as singular vertices and complex edges are introduced. Furthermore, we require that, $M^0$ must only consist of convex polygons to avoid the introduction of overlapping polygons in the subdivision step. We also note that, while other approaches—such as the generation of 3D Mandelbrot-sets [30] —can result in similar shapes; these representations must be converted to a 3D printable format, typically by implementing iso-surfaces extraction methods [31], which can result in loss of surface-detail or large file-sizes.

Two case study models were fabricated on a Stratasys J750 multi-material 3D printer, capable of printing several photopolymer resins simultaneously. During print time, the print head

simultaneously deposits resin droplets in various amounts that mix and immediately polymerize through exposure to UV light. By combing several types of base resins by spatial deposition, it is possible to achieve a wide variety of intermediate materials, which are rich in both color and structural properties. The standard workflow, available through the software interface to the 3D printer, uses predefined material combinations that can only be applied to individual disjoint model parts, which then have constant properties through the whole model part volume. While this workflow is sufficient for certain use cases, it is not applicable, nor is it ideal, for the production of parts resulting from our generative method. This is due to the fact that material properties are either encoded as vertex or face properties and can continuously vary across and between them. As such, we employ a custom slicing approach.

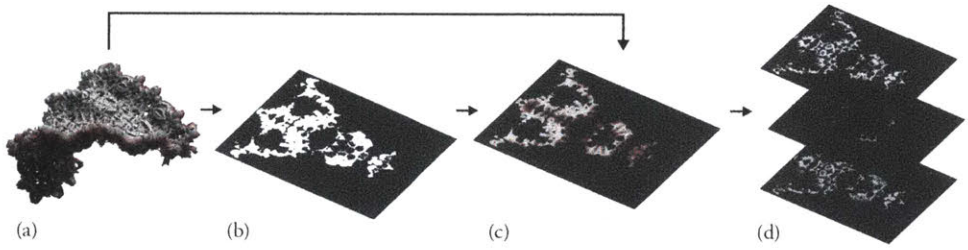


*Figure 18 – The slicing process.* (a) the input mesh; (b) the generated and rasterized slice; (c) contributing material information on the mesh is found per slice (d) dithering to 3 bitmaps describing droplet placement of three base resins.

As shown in Figure 18, we begin by generating a rasterized slice from $M^f$ . Following, we determine the material properties from the surface, and, finally we 3D dither the slices to bitmaps, one for each of the base-materials being deposited by the printer. These dithered slices are used for the control of droplet placement by the printer, where near-by placed droplets will diffuse to aggregate into intermediate materials depending on the given spatial configuration and the types of materials being deposited [32], [33]. Here we assume that $c_i \in C$ on $M^f$ is an n-dimensional vector, where n is given by the number of base materials that the printer can provide, and, further, we require that $|c_i|_1 = 1$. In order to find—based on the properties of $M^f$—the internal material properties of the slice $S_i$, a new property $C_V$ is associated with each voxel $u_i$ of the slice, such that: $u_i \in S_i$, $C_V = \{c_{V_1}, \dots, c_{V_M}\}$, $c_V: V \to C_V$, $c_{V_i} := c_V(u_i)$. We note that—while the property $C_V$ can encode for color by describing the mixing ratios of Cyan, Magenta, Yellow, Black, White and Transparent resins—it can also encode for the mixing ratios of arbitrary resins with different functional properties, such as shore-hardness. In order to find the properties from the surface, we use an approach similar to inverse distance weighting. For each voxel $u_j \in V_{s_i}$ in the slice $S_i$ we sample the $k$ closest points $K \subseteq V_M =$

$\{v_1, .., v_n\}$ that are visible from $u_j$. Where $v_i \in K$ is visible from $u_j$ if the line segment from $p(v_i)$ to $p_i(u_j)$ lies in $M$. From the points in $K$ we compute the new property by

$$c_i(u_j) = \frac{1}{\sum_{v_i \in K}(1 - \lambda(d(u_j, v_i))} \sum_{v_i \in K} (1 - \lambda(d(u_j, v_i))c(v_i)$$

where $\lambda$ is a smoothing function for example given $\lambda(d) = 6\left(\frac{d}{d_{max}}\right)^5 - 15\left(\frac{d}{d_{max}}\right)^4 + 10\left(\frac{d}{d_{max}}\right)^3$, $d_{max} = \max\left(d(u_j, v_i)\right) for\ all\ v_i \in K$ and $d$ is the Euclidean distance. If $M$ is coarse, additional sample points, $V_S$, can be generated on the surface $M$ and $V_M \cup V_S$ can be used to find the closest points, $K \subseteq V_M \cup V_S$. Following, for any additional $v_i \in V_S$, we compute $c(v_i)$ on $M$ implementing barycentric interpolation from the vertices adjacent to the triangle on which $v_i$ resides. An analogous approach can be used for properties associated with faces.

Furthermore, to each vertex $v_i \in V_M$ we can assign a maximum distance $maxd(v_i)$. We can then modify the set $K$ such that for every $v_i$, this applies: $v_i \in K$, $d(u_j, v_i) \leq maxd(v_i)$. This allows to constrain the influence region of each vertex within the enclosed volume. Following the identification of all internal material-compositions, the slice is dithered into n bitmaps, one for each base material, by a 3D-adaption of a process similar to Floyd-Steinberger [34] dithering. All the above can be efficiently implemented using common spatial data structures. We show two examples using different material combinations in Figure 19, printed on Stratasys J750 using seven materials simultaneously, creating a full color and transparency printed part.

*Figure 19 – Parts printed on a multi-material Stratasys J750 printer using seven base resins showcasing the geometric and material complexity that can be achieved.* The objects here were created as part of a collection by The Mediated Matter Group in collaboration with Stratasys for 'The New Ancient' collection.

## Conclusion

In this paper, we have presented an algorithm for the generation of complex 3-dimensional geometries incorporating heterogeneous material distribution for the generation of multi-material objects. The method presented promotes significant diversity in outcomes and, as such, is suitable for creative practice and design exploration. The ability to rapidly generate a wide yet diverse array of forms that are at once geometrically complex and materially heterogeneous makes it possible to design, and digitally fabricate, forms that are highly customizable. The method shown, therefore, introduces unique design opportunities that leverage, and lie at the intersection of additive manufacturing and generative design. Finally, the incorporation of material-based parameters with shape-generating methods opens up a new design space for generative modeling as well as new and exciting opportunities for creative practitioners including designers, artists and engineers. While our method generates material distributions informed by, and embedded within geometrical descriptions, future work may explore the simulations generation of geometrical and material modeling thus offering ways in which geometry and material can simultaneously interact within a generative system.

## Acknowledgments

The authors would like to acknowledge Naomi Kaempfer, Director of Art, Fashion and Design at Stratasys Ltd., and her team members—Gal Begun, Boris Belocon and Yoav Bressler—for their insights and dedication. The company's support has enabled the use of the Stratasys J750 seven material printer. The objects discussed and presented in this paper include study prototypes designed by The Mediated Matter Group for the 'New Ancient' collection by Stratasys to debut in late 2016.

# Programmable Matter

A vast variety of material structures in nature rely on continuous material property gradients within an objects volume to enable functional behavior. Examples include gradients in stiffness of tendon-to-bone attachments to alleviate stress concentrations at interfaces [35], refractive index gradients in lenses of aquatic animals to improve vision [36] and the differential swellability of plants to enable self-shaping [37]. This is in contrast to more common approaches of generating assemblies with homogenous materials throughout a model's geometry or even—as previously introduced—systems that infer material information from an objects surface. Therefore, design computation must shift from designing geometric features alone to more holistic approaches encompassing and considering heterogeneous material distributions, in order to allow designers to precisely mimic systems and mechanics found in nature.

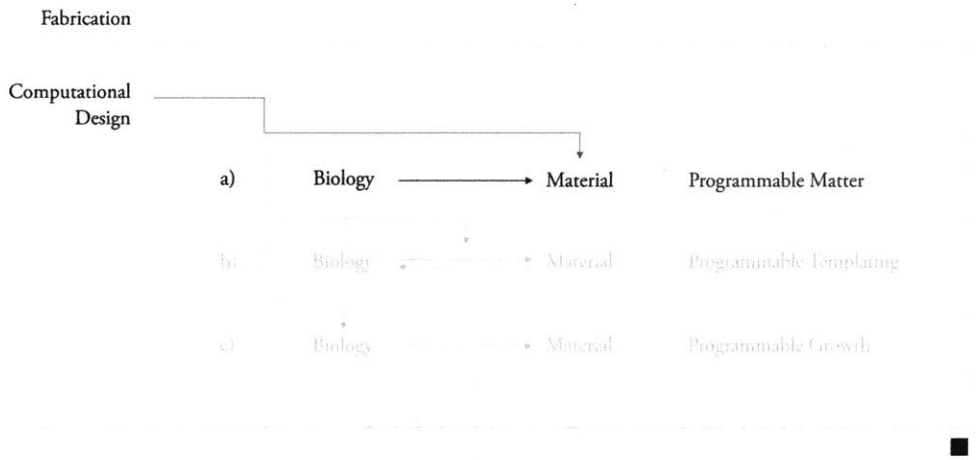


*Figure 20 – The programmable matter approach.* Utilizing computational design on synthetic material systems to enable biologically inspired design strategies.

Resolution and hierarchical complexity are one of the major themes when it comes to mimicking nature across scales visually and materially. However, accounting for the complexity observable in nature and fabricating similar systems in a controllable way is still a challenging endeavor as computational resources are finite while nature seems to transition scales continuously. Here we first introduce a data-driven material-modeling framework, enabling the production of materially heterogeneous objects, printed on a multi-material 3D printer at high resolution. In contrast to previous design approaches [38], [39], here one can specify multiple generated or acquired data sets, which are used to inform material distributions during slice generation.

However, some of the most inspiring material features found in nature are not only visual but functional or have the ability to change a specific property upon an external stimulus [40]. One prominent example is given by the humidity-driven self-shaping ability of plant systems such as pinecones and orchid tree seedpods [37]. Thus, the previous framework is extended, encompassing volumetric material modeling methods and forward evaluation approaches to enable more holistic design strategies adapted form nature. This framework is subsequently applied to a catalogue of 3D printable functionally gradable material properties to show how design computation can enable better biologically inspired designs.

# Data-driven Material Modeling with Functional Advection for 3D printing of Materially Heterogeneous Objects

Christoph Bader[1], Dominik Kolb[1], James C. Weaver[2] and Neri Oxman[1+].

*(as published in 3D printing and additive manufacturing, Volume 3, Number 2, 2016 – with minor edits)*

1. Mediated Matter Group, Media Lab, Massachusetts Institute of Technology, Cambridge, MA 02139, USA
2. Wyss Institute for Biologically Inspired Engineering, Harvard University, Cambridge, MA 02138, USA.

## Abstract

We present a data-driven approach for the creation of high-resolution, geometrically complex and materially heterogeneous 3D printed objects at product scale. Entitled *Data-driven Material Modeling* (DdMM), this approach utilizes external and user-generated data sets for the evaluation of heterogeneous material distributions during slice generation; thereby enabling the production of voxel-matrices describing material-distributions for bitmap printing at the 3D printer's native voxel resolution. A bitmap-slicing framework designed to inform material property distribution in concert with slice generation is demonstrated. In contrast to existing approaches, this framework emphasizes the ability to integrate multiple geometry-based data sources to achieve high levels of control for application in a wide variety of design scenarios. As a proof of concept, we present a case study for DdMM using functional advection, and demonstrate how multiple data sources used by the slicing framework are implemented to control material property distributions.

# Introduction

Recent advances in high-resolution 3D printing have enabled the design and digital fabrication of objects with unprecedented levels of structural complexity[41],[23]. However, while most commonly implemented methods for the production of 3D printable file formats rely on the generation of highly detailed surface meshes and object assemblies, they often neglect to address, or overlook, the functional need and design potential of heterogeneous material distributions that are *volumetric* in nature, and which take full advantage of the native resolution of a 3D printer.

Modern multi-material 3D printers [13] employ photo-polymerization of UV curable resins to construct 3D objects through an inkjet-like printing process by sequentially depositing layers as thin as 32 microns. This high-resolution 3D printing approach enables precise spatial control over the deposition of individual material droplets, where material composition is controlled at the droplet level by defining – for each deposited material – a binary 3D voxel matrix at the native resolution of the printer. This voxel-matrix, in turn, defines the material identityof the individual droplets and their spatial placement in space, resulting in *volumetric* binary material representations that can be used to define heterogeneous and continuously varying material composites at the resolution of the printer. This approach is often described as bitmap-based printing or voxel-printing [42].

Design approaches that rely solely on voxel-based representations [39],[38] for 3D multi-material compositions are often challenging to scale for the production of high resolution, large volume models. Since commercial multi-material 3D printers can offer build envelopes as large as 40,000 $cm^3$; defining binary 3D matrices at the native resolution of the printer, results in *billions* of individually addressable voxels, whose representations can become overbearing in size and challenging to handle.

In the following section, we present a data-driven design approach for the production of a materially heterogeneous object, printed on a multi-material 3D printer. We showcase a Data-driven Material Modeling (DdMM) approach in the form of a case study named *Lazarus*. In contrast to previous design approaches, this approach allows us to specify multiple generated data sets, which are used to inform material distributions during slice generation. Furthermore, *by partially reallocating data-transfer and data-modification to occur at the time of individual slice generation, we show how bitmap-printing in combination with function-driven material advection can be used for the design of highly complex and intricate material distributions.* Additionally, by employing a custom system for the direct input of bitmap-slices to control a 3D printer, this workflow, thus allows us to fully leverage the

native resolution of the 3D printer for large scale objects, highlighting the versatility, scalability, and usability of high-resolution bitmap-printing for design and engineering applications.

## Data-driven Material Modeling (DdMM)

### *Computational Framework*

To facilitate the use of external data-sources for the design of internal material distributions, and building on previous methods [32],[43],[44] our approach accounts for arbitrary external geometric data sets such as point-clouds, scalar and vector fields, curves and polygons, tetrahedral meshes, with their associated attributes, as shown in the case-study below. Using these external data sources, it is possible to drive the computation of hybrid evaluated and unevaluated heterogeneous material modeling methods[45] including distance-based[46] and source-based[47] approaches during slice generation for 3D-bitmap-printing. As such, this approach is designed to handle data-sources and to generate material-distributions *during* slice generation (on-slice-time) and, therefore, it permits the incorporation of external data as the primary design element in the creative process for multi-material 3D-printed objects. Despite these significant advantages, it should be noted, however, that only computational modifications to provided data-sets can be used with this approach for which either sufficient data can be pre-computed and provided during slicing, or which allow neighborhood-limited evaluation of material-distributions. An overview of this workflow is provided in Figure 21.

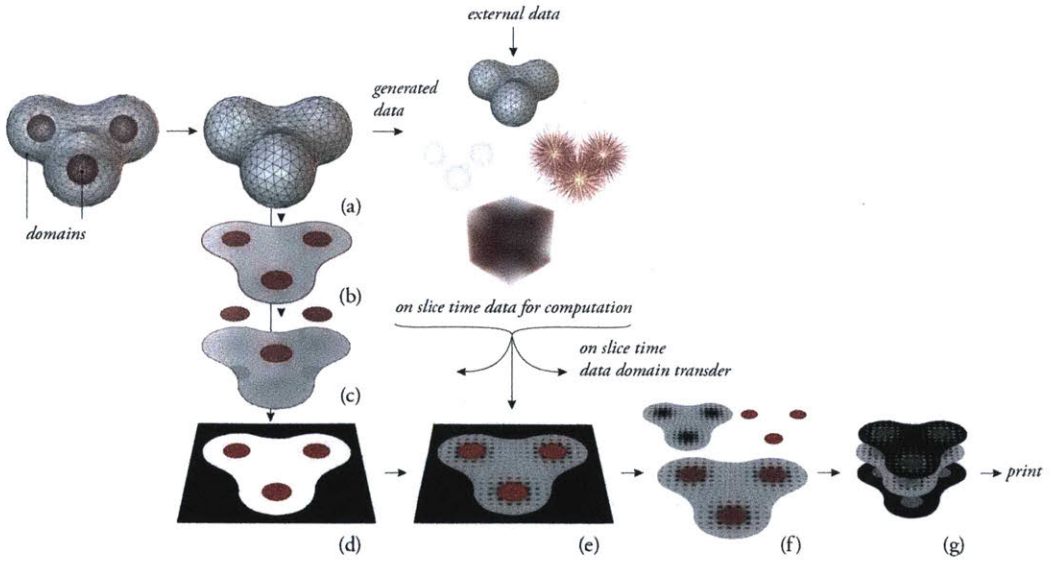


*Figure 21 – A data-driven computational framework for the production of bitmap-printable parts:* (a) Object-representation and data-generation; (b) Optional generation of a polygonal-slice; (c) Priority-ordering of specified material domains; (d) Rasterization; (e) On-slice-time data-transfer and data-modification; (f) Composition; (g) Material-dithering and bitmap printing system.

Our framework uses polygonal meshes, with user-defined material domains as source files. Each mesh is then sliced in the print-direction, resulting in a set of rasterized layers where each pixel/voxel can store, for example, material information, vectors for velocity fields, matrices, or other data structures. The resulting rasterized content is then dithered into $n$ binary bitmaps providing instructions for the material deposition of $n$ materials as defined by the printer. Furthermore, as mentioned above, we can integrate external geometry-based or user-generated data-sources of arbitrary dimensionality, which can then be used to influence the generation of the 3D-printable description at any stage of the description generation process. Figure 21(a) shows the object-representation and data-generation stages, where each object is indexed to a material-computation domain and additional data-sources can be computed and assigned for later use – for example – as part of the on-slice-time material generation step. We note that, while material-computation domains are discrete, their internal material-distributions can be continuous and heterogeneous. Figure 21(b)-(e) illustrates the rasterization of a bitmap slice obtained from a polygonal object, where we treat the generation of a polygonal slice as an optional stage. Figure 21(c) shows a priority-ordering step, describing, in a fully user-controlled manner, which material-domain has higher precedence. This approach is required in cases where two or more geometric material domains are overlapping, and, as a result, a defined priority has to dictate which material will be deposited. An example of data-driven priority-ordering is shown in Figure 22.

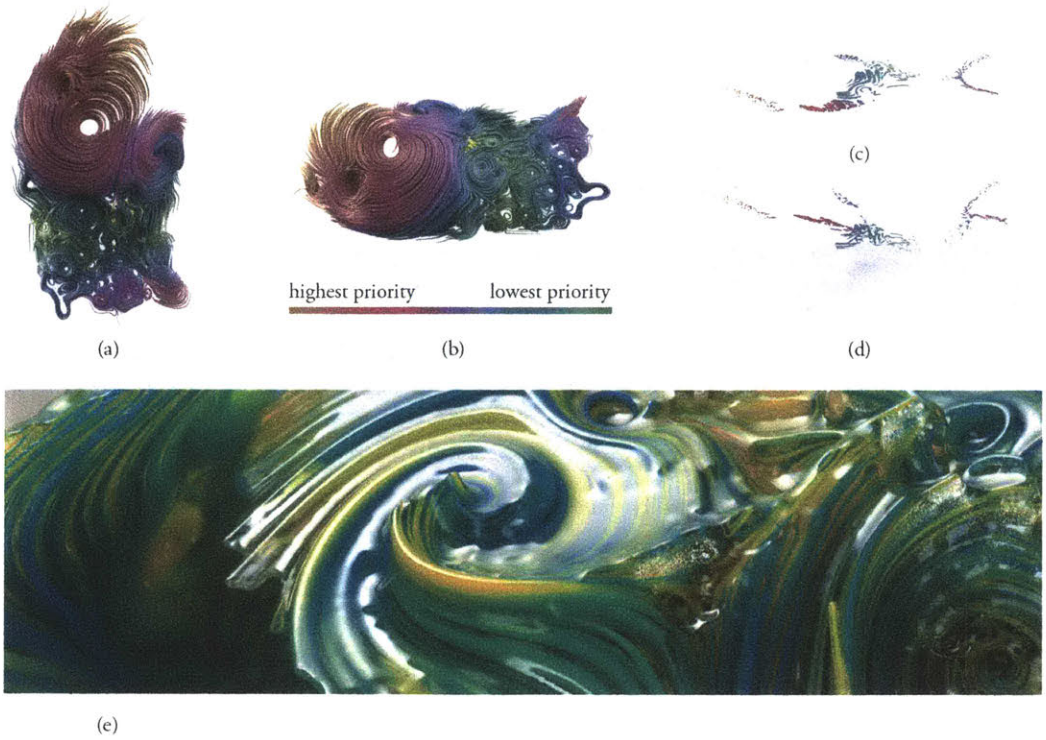


*Figure 22 – An example of data-driven priority sorting for the production of large and structurally complex objects[48]* In this example, the design consists of 15,543 polygonal tubes, curled and aligned to a predefined surface contour, which are encapsulated in a 41.2 by 30.5 by 16.7cm hull. Every tube can be assigned a uniquely different longitudinal material gradient and priority data is given by the distance from the surface contour. (a) A layering priority is assigned to each vertex of the polygonal tube according to its desired visibility in the final form, which varies as a function of distance from the underlying surface; (b) The design is aligned to the build-tray of the printer; (c) A slice is generated; (d) Visualization of the priority sorted segments of the design in the z-direction before rasterization; (e) Resulting 3D printed model. Photo: Yoram Reshef.

Figure 21 (e) illustrates the on-slice-time material computation step, whereby user-generated and external data sources, such as scalar and vector fields, from, for example, point-clouds and meshes, are transferred to a volume domain, and can then be used to influence and compute heterogeneous material distributions. A typical example of external data can include a voxel grid containing an n-dimensional property *per voxel*, describing relative material distributions, where each voxel describes a probability for a material to be deposited. As such, the provided volume can be coarser then the actual resolution of the printer whereby an *actual* material droplet description will be computed from the coarser volume during slice-time. We can *separate object-representation and material-representation* for the purpose of slicing. Figure 21(f) illustrates an example where several different material computation domains can be combined through common layering operations. Finally, Figure 21(g) shows the process of material dithering, using a modified version of Floyd-Steinberger[34] error diffusion dithering, where—for each material available to the 3D printer—a set of complementary slices is generated. These slices are directly input to a custom bitmap-printing system which controls

the deposition of material droplets by the 3D printer, such that no segmentation of material dithered slices to STL files is needed. This allows the production of objects with large volumes while still enabling continuous material distributions. An example of which is shown in Figure 23.

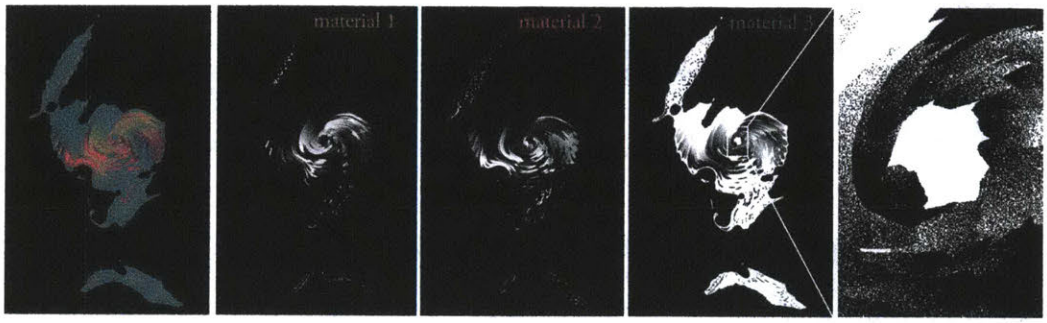


*Figure 23 – Object cross section illustrating variations in material composition of an object 3D printed with 3 different materials.* (a) Shows the composition of all 3 materials. Sections (b), (c), and (d) contain bitmaps that specify the droplet deposition for every material per object slice. Section (d) shows a close-up of section (c) whereby white pixels indicate material droplets deposited at each location.

To leverage the possibilities enabled by the design of data-driven material property variation during slice-time, we showcase function-driven advection as one example for a hybrid method to generate and influence high-resolution and heterogeneous material distributions. We denote by $\mathrm{m}(t_0, \mathrm{x}(t_0))$ an initial material distribution and describe the evolution of $\mathrm{m}$ through a velocity field $\mathrm{v}(\mathrm{x})$, defined at all positions, by the advection equation $\frac{\partial \mathrm{m}}{\partial t} + \nabla \mathrm{m} \cdot \mathrm{v}(\mathrm{x}(t)) = 0$. Using the framework shown in Figure 21, we use a coarse volumetric representation of the initial material distribution of the confining object, as well as either a functionally defined or an externally given vector field, as a secondary volume-data set, in the on-slice-time computation step shown in Figure 21(f). Lagrangian paths can be generated by integrating the flow. By performing a few steps of semi-Lagrangian advection[49] using a fourth order Runge-Kutta method, on only a few slices at a time, we can defer and distribute complex computations towards individual slice generation. Further modification can be achieved such that a simple diffusion term can be incorporated, or materials can be perturbed along the gradient of a predefined distance field. This, combined with the framework described earlier, enables the evaluation and transfer of data-sets in the material generation steps - as shown in the design case study given next - during slice generation. Further data-driven 3D printed variations using a Stratasys J750 full-color printer and designed implementing our methods are presented in Figure 24

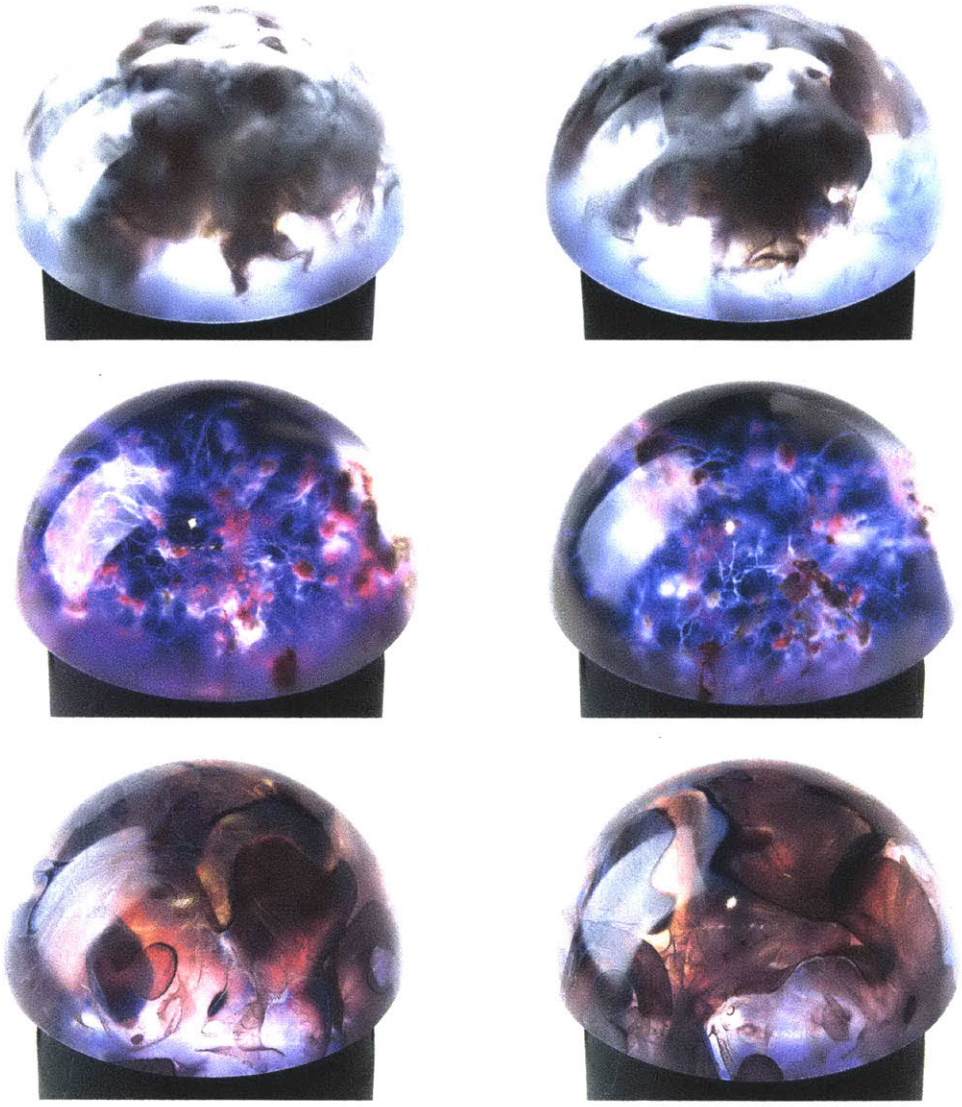

*Figure 24 – A collection of three general examples of the DdMM approach, illustrating an array of internal material compositions achieved through the implementation of the described methods to achieve visually complex patterns.* Such material compositions are uniquely obtained through our computational framework in combination with on-slice-time advection. The first row shows an example of advection driven by a given velocity field. The second row shows a volumetric data set where advection in the normal direction is used to create a diffusive effect in dense areas. The third row shows a periodic implicit function perturbed by a velocity field. For each set of 3D printed objects, the two photographs depict the object from different viewing angles. Photos: Mediated Matter.

## Data Driven Design

To demonstrate the DdMM approach in a design setting, we present *Lazarus*, a wearable mask designed to contain the wearer's last breath. The mask was designed as part of a collection whose design is ongoing, speculating upon, and offering a new interpretation of the ancient death mask. Traditionally made of wax or plaster to represent a person's face following death, *Lazarus* serves as an

"air urn" memento that is 3D printed, carrying a loved one's final exhale. As such, the mask offers a new form of portraiture combining the wearer's facial features while preforming as a spatial enclosure for their last breath. The mask's surface area is modeled after the face of the dying, while its material composition is informed by the physical flow of air and its distribution across the surface. Unlike its traditional hand-made analog, the design of *Lazarus* is entirely data driven, digitally generated and additively manufactured, approaching the resolution of the physical phenomenon it is designed to capture. Data fetched to inform the distribution of air flow can be acquired from the wearer, or, it can be digitally generated by a computational process incorporating the wearer's data, thereby creating a unique artifact perfectly customized to fit the wearer and her last breath.

For this speculative design, and its related (and specific) application, our design approach is illustrated in Figure 25 and is implemented as follows. First, the data designated to drive the material distribution is acquired or generated. In this example, only generated data is used, while - as stated above - external data-sources can also be employed and used with the described method. This data is then transferred from the domain of its origin (e.g. a human face), to a target domain (e.g. a mask designed around the human face). As the data from the original domain is insufficient to compute material distributions in a volumetric domain, this step is necessary to render the provided data suitable for further computation and evaluation. The collected data sources are subsequently used to inform the generation of material distribution. The material generation step is performed *during* slice generation, and as such, allows for the controllable design of material distribution at the resolution of the printer, while optimizing the use of available computational resources.

To simplify, we denote the closed parameterized surface (i.e. the face of the wearer) as $\partial\Omega$, and the target volume domain (the mask) as $\Omega$, shown in Figure 25 (d) - left and right - respectively. In this workflow, we implemented three different data-sources to drive material generation. First, as shown in Figure 25 (a), a heat map derived from solving for $u(\cdot,t): \partial\Omega \to \mathbb{R}$ in the adapted heat-equation[50] $\partial_t u(x,t) = k\Delta_\Omega u(x,t) + \frac{Q(x,t)}{c\rho}$, where $\Delta_\Omega$ is the surface laplacian, and an initial temperature $u(x,0) = u_0(x)$, is given. While in this case, the heat map is synthetically generated, it could equally well be acquired from a thermal imaging camera where the acquired data can be mapped to $\partial\Omega$ and similarly processed at a later time in the workflow, as described below. Secondly a geometrically determined normal-map as shown in Figure 25(b), from $\partial\Omega$, determined by $n(s) = \frac{(\partial_{s1}X(s)\times\partial_{s2}X(s))}{|\partial_{s1}X(s)\times\partial_{s2}X(s)|}$ is generated. Lastly, we use a velocity field (Figure 25(c)) acquired from a

computational fluid simulation mimicking simplified human respiration where $\partial\Omega$ was used as a rigid collision object.

Figure 25(d) shows the target 3D object, which was designed specifically to fit to our region of interest. On this "template", we model material distributions such that they are informed by the combined source data-sets. In order to transfer the previously computed data-sources to the volume domain, we use three different methods; Extrapolation, re-representation, and a simple change of domain. First, for $\Omega$, we generate a signed distance field[51] $d_{\partial\Omega}(x) = s_{\partial\Omega}(x) \cdot m_{\partial\Omega}(x)$, and $m_{\partial\Omega}(x) = \inf_{y \in \partial\Omega} d(x,y)$ and $s_{\partial\Omega}(x) = \{-1 \text{ if } x \text{ is interoir } \partial\Omega, 1 \text{ if } x \text{ is exteroir } \partial\Omega\}$, similarly we generate $d_{\Omega} = s_{\Omega}(x) \cdot m_{\Omega}(x)$, and $m_{\Omega}(x) = \inf_{y \in \Omega} d(x,y)$ and $s_{\Omega}(x) = \{-1 \text{ if } x \text{ is interoir } \Omega, 1 \text{ if } x \text{ is exteroir } \Omega\}$. For the heat map, we use a one-way extrapolation[52] of $u$ from the interface along the normal-direction such that $u + (\nabla u \cdot \nabla d_{\partial\Omega}) = 0$ as depicted in Figure 25(e). For the normal-map, we choose to re-represent by $\nabla d_{\Omega}$ instead of the surface normal, as $\nabla d_{\Omega}$ is defined over all of $\Omega$. In a similar fashion, other geometric properties such as curvature can be made useable to the volumetric domain. Finally, for the velocity field in Figure 25(g), we simply change the region where the field is sampled from $\partial\Omega$ to $\Omega$. We note, that the transfer step is not necessary if the provided data is already specified in the target domain. However, this example serves to outline how this transfer can be accomplished if the provided data-sources are not specified as needed.

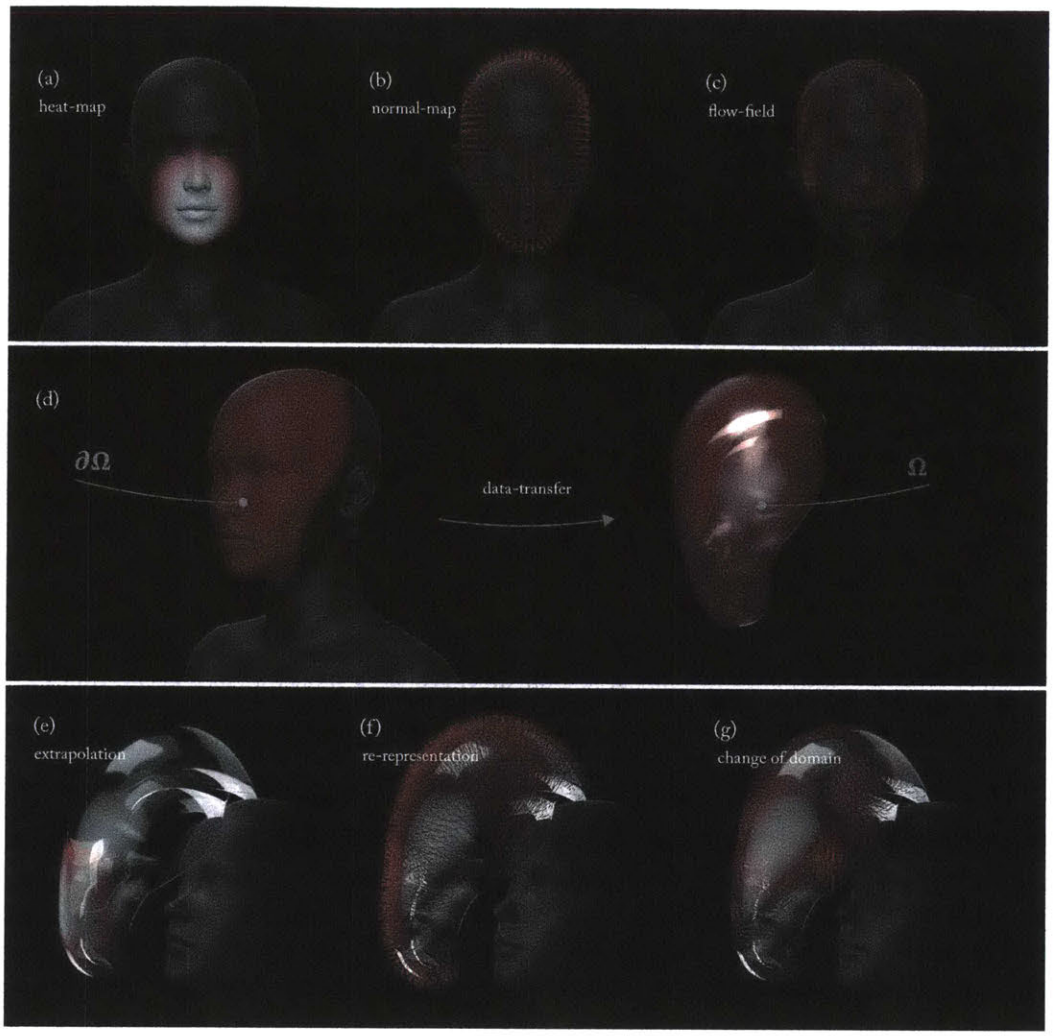


*Figure 25 – Visualization of the design approach for* Lazarus. In (a), (b) and (c) data-sources are generated. (a) shows the generated heat-map; (b) shows the generated normal-map and (c) shows the velocity-field computed over $\partial\Omega$. In (d), the data-sources are transferred to the object of interest, which is detailed in (e), (f) and (g).

From this transferred data, we compute material distributions implementing a three-step strategy. The contribution of each external data-source is shown in Figure 26, where the first material is depicted as opaque, and the second as transparent. The heat map provides coarse initial guidance for the grading of material distributions, such that areas with high temperature use the first, transparent material while regions with low temperature use the second, opaque material. Afterwards, the velocity field perturbs material voxels according to the above described advection process. The normal field, in turn, aligns the flow and confines the emerging patterns to the contour of the face as well as its surrounding boundary, by projecting the velocity to the gradient of $\mathrm{d}_{\partial\Omega}$. As described above, by providing data-sources *during* the generation of each slice, this processes can be carried out *per slice*. This allows the material distribution to be computed at the resolution of the printer without requiring

significant computational overhead, and, as such, high spatial complexity in the patterns generated can be achieved.

The resulting object was produced on a Stratasys Objet 500 Connex 3 printer[53] with opaque VeroWhite (RGD835) and optically transparent VeroClear (RGD810) materials, and is shown in Figure 26. Throughout the entire design process, the sequential design iterations were all reviewed using standard volumetric visualization methods[54], as shown in Figure 27.

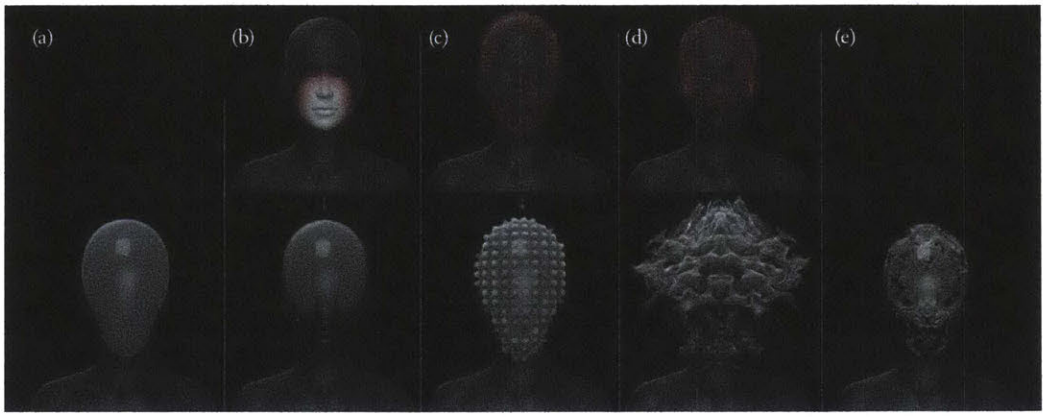


*Figure 26 – Volumetric visualization of the contribution of each original data-source for the generation of internal material distributions.* Grey areas represent VeroWhite (RGD835) material and transparent areas represent VeroClear (RGD810) material. For clarification purposes, only the distribution of the rigid white material in the final 3D printed prototype is emphasized. (a) Initial material distribution; (b) Contribution of the heat-map as an indicator for material grading; (c) Contribution of the normal-map to align advection with the geometry of the face, here visually empathized by a displacement; (d) Contribution of the velocity field to perturb material-distribution; (e) Final combined effects in a pre-visualization.

While the case study in this example is design driven, the above described methods can be employed for many different applications. For example, this method can be used for direct visualization of data sets, such as z-stacks acquired from biomedical imaging studies, physical visualization of multi-field computational simulations, or visualization of point-clouds acquired from geospatial sources. Furthermore, these external data sets could be functionalized and used for the evaluation of heterogeneous material modeling methods. This could potentially allow for the production of materially optimized prosthetic sockets[42], in finite element analysis for material optimization, or even materially adapted habitats for microbial assemblages.

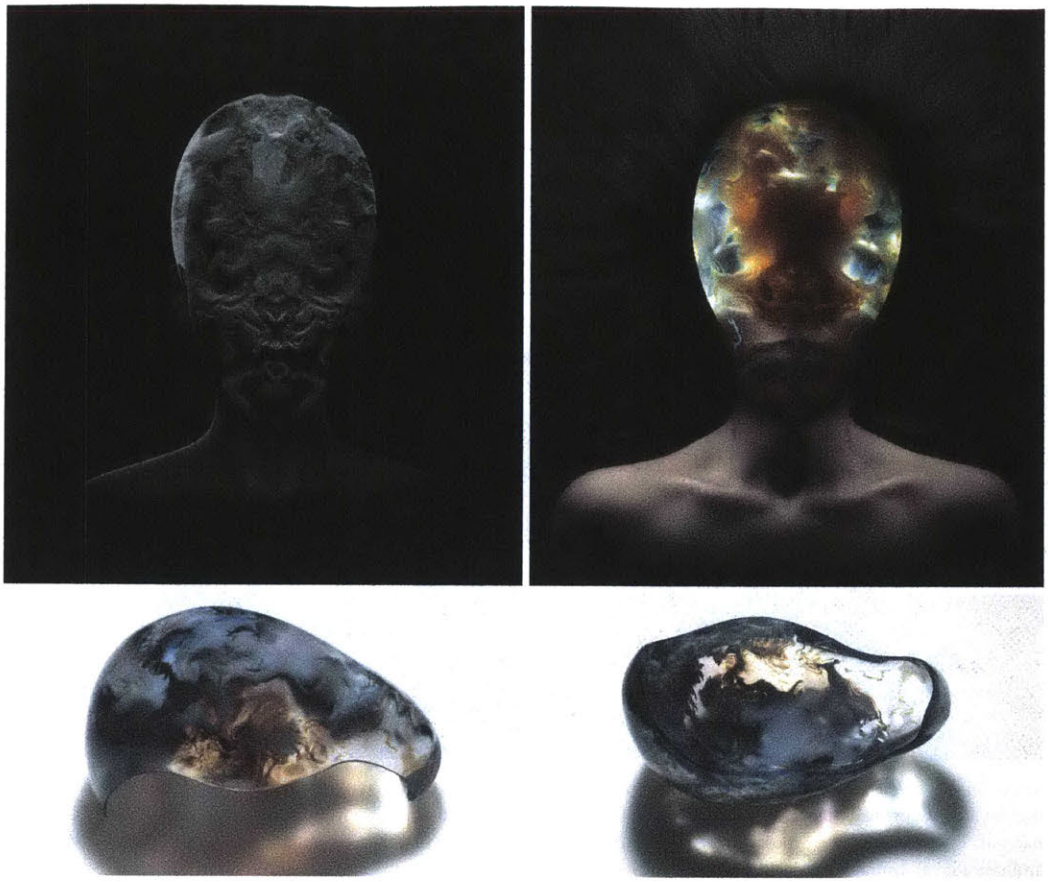

*Figure 27* – Lazarus, *2016. Designed by Neri Oxman and The Mediated Matter Group in collaboration with Stratasys.* Using a functional advection workflow, the resulting 3D printed mask - printed from rigid white and transparent materials - is shown alongside its corresponding 3D rendering. Photos: Yoram Reshef, courtesy of Mediated Matter.

## Conclusion

The DdMM computational approach and its related case study presented herein, serve to demonstrate a data driven material modeling work-flow, combining slice processing and material distribution generation with high-resolution bitmap-based 3D printing. It provides a powerful tool for the generation of complex 3D objects with volumetric heterogeneous material distributions.

In addition to capturing, processing, generating and digitally fabricating complex volumetric material distributions shown herein, the DdMM computational approach and its related methods can contribute to the enablement of a wide array of applications including the production of high-resolution lens arrays, detailed surface topographies and lattice structures, as well as protocols associated with the retrieval of material properties from geometric representations. Such applications and related protocols could be produced with on slice-time methods at the native resolution of the

printer, without the need to design or generate additional geometrical content and as such with minimal memory overhead.

## Acknowledgments

The authors would like to thank Naomi Kaempfer, Director of Art, Fashion and Design at Stratasys, and team members - Gal Begun, Boris Belocon and Yoav Bressler - for their insights and dedication in producing *Lazarus*. The company's support has enabled the use of the Stratasys Objet 500 Connex3 color, multi-material 3D printer and Stratasys J750 seven material printer. The authors also wish to acknowledge Yoram Reshef for his photographs.

# Design of 3D Printable Functionally Graded Material Systems

Christoph Bader[1], Dominik Kolb[1], James C. Weaver[2] and Neri Oxman[1*].

*(in preparation)*

1. The Mediated Matter Group, Media Lab, Massachusetts Institute of Technology, Cambridge, MA 02139, USA
2. Wyss Institute for Biologically Inspired Engineering, Harvard University, Cambridge, MA 02138, USA.

## Abstract

Material systems in nature are fundamentally heterogeneous and thereby offer advantages such a functional optimization and response tunability. However to leverage such advantages in synthetic hybrid material systems designers and engineers alike have to think beyond geometry-driven linear CAD tools and consider implementing hybrid design workflows. Combining parametric geometric modeling, parametric volumetric modeling, high resolution material dithering, common design evaluation methods and mutli-material 3D printing we propose an integrated design workflow and explore associated design space of 3D printable functionally graded material systems. Specifically, we demonstrate how common material properties found in natural systems and employed in biomimetic designs—including color and opacity, stiffness, softness, shape memory, swellability, expansion, wettability and refractive index— can be seamlessly tuned, fabricated and leveraged in design applications. Thereby offering a hybrid design strategy to mimic natures hybrid systems. Finally, we demonstrate how the introduced concepts can be employed in a design context reinterpreting the collagen structures of tendon to bone attachments in *Rottlace*, a mask for the Icelandic singer Björk worn for a performance at the Tokyo Miraikan Museum.

## Introduction

A vast variety of material structures in nature rely on continuous material property gradients within an object to enable and enhance multi-functional behavior. Examples include gradients in stiffness of tendon-to-bone attachments to alleviate stress concentrations at interfaces [35], refractive index gradients in lenses of aquatic animals to improve vision [36] and the differential swellability of plants to enable self-shaping [37]. The characteristics of such biological material systems, both fascinate and inspire designers operating across scales and disciplines. The dichotomy between biological and synthetic structures is embodied in the former frequently exhibiting multi-functionality, hierarchal organization, and adaptability [55]. Most importantly, biological structures are heterogeneous systems. These hybrid systems with different properties in the same structure can result in architectures whose properties are designated and optimized for specific purposes. Thus, nature-inspired synthetic material systems utilizing functionally graded materials have been developed and enable the reduction of interfacial failure and increase material tunability [56]. However, processing techniques to fabricate such objects are often either cumbersome or limited in the spatial material distributions and geometric complexity that can be achieved. Multi-material 3D printing circumnavigates this, by allowing the free placement of multiple materials within a single part. These technologies enable the digital fabrication of geometrically complex and materially heterogeneous objects with high spatial resolution in manufacturing. Yet, such advancements challenge designers, architects and engineers alike, to move beyond shells designed with pre-determined shape, and material composition; and to consider an expanded design space encompassing internal material compositions. However, current workflows, do not typically take these recent advancements into consideration, thereby missing out on significant design opportunities that lie at the intersection of digital modeling and fabrication. Thus to mimic natures hybrid system we propose a hybrid design system.

## Extensions to the Data-Driven Design Framework

The application and design of functionally graded materials is largely limited due to challenges associated with modeling, characterization, evaluation and fabrication of heterogeneous material objects. Here we outline an integrated framework leveraging multi-material 3D printing as a fabrication technology and accounting for these challenges. Multi-material 3D printers [57] can employ the placement of individual build materials to construct 3D objects through a droplet deposition printing process by sequentially jetting layers of said droplets onto a build platform.

Material compositions can be controlled at the droplet level by defining—for each depositable material with distinct properties—a set of layers in a raster-format at the native depositing resolution of the printer. This set of layers, in turn, defines the material "identity" of the individual droplets and their spatial placement in space. As nearby droplets mix, this spatial placement determines the intermediate material characteristics the resulting object will have in the specified regions. The layers can for example be given as binary material representations in a raster file format, one set for each deposited material the 3D-printer provides, defining where a droplet should be placed or not. This droplet deposition description in form of a set of layers is then used by the printer to fabricate objects with heterogeneous and continuously varying material properties. This approach is often described as bitmap-based printing [58] or voxel-printing [59]. Models shown herein where printed on Stratasys Objet500 Connex multi-material 3D printing system and materials used are stated in their respective section.

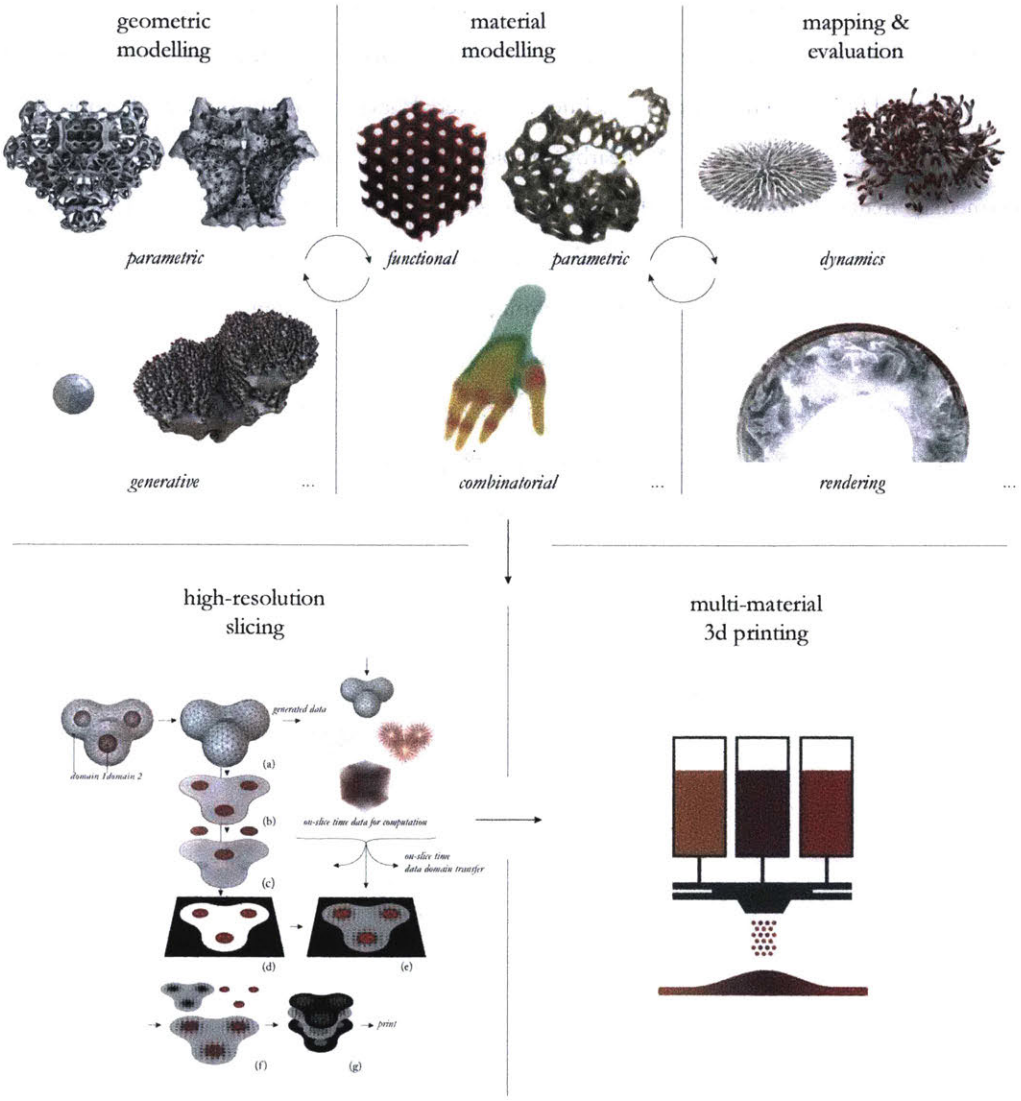


*Figure 28 – Proposed design framework.* We propose to combine parametric geometric modeling and parametric volumetric modeling into one integrated modeling workflow. Volumetric material information can be mapped to functional material properties which then can be evaluated through design evaluation methods such as simulation of the dynamics of an actuation systems or visualization of internal opacity gradients through volumetric-rendering. Geometry and material information can be combined in a slicing workflow and fabricated through multi-material 3D printing.

The proposed framework contains five parts as shown in Figure 28. First, parametric geometric and volumetric modeling are implemented to model geometry in conjunction with material distributions. Parametric geometric modelling refers to the ability to describe the generation of a geometric object through a set of generators and operators and the control of this generation description through parameters. This is advantageous as a change in parameters, results in re-evaluation of the generation description and a new geometric object according to parameter specification. Volumetric parametric modelling is similar to this as the generation of a volumetric region and associated property fields in

space are described by a network of operators and generators controlled through a set of parameters. The volumetric descriptions can be given in form of a voxel representation describing material distributions as a set of material vectors of mixing ratios and additional data organized in a spatial data structure. This material vector, associated additional data and the property-to-material lookup tables (described below) are then used to compute the final multi-material droplet deposition instruction at the resolution of the printer. Parametric geometric and parametric volumetric modelling methods are combined by using geometric properties as parameters in the volumetric modelling workflow and vice versa.

Material distributions are mapped to experimentally characterized material properties such as opacity, stiffness, or others as discussed below. This mapping is enabled through two processes. First, the characterization of material mixing ratios through which associated property-to-material lookup tables can be generated. Secondly, the continuous material tunability through high resolution material dithering which allows to use the property-to-material lookup tables to map a desired material behavior to volumetric descriptions of material mixing ratios.

The material tunability and the volumetric material description allow to perform design evaluation of material behaviors by either rendering or simulation. This can be in the form of the simulation of the non-linear dynamics of an actuation system or the evaluation of optical properties through volumetric rendering. Significantly, geometry and material representations are kept distinct and are only combined if necessary for example in the simulation or slicing process to achieve scalability. Geometry, volumetric material descriptions, and property-to-material look up tables are then processed through a slicing process to generate the above described layer based instructions for the multi-material fabrication system. This slicing process uses the gathered data-sets to perform additional computational processes during slice time to achieve high-resolution composite generation. All of these contributing towards a *holistic* design approach for programmable materiality. In the following we showcase and explore this emergent design space.

# Applications – Exploring the Design Space

## *3D printable opacity gradients*

Mimicking nature starts with the observable. Thus control over shape and color are essential elements in the replication of nature's rich visual expressions. We can use the high-resolution spatial droplet descriptions as described above to achieve optical transparency gradients and color gradients by using transparent VeroClear (RGD810) and opaque VeroWhitePlus (RGD835) resins (Figure 29).

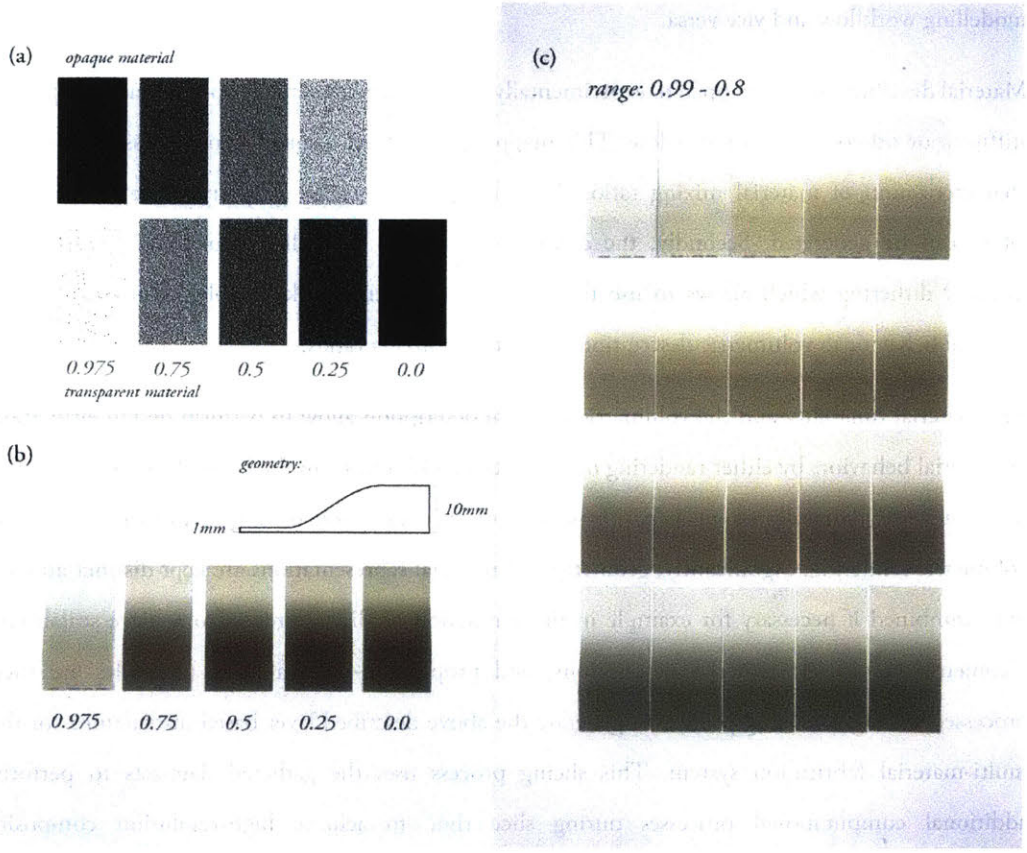


*Figure 29 – Examples of opacity gradients.* (a) Zoomed in section of one layer from the material dithering process, separating transparent and opaque material droplets with various material mixing ratios. This raster-description instructs the printer to deposit transparent and opaque material droplets, whereby white pixels in the bitmap result in physical material droplets on the 3D printer's built tray. White pixel in the upper row describes the opaque material distribution, while the white pixels in the lower row describe the transparent material distribution. In combination, the two material descriptions result in an opacity gradient. The corresponding objects are shown in (b). Here, it is apparent that visual characteristics are not linearly related to material mixing ratios. In (c) we show that perceivably separable differences accumulate at mixing ratios of high clear material content. Small changes in additionally deposited opaque material droplets can have a drastic change in visual appearance and turn the transparent material opaque.

This material feature space enables two key characteristics interesting for the translation of visual characteristics from data sets to physical visualization:

1) Visual gradients: Close by placed droplets diffuse and aggregate before UV-curing giving them a chance to mix. By varying spatial and local density of droplets belonging to different materials, visual gradients in color and opacity can be achieved
2) Preservation of detail: Very detailed structures can be fabricated inside clear enclosings and very small features-sizes can still be reliably perceived

This allows for a direct digital manufacturing approach to physical data-visualization through voxel-printing. Generally, first for a given data-set an approximating hull is generated, this can be an accurate boundary representation, a convex hull or a simple bounding box. This hull determines together with the resolution of the 3D printer the number of layers the printer needs in order to fabricate the representation. For each layer internal material information is then computed from the given data set. This per layer material information can then further be materially-dithered [60] into material droplet deposition descriptions form which the 3D printer then determines where to deposits which material. By this high-resolution deposition of different materials during print time, visual gradients can be achieved. Multi-material 3D printing with photopolymeric materials, as described above, enables the use of several materials at once. This in turn allows the use of dedicated Cyan, Magenta, Yellow, Black, White and Transparent resins to create full color models. The ability to fabricate objects with transparent shells and multiple colors enables the physical visualization of compact n-manifold ($n \leq 3$) data sets such as unconnected point cloud data, lines and curves, open surfaces and volumetric data by directly rasterizing said data to the slices. Therefore this allows to fabricate a plethora of representations commonly utilized for data-visualization in scientific applications and thereby it becomes possible to obliterate the digital/material boarder by providing a unified bridge between the digital on-screen and the physical visualization. This again allows to replicate volumetric biological material structures through for example density scans obtained from magnetic resonance imaging (MRI) or image stacks obtain from microscopic imaging. An example of this process is schematically illustrated in Figure 30 and examples are given in Figure 31.

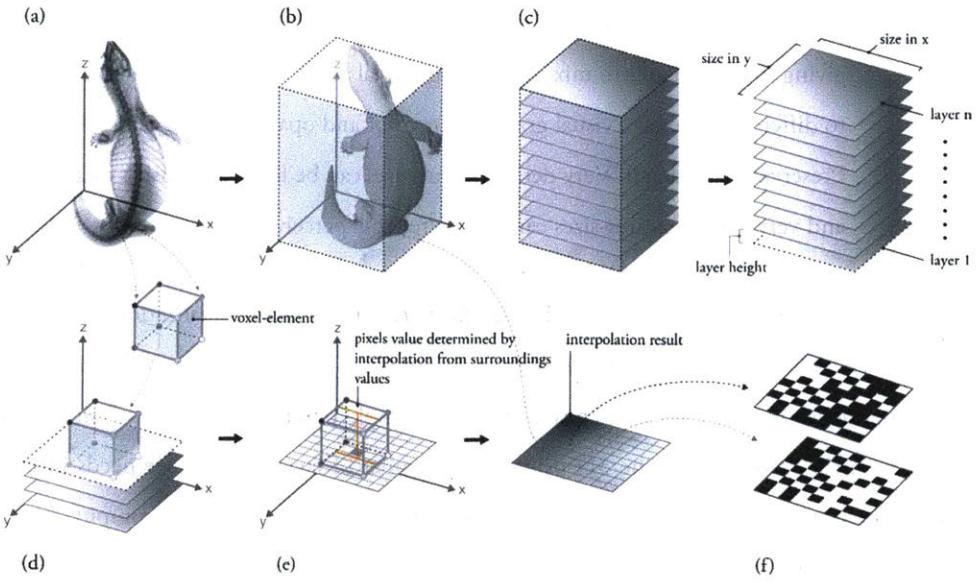


*Figure 30 – Example of 3D printing volumetric datasets.* (a) Shows the initial volumetric data set to be 3D printed. (b) Determination of an outer enclosing for the volumetric data set. (c) From this, the number and dimensions of layers is obtained. (d) Each layer is processed in parallel. Here one particular voxel intersecting a layer is shown. (e) For each pixel in a layer, its position information is used to sample the volume to give the final pixels' material data. (f) The material information is dithered into binary material deposition descriptions. Here white denotes deposition of material at the pixels' location in the build space while black denotes no deposition.

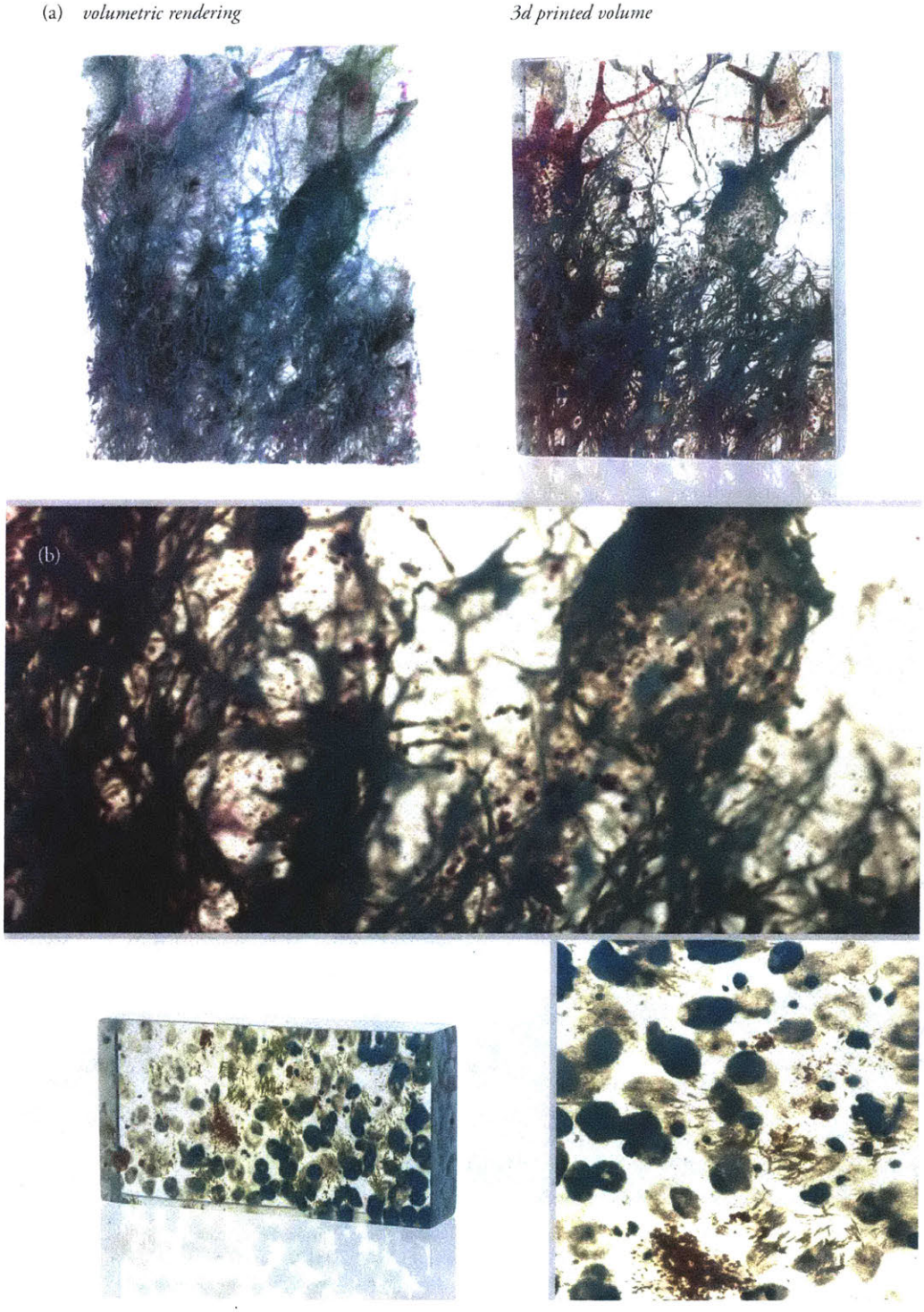


*Figure 31 – Example of a biological tissue datasets directly fabricated through the voxel printing process.* Here, (a) shows the comparison of a volumetric rendering preview to the actual 3D printed object and (b) shows a close up detailing fine features representative of the level of material deposition control achieved through our method.

### *3D printable modulus gradients*

Equivalently to the opacity gradients above, continuous gradients in modulus can be achieved. In living systems such gradients between tissues with highly disparate mechanical properties are needed to reduce high interfacial stresses in the joining of dissimilar materials [61]. Remarkably robust interfaces can be achieved between mechanically mismatched tissues through material property gradients. Such mechanical gradients are exhibited, by example, in human teeth [62] and tendon to bone attachments, in the exoskeleton of crustaceans [63] and in the beak of squids [64]. Through multi-material 3D printing and the previously introduced framework, such continuous gradients in stiffness within a modulus range from 1MPa to 1GPa can be fabricate by leveraging flexible TangoBlackPlus (FLX980) or Agilus30 Black (FLX985) materials and rigid materials such as VeroClear (RGD 810). Here, parametric material distributions—as shown in Figure 32(a)—are mapped to soft and stiff materials and allow to fabricate intricate geometries with complex material logic (Figure 32(b)).

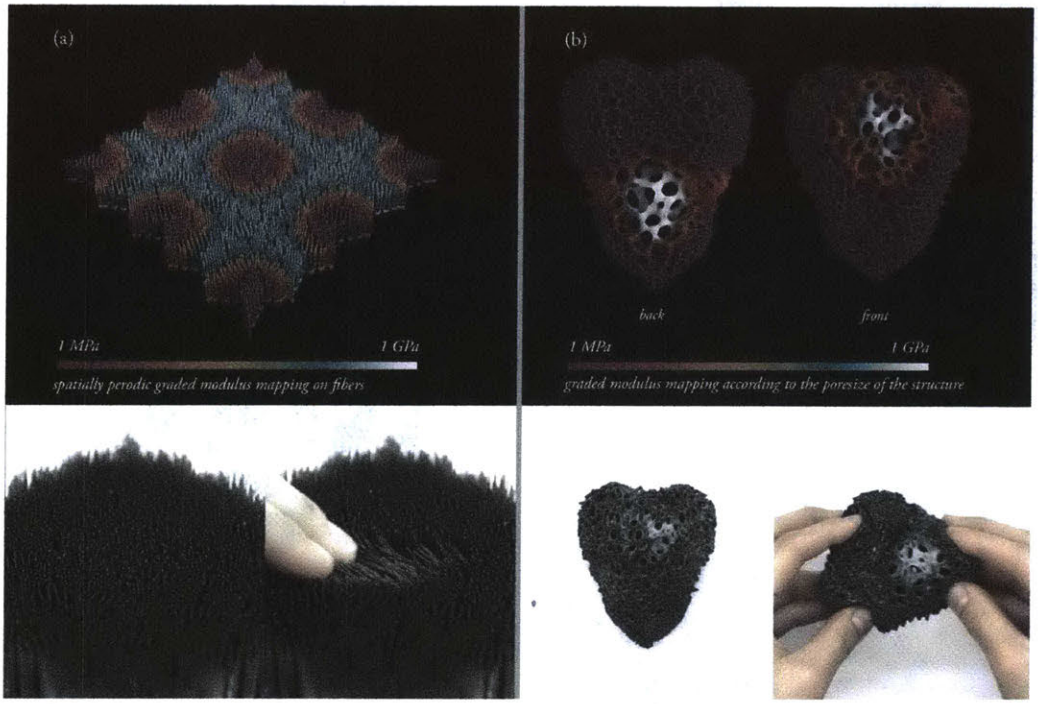


*Figure 32 – Examples of objects with gradients in elastic modulus.* (a) Shows a 3D printed part made out of 1mm thick fibers fabricated using flexible TangoBlackPlus (FLX980) and rigid VeroClear (RGD810). Parametric and continuous material distributions between stiff and flexible are computed independent from geometry and in this case are given by a 2 dimensional $C^{\infty}$ periodic function into the material space resulting in flexible fibers in a dot like pattern and rigid fibers elsewhere. (b) Shows a porous structure with modulus gradients from 1 MPa to 1 GPa parameterized through the geometry according to the pore size of the sponge like structure.

*3D printable shape memory gradients*

The introduced framework can be utilized to design and fabricate objects with spatially gradable stimulus response. Similar 3D-printed systems have been proposed by [65] and [66] however, in the first case material tuneability was not achieved and the degree of shape-change was largely guided by geometry; in the second case no continuous material transitions in a single object could be achieved by virtue of the fabrication method used.

Stimulus response is a basic property of living systems. A prominent example includes the humidity-driven self-shaping ability of plant systems such as pinecones and orchid tree seedpods [37]. Synthetic stimuli-responsive materials embody a large range of applications; spanning biomedical devices, drug delivery systems and self-healing composites [67]. One specific class of stimuli-responsive materials are shape-memory materials [68]. Objects made out of such materials exhibit the ability to memorize macroscopic shape often through a sequence of stimulus enabled programming, shape memorization, and shape recovery initiated again by an external stimulus. Often this process is driven by a thermo mechanical cycle and includes, first exciding the glass transition or melting temperature ($t_g$) of the material, secondly deformation as programming step, thirdly cooling to store a temporary but fixed shape, and finally heating to restore the permanent shape. This process is shown schematically in Figure 33(a). The ability of a material to store shape is often specified by its shape fixing ratio $R_f = \frac{\varepsilon_u(N)-\varepsilon_p(N-1)}{\varepsilon_l(N)-\varepsilon_p(N-1)}$, where $\varepsilon_u$ is the strain after unloading, $\varepsilon_l$ is the strain under load, and $\varepsilon_p$ is the permanent strain, all at the Nth iteration of the cycle. Here, we can use the aforementioned framework, and the use of two base resins (RGD810 and FLX 980) to design objects with gradable shape fixing ratio, thereby controlling how much an object remembers the induced shape (Figure 33 (b) & (c)).

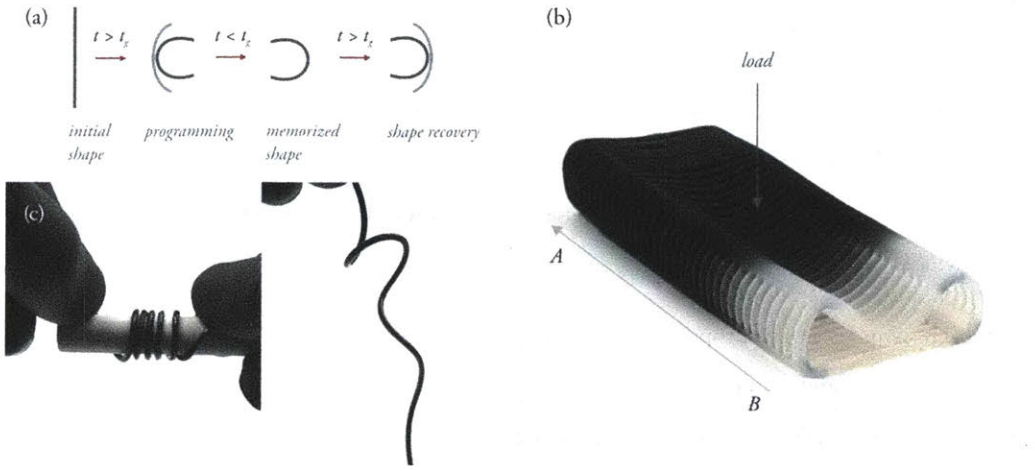


*Figure 33 – Graded shape memory objects.* (a) The lifecycle of a thermally programmable shape memory polymer. First the initial configuration is heated up beyond the glass transition temperature. In this state it is deformed, fixed and cooled down to memorize a specific shape (programming). Finally, the initial shape can be recovered by exceeding the glass transition temperature again. (b) Additively manufactured object with a continuous gradient from material A (FLX 980) to material B (RGD810) exhibiting a gradient in shape fixing ratio after the previously described programming process. Here a cylindrical metal rod was applied as a load, deforming the object. Another example of a shape fixing ratio gradient of a cylindrical wire is given in (c). Here, material A and B are at opposing longitudinal ends of the wire with a continuous linear gradient between both. The wire is coiled around a rigid cylinder in the programming phase, then cooled down and subsequently unwound showcasing a smooth transition from a coiled fixed shape to the initial linear shape according to the material gradient.

### *3D printable expansion gradients*

Another stimulus response can be achieved by materials which expand through swelling induced by the environmental conditions they are exposed to. Spatial differences in swellability and expansion can then cause macroscopic shape change, resulting in motions such as bending, twisting or bulging [69]. This induced shape change is essential in the life-cycle of plants from the dispersal of seeds[70], over the climbing movement of vines, the dynamic rotational arrangements of leaflets towards the sun and for the survival of carnivorous plants [71], to the actuation of dead tissues in a controlled manner by changes in external conditions [72]. Here, we leverage a material system of three base materials, and gradients between each, responding differently to similar environmental conditions. TangoBlackPlus (FLX 980) expands in isopropyl alcohol (IPA), but not in water, Support (SUP705) will expand in water but not in IPA (Figure 6(a)), while VeroClear (RGD810) does not expand in either of these substances. All three materials can be combined in a single object allowing graded stimulus response based on concentrations of previously mentioned materials and liquids. Here, several advantages of aforementioned framework are showcased in Figure 34. First, generative design can be utilized to design shapes, which contain geometric information to guide material modeling methods. Secondly, parametric volumetric modeling can be utilized to infer volumetric material descriptions during slicing which allows the decoupling of geometry and material behavior partially

or fully (Figure 34(c), (d) & (e)). Thirdly, forward design evaluation by finite element expansion simulations enabled by characterization of material behavior can be used to explore the given design space (Figure 34(c), (d) & (e)).

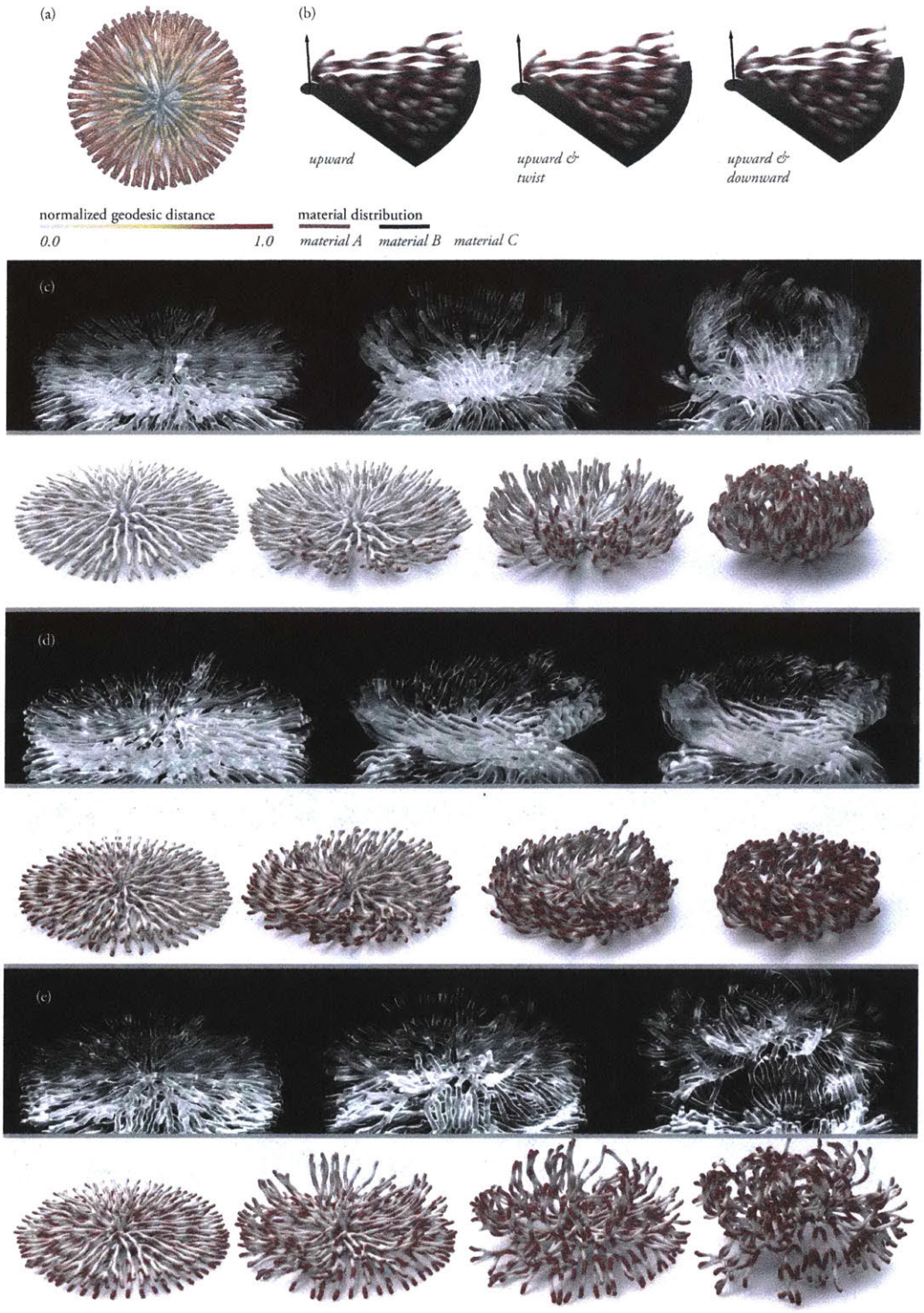

*Figure 34 – Designing objects with spatially tunable expansion.* (a) First a shape is geometrically grown [73] and a geodesic distance parameterization from its source point is generate by the growth process. (b) The geometric shape and its volumetric parameterization is then used to model material distributions inside the object. Material A is the in IPA expanding TangoBlackPlus (FLX 980), material B is the flexible in water expanding Support (SUP705) and material C is the rigid VeroClear (RGD810). Here, three different distributions are computed for upward curling, twisting and upward and downward movements. This results in three objects with the same geometry but different material distributions and therefore three different behaviors solely varied by the materiality of the objects as shown in (c), (d) and (e). The objects behavior is previsualized by simulating the expansion of material A, B and C using model-reduced finite element methods with the assigned expansion behaviors according to the parameterized volumes (c), (d) and (e) lower parts respectively. The objects are then fabricated and tested showcasing the desired behavior (c), (d) and (e) upper parts.

### *3D printable hydrophilicity gradients*

In nature we find numerous structures with graded features enabling controllable hydrophilicity or wetting. Water transport direction in wetted spider silk [74], directional liquid adhesion of butterfly wings [75], hydrophobic patterns the back of a beetle to allow fog or dew collection [76] or the well-known ultra-hydrophobic water repellent lotus leaves are only a few examples [77]. Similar material architectures can be created by the use of multi-material 3D printing in combination with the introduced framework. Here, we can use VeroClear (RGD810) and Support (SUP705) to fabricate continuous gradients of hydrophilicity shown in Figure 35.

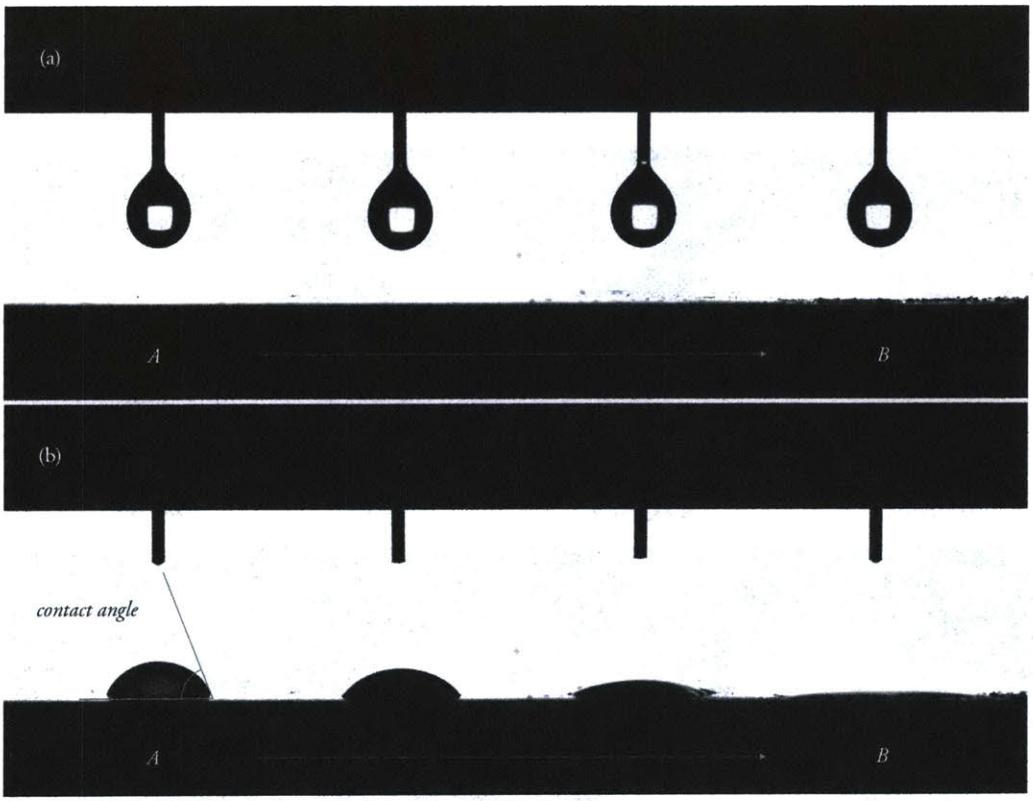


*Figure 35 – Wettability gradients.* (a) Here the contact angle of different 3D printed material ratios between material A (VeroClear RGD810) and material B (Support SUP705) is shown. The apparent contact angle is the angle between the air liquid interface of a droplet placed on the surface to the tangent plane of said surface. (b) This angle characterizes the wettability or hydrophilicity/hydrophobicity of a surface, where low angles indicate higher wettability/hydrophilicity. Here material A

shows a medium wettability while material B exhibits almost perfect wetting, with tunable intermediated contact angles shown between A and B.

### *3D printable refractive index gradients*

Gradients in refractive index can be found in several aquatic animals such as box jellyfish [78] and squids [79] to improve vision. Here, grading prevents spherical aberration through the direction of beams entering different regions of the lens onto the retina. However, such gradients can also be observed in the air-material interface of the wings of hawkmoths [80]. For the production of their synthetic analogs, gradients in refractive index are achieved by using clear resins with different optical properties. Specifically, the transparent VeroClear (RGD810) and the quasi-clear TangoPlus (FLX 930) have different refractive indices. Yet, when printing with the flexible TangoPlus (FLX 930), due to the need for a surrounding support material during printing, the flexible material will be partially roughened and not be clear. By printing TangoPlus (FLX 930) inside a VeroClear (RGD810) shell and modeling internal gradations through above described volumetric material modeling methods we can fabricate objects with internal refractive index gradients.

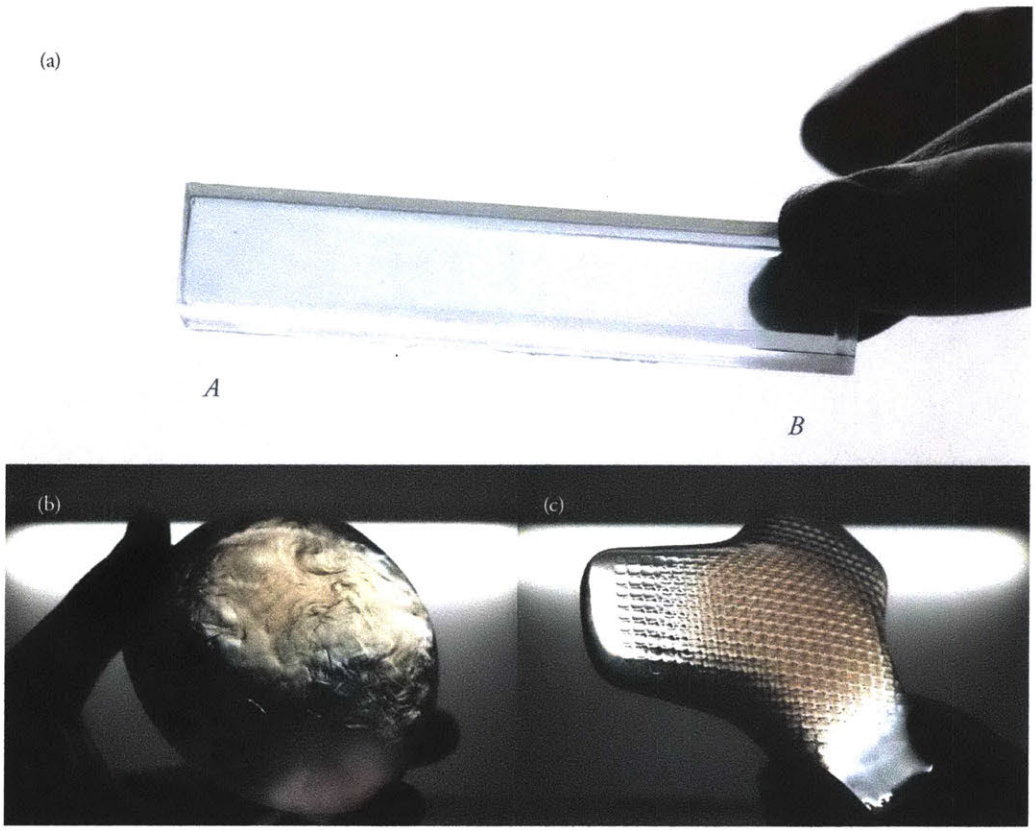


*Figure 36 – Examples of objects with refractive index gradients.* (a) Shows a VeroClear (RGD810) block with a gradient from Material A (VeroClear) to Material B (TangoPlus) left to right inside of it. (b)&(c) show more complex optical gradients with intricate material distributions allowing complex graded refractive index effects (b) and gradients in refractive index and opacity (c).

## Rottlace, a Mask for Björk

As an application of the principles introduced here we showcase *Rottlace* as part of a family of masks designed for Icelandic singer-songwriter Björk (Figure 37). The design is informed by the geometrical and material logic that underlie the human musculoskeletal system. As in the human body—where continuous, collagenous elements alter their mechanical properties as a function of the tension they exert or endure—each mask is designed as a synthetic 'whole without parts'. Inspired by complex structure of muscles, connective tissues, tendons, and ligaments and conceived as 'muscle textile,' the masks are bundled, multi-material structures, providing formal and structural integrity, as well as movement, to the face and neck. *Rottlace* is printed as a single, multi-functional material system, composed of rigid materials (VeroWhite) combined with nano-enhanced, elastomeric structures (Agilus). The intricate fibrous tissue is made of soft and flexible materials designed to accommodate facial movement. The materials' durometer varies as a function of the structural type they are intended to provide. Continuous property transitions—ranging from stiff bone-like structures to semi-flexible ligament-like structures, to flexible fiber-based connective tissue structures—are computationally generated and digitally fabricated. Specifically, the fibrous tissue is computationally generated as modified principal curvature directions of Björk's facial scan—obtained as point cloud data—while the bony-like tissue emerges as support structure at points of high divergence from the principal curvature field. While bone-like locations are geometrically informed, their material composition is continuously graded—from stiff to flexible, and from opaque to transparent—as a function of geodesic distances from the bones given by the face-scan. Here we use the computational framework to enable micron scale control of 3D printable material placement over a highly complex domain. This enables the design and 3D printing of complex, large-scale objects with continuous variations of modulus and transparency, within a single build. Properties, such as structure to material composition, of the mask include a number of length-scales, informing their mechanical properties and behavior: (1) on the centimeter scale, the 3D printed musculoskeleton is designed to allow for flexible movement, while providing integrity to, and support of, its overall form; (2) on the millimeter scale, the fusing and parting of fibers with varying material compositions enables the overall structure to be self-supporting; and (3) on the micron scale, material droplets are placed, diffused, and spatially aggregated to provide continuous material variation—just like its biological counterpart—within a single 'muscle-skin' object. *(This section is partially taken and adapted from* [81] *with permission from the authors)*


*Figure 37* – Rottlace, *2016.* (a) and (b) show Björk wearing *Rottlace* designed by Neri Oxman and The Mediated Matter Group, 3D printed in collaboration with Stratasys for her performance at the Tokyo Miraikan Museum, Photo: Santiago Felipe. (c) shows the modulus gradients from the stiff bone-like structures to the flexible fiber bundles.

# Conclusion

We have shown that a wide variety of hybrid systems found in nature, can be directly fabricated to nature mimetic entities by employing voxel-printing. By utilizing methods described herein we show that the barrier between the digital description of material behaviors and the physical reality can be obviated more easily. Therefore, the design with 3D printable functionally graded materials through an appropriate framework can open up a wide design space towards improved biomimetic design workflows. Enabled through computational design strategies such as parametric geometric, parametric volumetric modeling and design evaluation in combination with high-resolution slicing and multi-material 3D printing we point towards an integrated workflow encompassing means to work with geometric and material structures efficiently and creatively. Such design workflows will in the future enable designers to precisely mimic systems and mechanics in nature and inspire and improve the associated design embodiments.

# Vespers – Series 2

*"The custom of the death mask in the ancient world was believed to strengthen the spirit of the deceased and guard their soul from evil spirits on their way to the afterword. In this view, death is a conduit to a form of rebirth. The mythical notion that the soul can be guided from a state of death to a new state of life inspired the design of the masks in the second series. The second series explores the transition between life and death implying the progression of the death mask from a symbolic cultural relic (in the first series) to a functional biological interface (in the third series). It moves beyond the exterior surface and into the interior volume of the mask, employing a contemporaneous interpretation of the soul's journey.*

*The inner structures are entirely data driven and are designed to match the resolution of structures found in nature. Expressed through changes in formal and material heterogeneity—from discontinuous to smooth, from surface to volume, from discrete to continuous —this series conveys the notion of metamorphosis. Using spatial mapping algorithms, the culturally coded surface colorations and truncated geometries in the first series are transformed into colored, internal strands within transparent, smoothly curved volumes in the second. For example, the distribution of colors across the 'crown of thorns' mask in the first series becomes internal nerve axons in its mask in the second series.*

*In this series, it is the interplay of light that reveals these internal structures. Like spirits (from Latin spiritus, meaning "breath"), the internal structures reference the distribution of the wearers last breath." [2]*

*Figure 38* – Vespers. *Series 2 Mask 5. Bottom view.* Designed by Neri Oxman and members of The Mediated Matter Group for The New Ancient Collection curated and 3D printed by Stratasys, 2016. Photo: Yoram Reshef.

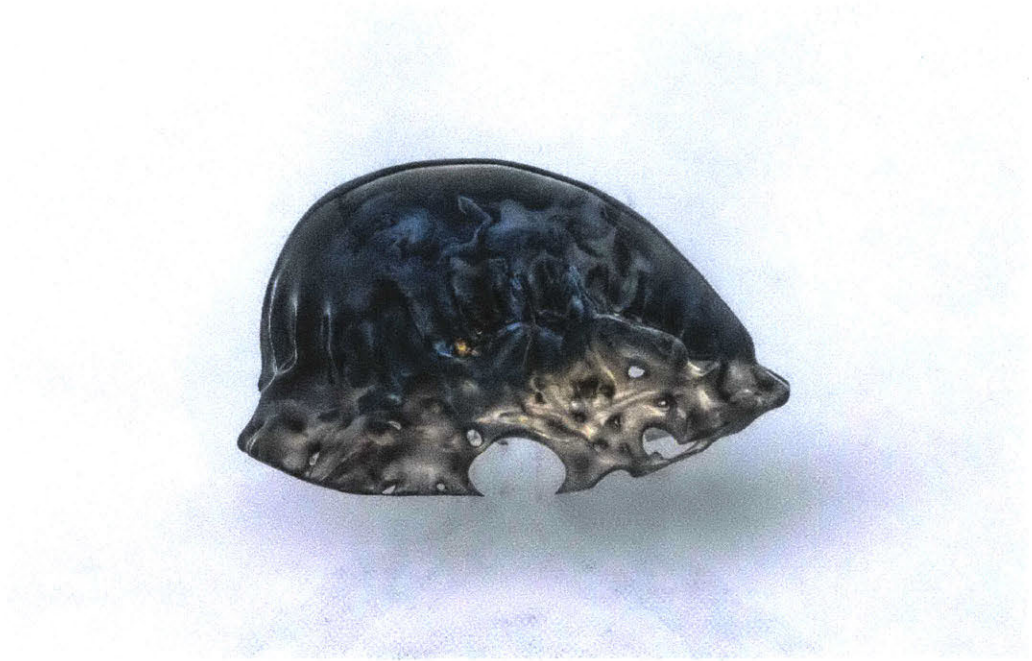

*Figure 39* – Vespers. *Series 2 Mask 2. Side view.* Designed by Neri Oxman and members of The Mediated Matter Group for The New Ancient Collection curated and 3D printed by Stratasys, 2016. Photo: Yoram Reshef.

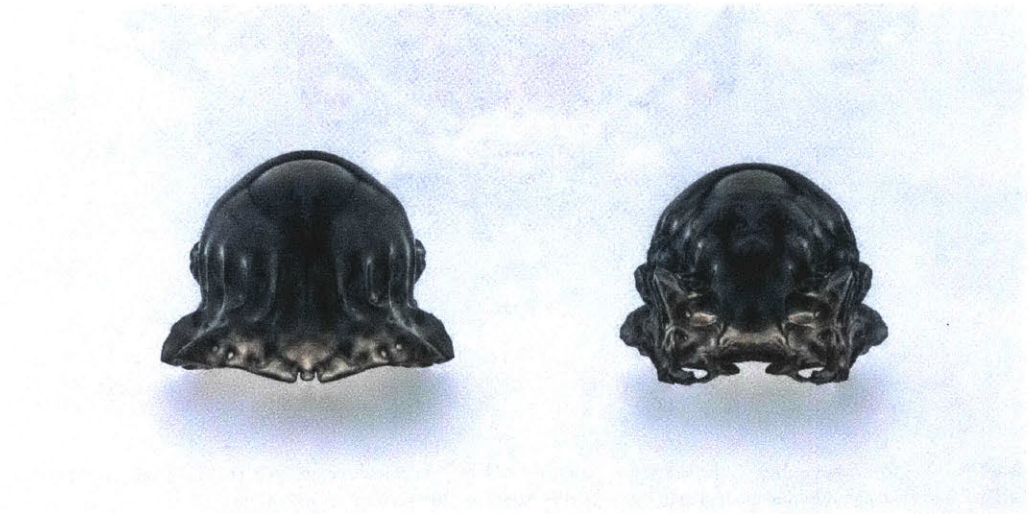

*Figure 40* – Vespers. *Series 2 Mask 2. Top and bottom view.* Designed by Neri Oxman and members of The Mediated Matter Group for The New Ancient Collection curated and 3D printed by Stratasys, 2016. Photo: Yoram Reshef.

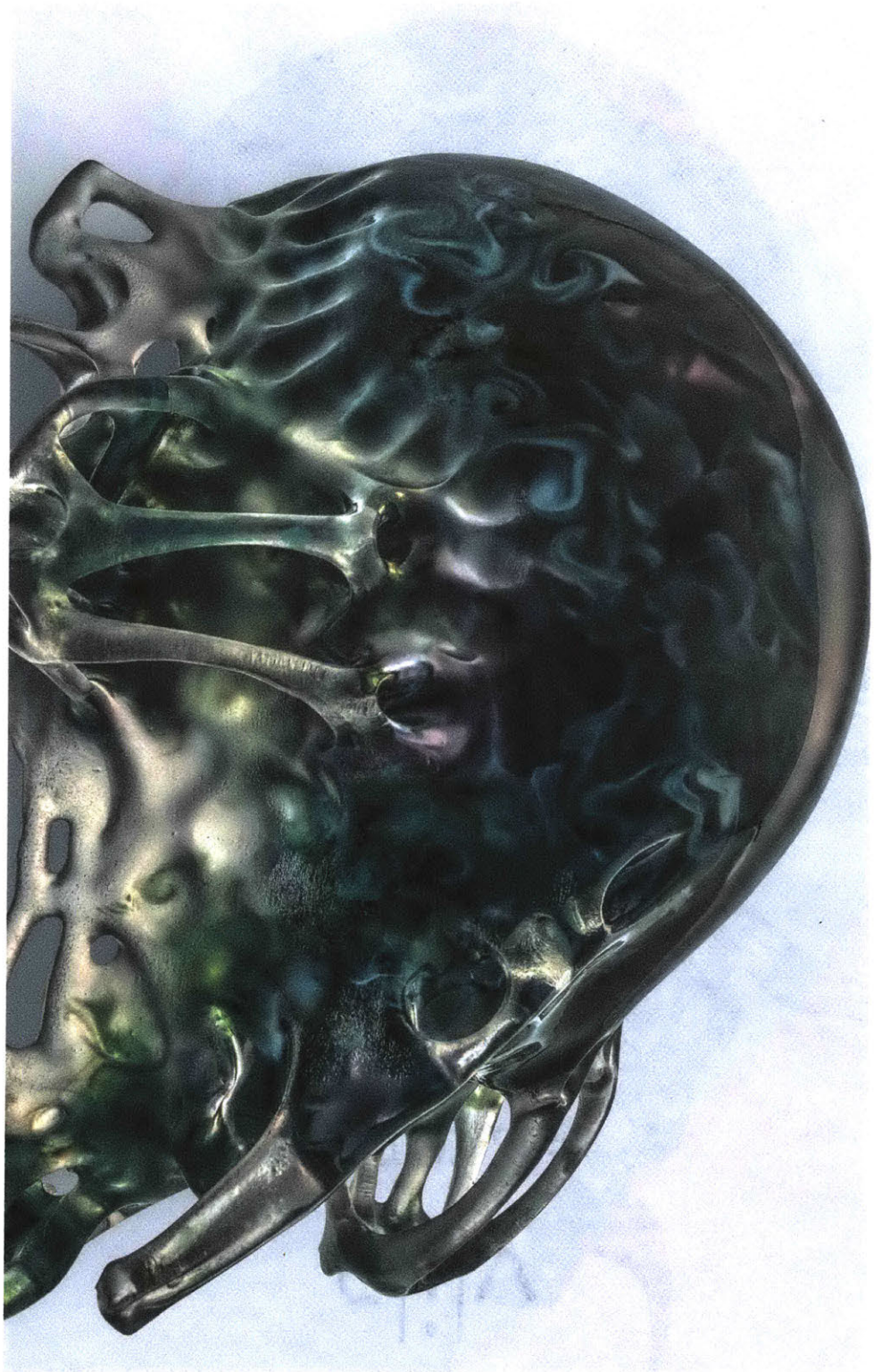

*Figure 41* – Vespers. *Series 2 Mask 3. Side view.* Designed by Neri Oxman and members of The Mediated Matter Group for The New Ancient Collection curated and 3D printed by Stratasys, 2016. Photo: Yoram Reshef.

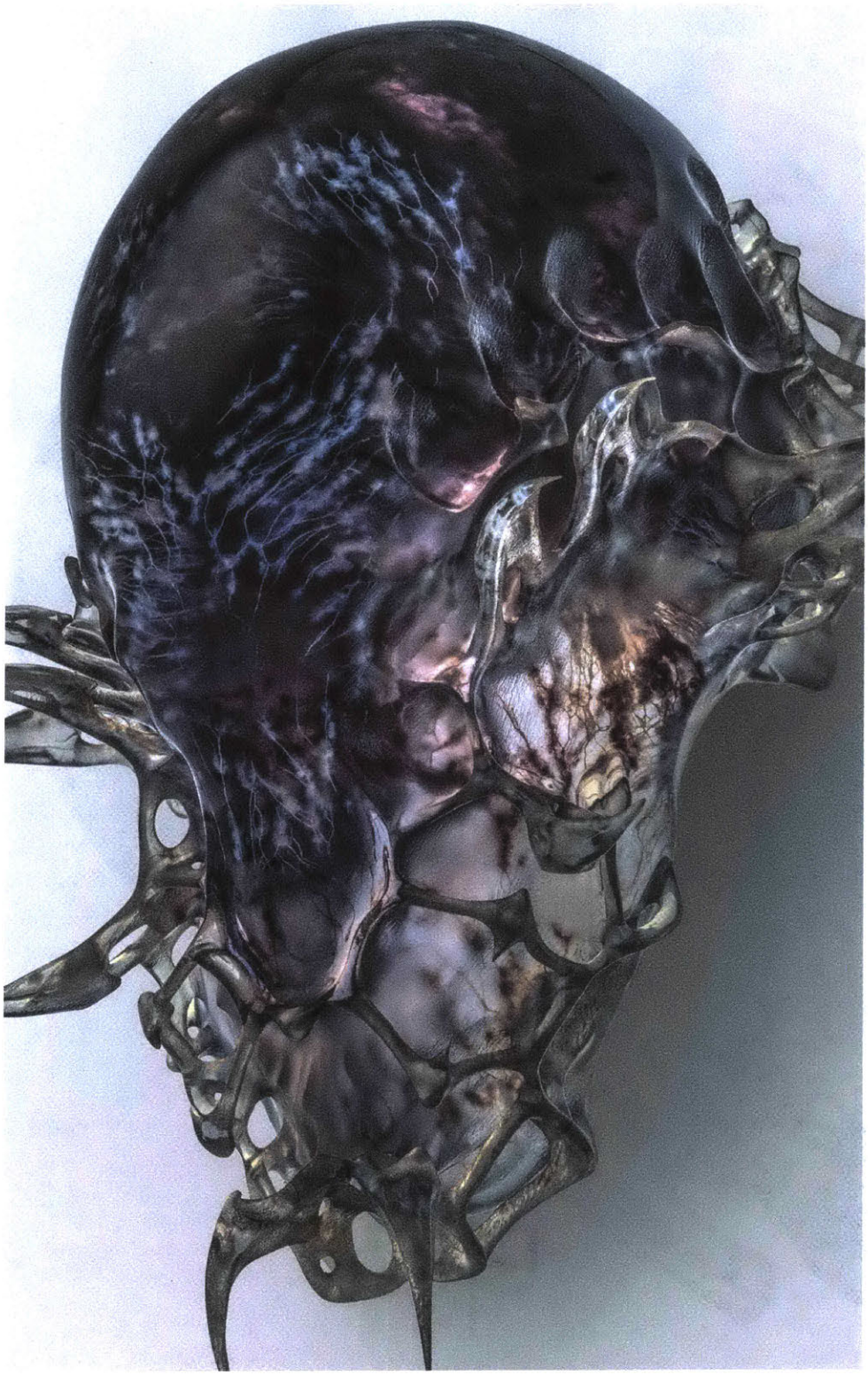

*Figure 42* – Vespers. *Series 2 Mask 3. Side view.* Designed by Neri Oxman and members of The Mediated Matter Group for The New Ancient Collection curated and 3D printed by Stratasys, 2016. Photo: Yoram Reshef.

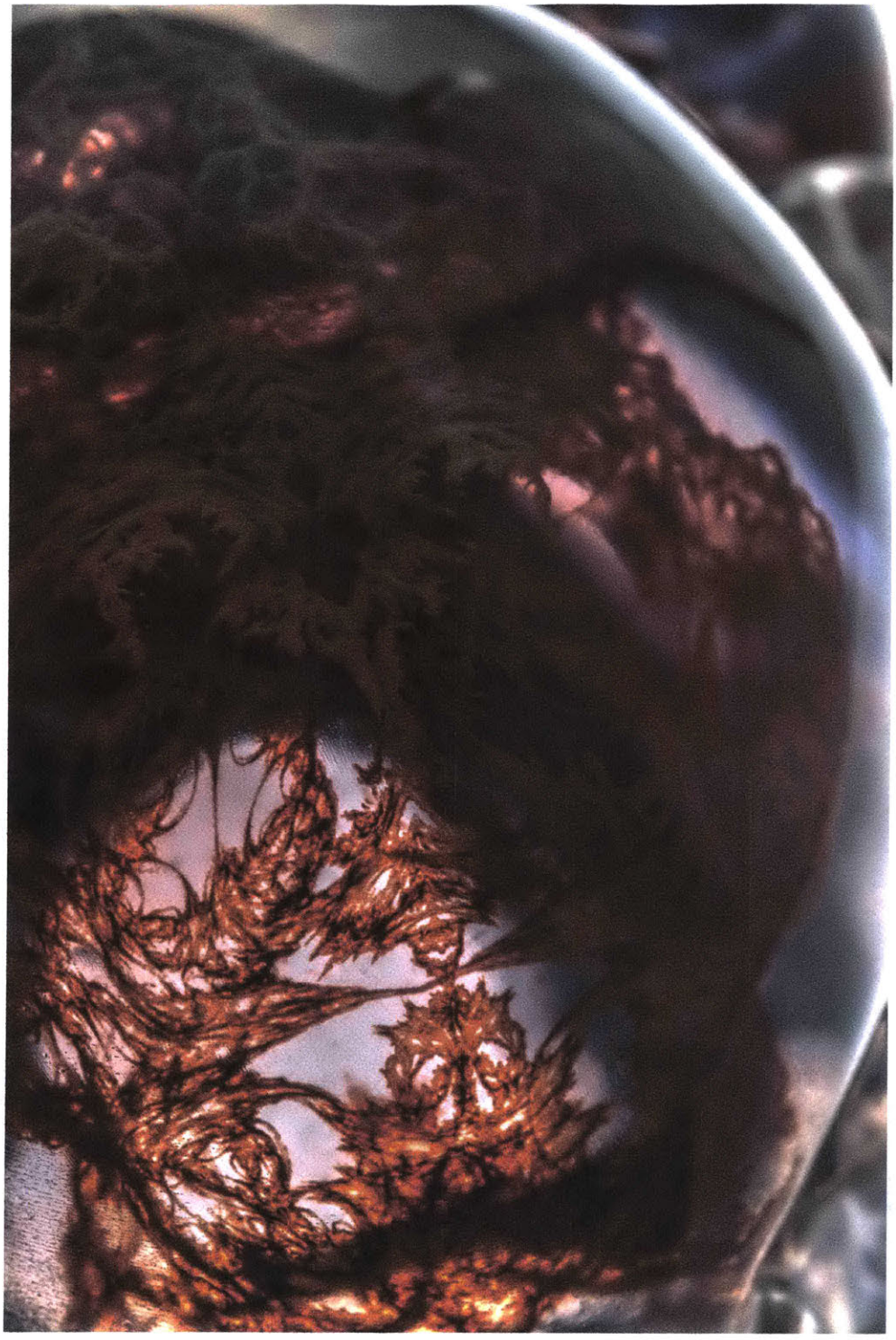

*Figure 43* – Vespers. *Series 2 Mask 5. Bottom view.* Designed by Neri Oxman and members of The Mediated Matter Group for The New Ancient Collection curated and 3D printed by Stratasys, 2016. Photo: Yoram Reshef.

*Figure 44* – Vespers. *Series 2 Mask 2. Back and front view.* Designed by Neri Oxman and members of The Mediated Matter Group for The New Ancient Collection curated and 3D printed by Stratasys, 2016. Photo: Yoram Reshef.

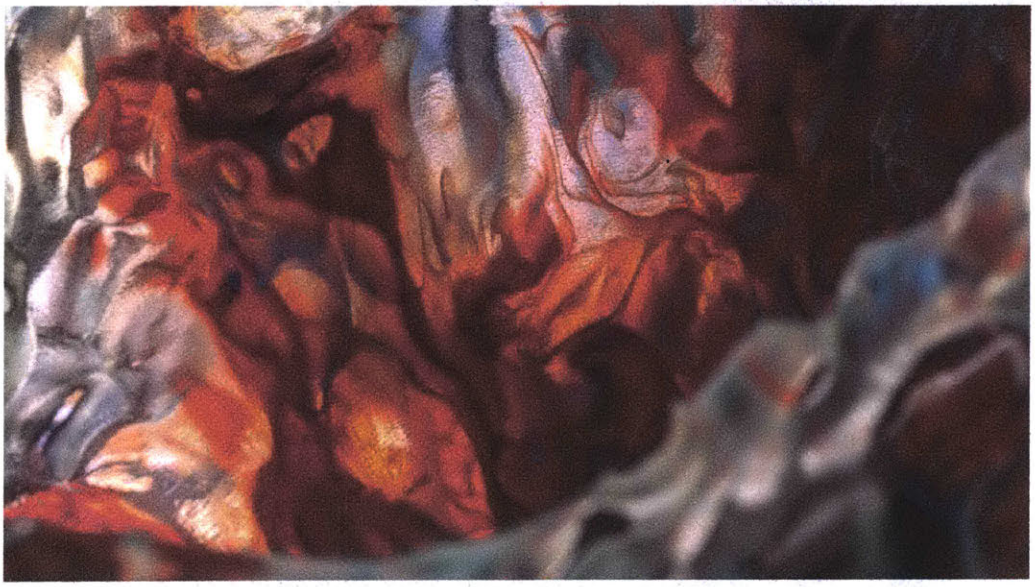

*Figure 45* – Vespers. *Series 2 Mask 2. Top and bottom view.* Designed by Neri Oxman and members of The Mediated Matter Group for The New Ancient Collection curated and 3D printed by Stratasys, 2016. Photo: Yoram Reshef.

*Figure 46* – Vespers. *Series 2 Mask 3. Front view.* Designed by Neri Oxman and members of The Mediated Matter Group for The New Ancient Collection curated and 3D printed by Stratasys, 2016. Photo: Yoram Reshef.

# Programmable Templating

While nature serves as inspiration and guidance for design and engineering, design by its virtue operates in a top down modus compared to the bottom-up processes found in nature. However, facilitating synergies between the designed and biological necessitates a shift towards a design-inspired nature, pointing to the need to be able to design both the synthetic and the biological and their relationship [82]. Here we demonstrate the intersection of a programmable material environment and programmable living entities mediated through computational design, and thereby constructing a 'synthetic ecology'.

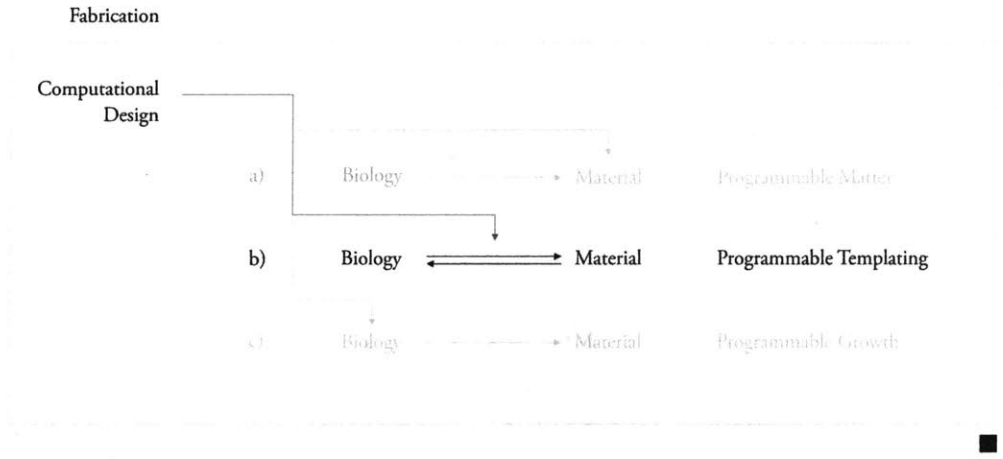


*Figure 47 – The programmable templating approach.* Utilizing computational design at the intersection of synthetic and biological systems.

We introduce a computational design environment for additive manufacturing of geometrically complex and materially heterogeneous fluidic channels. Using the framework as previously introduced in combination with a novel liquid support material, here a synthetic habitat is designed in the form of a wearable, *Mushtari*. While adapted to the human body, the wearable habitat is geometrically designed to potentially host a symbiotic co-culture of phototrophic and heterotrophic bacteria and materially designed with continuous opacity gradients to template the relationship between the two cultures.

Yet, a persisting challenge in this development is to derive a meaningful interaction between inert material fabrications and biologic function. A material can act as more than an environment in which inhabiting organisms grow, rather it can act as a spatial template to direct how these organisms behave. Engineered bacteria can be designed with promoter's sensitive to specific small molecules

allowing to activate the expression of a specified gene and thereby the production of a desired product. This chemical induction process is sensitive to the concentration gradients activating the production. Embedding small molecules into the 3D printable material, 3D printing a multi-material system with properties as previously shown, and growing bacteria on top of the 3D printed substrate, a relationship between material and organisms can be achieved through diffusion of the embedded chemical signal. Combining materials with and without small molecules allows to 3D print concentration gradients regulating the gene expression of the cell population. Thereby, here we show how a material can convey a signal that an engineered organism is capable of sensing and responding to.

# Grown, Printed, and Biologically Augmented: An Additively Manufactured Microfluidic Wearable, Functionally Templated for Synthetic Microbes

Christoph Bader[1*], William G. Patrick[1*], Dominik Kolb[1], Stephanie G. Hays[2,3], Steven Keating[1], Sunanda Sharma[1], Daniel Dikovsky[4], Boris Belocon[4], James C. Weaver[3], Pamela A. Silver[2,3], and Neri Oxman[1+].

*(as published in 3D printing and additive manufacturing, Volume 3, Number 2, 2016 – with minor edits)*

1. MIT Media Lab, School of Architecture and Planning, Massachusetts Institute of Technology, 75 Amherst St. Cambridge, MA 02139, USA
2. Department of Systems Biology, Harvard Medical School, 200 Longwood Avenue, WAB 563, Boston, MA 02115, USA
3.Wyss Institute for Biologically Inspired Engineering, Harvard University, Cambridge, MA 02138, USA.
4. Stratasys, LTD. 2 Holtzman St., Science Park, P.O.Box 2496, Rehovot 7612401, Israel.

## Abstract

Despite significant advances in synthetic biology at industrial scales, digital fabrication challenges have, to date, precluded its implementation at the product scale. We introduce a computational design environment for additive manufacturing of geometrically complex and materially heterogeneous fluidic channels. We present, Mushtari, a multi-material 3D printed fluidic wearable designed to culture microbial communities. Thereby we introduce a computational design environment for additive manufacturing of geometrically complex and materially heterogeneous fluidic channels. We demonstrate how controlled variation of geometrical and optical properties at high spatial resolution can be achieved through a combination of computational growth modeling and multi-material bitmap printing. Furthermore, we present the implementation, characterization and evaluation of support methods for creating product-scale fluidics. Finally, we explore the cytotoxicity of 3D printed materials in culture studies with the model microorganisms, Escherichia coli and Bacillus subtilis. The results point towards design possibilities that lie at the intersection of computational design, additive manufacturing, and synthetic biology; with the ultimate goal of imparting biological functionality to 3D printed products.

# Introduction

## *Vision*

How can we design relationships between the most primitive and the most sophisticated life forms? Can we design wearables embedded with synthetic microorganisms that enhance and augment biological functionality? We explored these questions through the creation of *Mushtari* (Figure 48), a 3D printed wearable comprised of 58 meters of internal fluid channels. The wearable concept-piece was designed to function as a "microbial factory" that uses genetically modified microbes to make useful products for the wearer. Optimally, *Mushtari* could enable and inform a symbiotic relationship between two microorganisms: photosynthetic autotrophs, such as microalgae or cyanobacteria; and compatible heterotrophs, such as *Escherichia coli* or *Bacillus subtilis*. The photosynthetic microbes could convert sunlight into nutrients for the heterotrophs, which could in turn produce compounds for specific applications. This form of microbial symbiosis, a phenomenon commonly found in nature [83], builds upon the inherent symbiosis present between the wearer and the microbes *within* the wearable. Based on the demonstrated biocompatibility for microbes shown in cytotoxicity tests of the 3D printed materials used in this study, we ultimately envision a fully functional photosynthetic prototype that contains engineered heterotrophs such that the wearer would be able to trigger microbial production of specific compounds of interest, including scents [84], pigments [85], and fuels [86].

While 3D printing has been previously demonstrated as a viable means for the production of bespoke wearable-scale products [87], this technology has not previously been used to print a wearable with an inner fluidic network. Until recently, additive manufacturing has been utilized to produce microfluidic devices[88], but only in a single material and/or typically at a small scale – usually below feature sizes of 10 cm - when compared to the scale of a typical wearable. *Mushtari* is the first of its kind fluidic device with channels as thin as 1 mm in diameter. It was digitally fabricated at a wearable scale and examines the material ecology [89] within a 3D printed wearable that incorporates functional microbial communities.

## *Approach*

Functional templating [82] of microbial activities through 3D printing of heterogeneous material-distributions, or the ability to design a top-down material system that can inform bottom-up biological processes (such as guiding microbial growth for the purpose of photosynthesis), is a fundamental concept for the design of biologically augmented wearables. Our approach for designing

*Mushtari* focuses on methods by which heterogeneous multi-material 3D printing for the design of custom intermediate materials, in combination with novel additive manufacturing strategies, can be used for the fabrication of complex fluidic channels that create an artificial habitat for microbial growth.

*Organization*

The paper is organized in three sections: (1). **Growing** *Mushtari*, (2). **Printing** *Mushtari*, and, (3). **Augmenting** *Mushtari*. In the first section we show how complex channel geometries were generated, and how heterogeneous material distributions within these channels were modeled. In the second section we present a digital fabrication method for controlling material distribution using multi-material 3D printing, employing a novel liquid support-material, which enables the fabrication of a vast interconnected network of internal channels. Finally - in the third section - we demonstrate the biocompatibility of the 3D printed materials in the context of microbial growth studies. The aforementioned three sections relate to their respective knowledge domains –computational design, additive manufacturing, and synthetic biology - that coalesce to a first-of-its-kind implementation of synthetic biology in the domain of 3D printing, and vice versa.

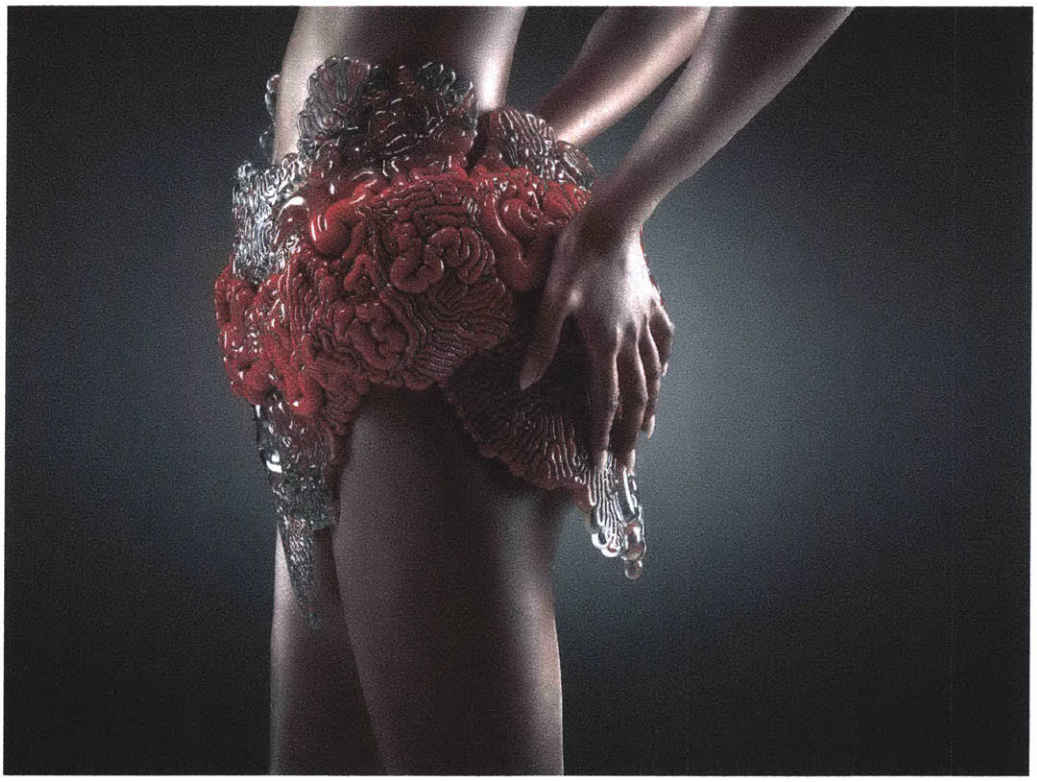

*Figure 48 – Side-view of Mushtari.* The 3D printed wearable combines a continuous internal network of biocompatible fluidic channels with variable optical transparency through the use of bitmap-based multi-material additive manufacturing. Photo: Yoram Reshef.

## Growing Mushtari

The design motivation behind *Mushtari* was to create a full-scale wearable with fluidic channels circumnavigating the human body in a dense, space-filling manner. To achieve this, the design involved computational processes that emulate natural growth in a controlled manner. This, in turn, led to the development of natural and organic-like structures, culminating in a design "symbiosis" between artificial (computational) growth of the *containing* environment, and the natural (biological) growth of the *contained* microorganisms. As such, *Mushtari* was designed using a generative growth algorithm, which emulates biological growth by developing complex geometries over multiple iterations. Similar processes include, for example, Lindermayer-Systems [90] (L-Systems), which are a widely used formal grammar, where rules are applied in parallel to generate branching structures. Reaction-Diffusion equations provide another example, where partial differential equations are implemented for modeling the distribution of components within a reaction, mimicking phenomena of pattern-formations that are characterized by variation of properties using multiple species (e.g. materials) [91]. More recently, the usage of a simplified mass-spring system over a mesh with a selective refinement strategy has been proposed for the generation of cellular forms [92].

Implementing a similar system, our approach allows us to inform the global or overall geometry, the local mesh geometry, as well as variations in material property distribution across length scales, by altering the relative strength of relaxation, attraction and repulsion over several iterations as described below. This approach enabled the design of a *single* channel that "grows" over numerous iterations to generate a wearable with 58 meters of hollow internal structure. The channel employs variations in diameter - from 1mm to 25mm - as shown in Figure 49; as well as variations in transparency; locally graded within the wearable to create areas where photosynthetic microbes could receive light, thrive and grow.

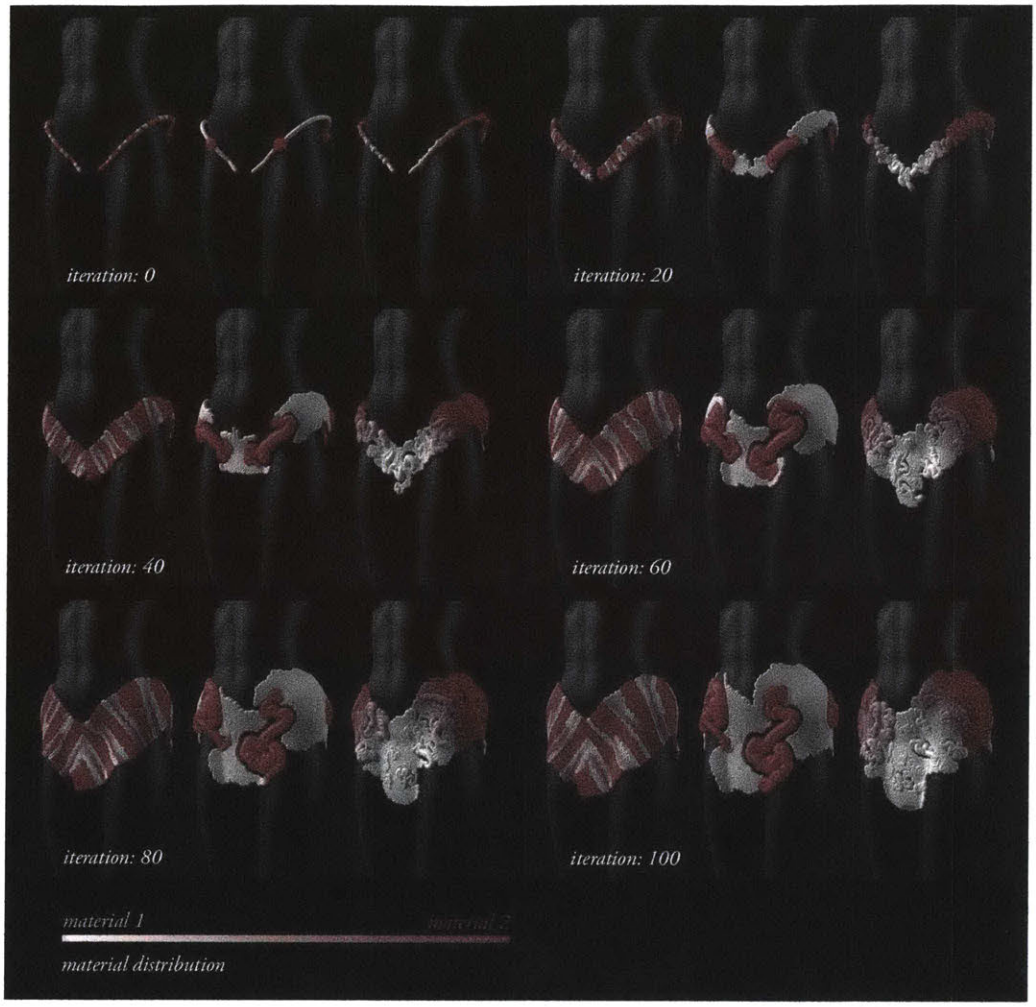


*Figure 49 – Visualization of 100 iteration steps from three different growth variations used to generate the fluidic wearable, Mushtari* (left, middle, and right orientations - in each panel). Shown are global-, and local-scale controls over the generation of the fluidic channels, as well as the ability to tune material properties during computational growth. Materials shown in red represent transparent areas, while materials shown in white represent opaque areas. The left-most approach (in each panel) varies transparency as a periodic function of the length of the strand. The center approach varies transparency by the diameter of the tubing. In the right-most approach, material properties are assigned by regions.

### *General Framework*

The general framework driving the generation of *Mushtari* is shown in Figure 50. A geometric input representation (e.g. a triangle mesh, a set of line segments, or a point cloud) is first transformed into an intermediate representation. From this intermediate representation, a coarse implicit representation is generated. Information from these three representations is then used to deform the initial geometric representation. Lastly, the deformed initial representation is topologically modified to react to the deformation of the object. This is done iteratively, such that a given input representation is continuously deformed and refined. As the process repeats, the deformations

aggregate into the growth of a coherent form. For an exhaustive presentation showcasing 15 different derivations of this process, we refer to [93].

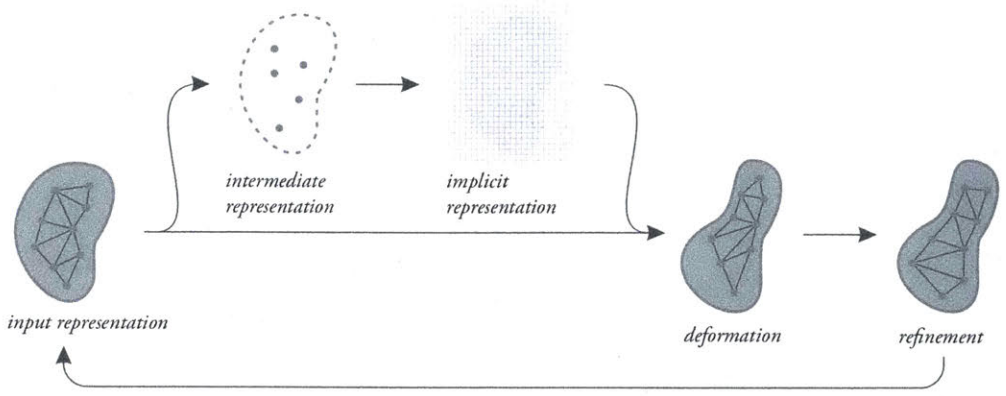


*Figure 50 – Schematic overview of the general framework used for the generation of computationally grown structures.*

### *Growth of Polygonal Lines*

Figure 4(a) shows how the general framework can be adapted to animate the growth of a polygonal line that acts as a backbone for the fluid channel of the wearable. In this case, the input representation is a polygonal line while the intermediate representation is a point cloud. The implicit representation is a distance field[51] given by the distances to the points of the intermediate representation and their associated radii. The deformation is described by a displacement of the vertices of the polygonal line. The subsequent topological transformation is performed by resampling of the line. The iterative nature of this process results in a continuous deformation of the input polygonal line.

We assume the polygonal line $L$ is given by a set of vertices $V_L = \{v_1, .., v_n\}$ and edges $E_L = \{e_1, \dots, e_m\}$, $e_i \in V_L \times V_L$ where a position $p_i = p_L(v_i)$ in $\mathbb{R}^3$ is associated with each vertex $v_i \in V_L$. Then, the intermediate representation is given by a point cloud $P = \{w_1, .., w_n\}$, containing $n$ points, one for each vertex of $L$, with positions $p_P(w_i)$ offset along the edges of $L$ and associated radii $r(w_i)$. From this, the implicit representation is given again by a distance field $d_P : \mathbb{R}^3 \to \mathbb{R}$ such that $d_P(x) = \inf_{y \in \partial B} \|x - y\|$ where $\partial B$ is the boundary of

$$B = \bigcup_{i=1}^{n} \{y \in \mathbb{R}^3 | \, \|p_P(w_i) - y\| \leq r(w_i)\}$$

In each iteration, the deformation from the input polygonal line $L_j$ to the deformed line $L_{j+1}$ is described by the displacement function $\delta$ which associates with each vertex $v_i$ a displacement vector $\delta_i = \delta(v_i)$ such that $L_{j+1} = \{p_i + \Delta t\delta_i \mid v_i \in V_{L_j}\}$ and

$$\delta_i = -a\Delta d_P(p_i)\nabla d_P(p_i)$$

Where $a$ is a free parameter, $\Delta d_P$ is the laplacian and $\nabla d_P$ is the gradient of $d_P$. After the displacement, the polygonal line is resampled such that all edges have the same length. An example of this process is shown in Figure 51(b). For the final 3D printable geometry, we extracted a surface representation by volumetric expansion from the 1-dimensional strand, where the stand's local proximity to nearby points guides the enlargements of the 3D geometry.

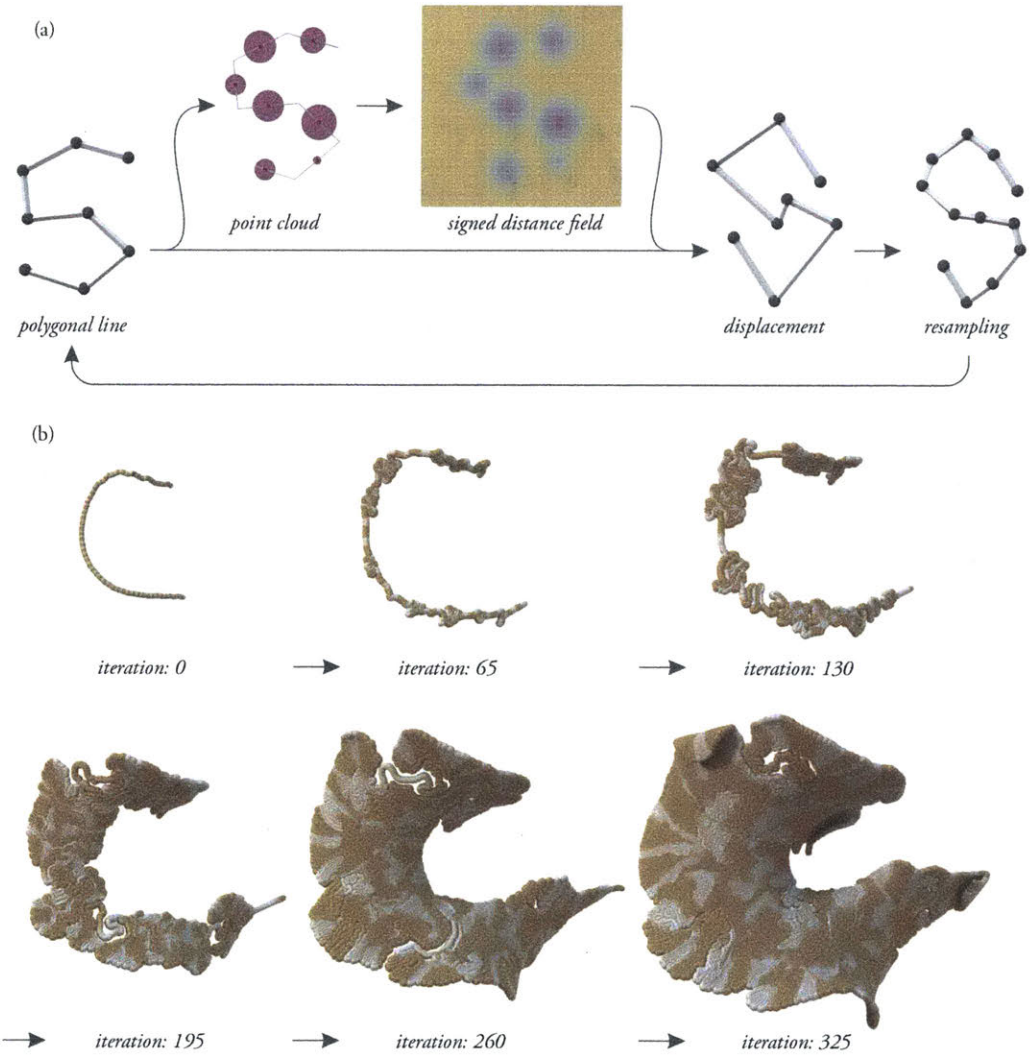

*Figure 51 – (a) Example of the general framework applied to a polygonal line.* (b) Several iterations of this process ultimately resulting in a compact coiled architecture. In this figure, the process is constrained to the tangent space of an underlying guiding triangular mesh (not shown).

### *Functional Templating*

The core motivation associated with biological augmentation of the device was to contain a sustainable co-culture of photosynthetic microbes capturing solar energy and nourishing other heterotrophic microbial communities. The design required and involved *functional templating*[82], achieved through high-resolution tunability of material properties, such as opacity. Transparent or translucent channels would enable the phototrophs' exposure to sunlight, and the subsequent transfer of chemical energy in the form of fixed carbon to heterotrophic bacteria such as *B. subtilis* and *E. coli*. Our design approach therefore necessitated the *parameterization of material properties for functional templating*. This approach is presented in Figure 52.

To enable functional templating via continuous control over transparent and opaque regions, we employed heterogeneous material modeling techniques [45]. Material properties were either specified as a function of the path-length of the grown strand, or globally defined by specifying external sources [94]. While the parameterized approach allows better control over local variation, the global approach yields better control of overall material distribution (the latter was chosen for *Mushtari* as shown in Figure 52(b)). Figure 52(c) shows the generated fluid channel in its unfolded state, illustrating local material distributions required to achieve the global distribution in the final folded form. Modeled material distributions were subsequently fabricated using a Connex3 multi-material 3D printer (Stratasys) by employing the transparent VeroClear (RGD810) and rigid, opaque VeroRed materials [13].

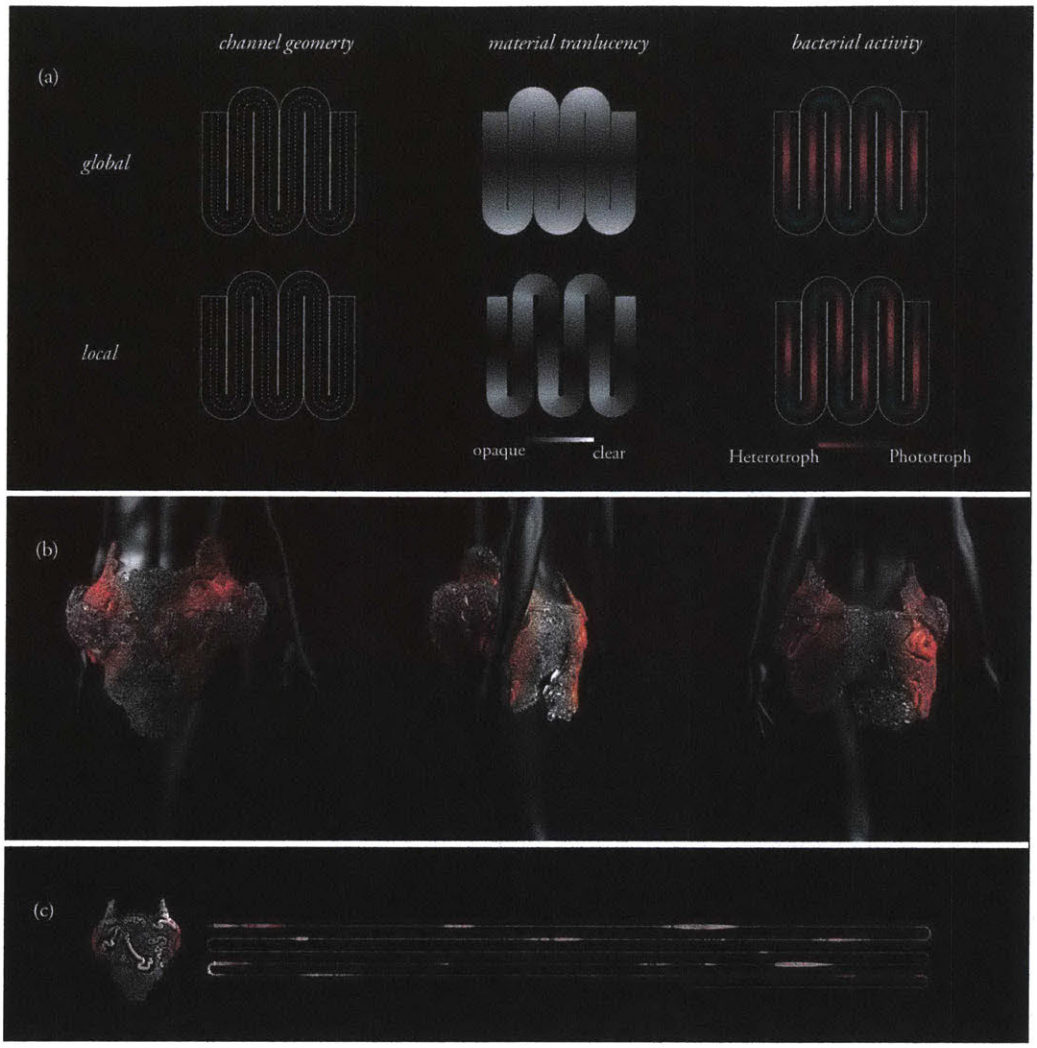


*Figure 52 – (a) The desired effect of material transparency on microbial activity.* In translucent regions, the co-culture receives light, increasing phototrophic activity (right column). In opaque regions, the co-culture is dark and the heterotrophs would consume the photosynthates, thus increasing their metabolic activity. Transparency can be controlled globally, as shown in the upper middle column, independently of the strand; or - locally, shown in the lower middle column, using path-length parameterization as a guide for material-distributions; (b) Implementation of the global heterogeneous modeling approach on the wearable; (c) Visualization of the unfolded strand showing how the overall ("global") source-based approach influences local changes in opacity along the strand.

# Printing Mushtari

## *3D printing a Materially Heterogeneous Tract*

In order to effectively template the containment and activity of fluid media within the wearable, it is necessary to digitally fabricate channels that are geometrically complex as well as materially and optically heterogeneous. The production of an optically heterogeneous single conduit poses significant technical challenges from an additive manufacturing perspective. Specifically: to fabricate a single channel with variable properties, the use of multi-part assemblies with pre-defined and

consistent properties, or – similarly – the use of tube inserts post fabrication was deemed impractical. As such, to fabricate a continuous tract that is at once materially heterogeneous and hollow, we employed a bitmap-printing approach to create controllable opacity gradients and leveraged a novel liquid support-material strategy enabling the fabrication of vast channel networks.

*Multi-Material Voxel-Printing of Fluidic Channels*

In order to 3D print materially heterogeneous channels we implemented a voxel-based 3D printing technique [42], which enabled the digital fabrication of material property gradients. Modern multi-material 3D printers[13] employ an ink jet-like printing approach to construct parts by depositing UV-curable droplets of photopolymer resin in a layer-by-layer fashion. By depositing distinct material droplets of base resins in high-resolution (600 dpi in $x$ and 300 dpi in $y$), nearby material-droplets will diffuse at a micron-level, resulting in the formation of hybrid materials with intermediate properties. Controlling this high-resolution placement enables the creation of functionally graded materials at a fine scale. To achieve this level of control, we implemented a custom 3D slicing and material-distribution method [95], which allows for the utilization of external data-sources to evaluate heterogeneous material modeling methods ***during*** slicing, and, as such, enables for the computation of material distributions in high spatial resolution. These material-modeling descriptions are used to generate binary 3D voxel-matrices containing spatial droplet deposition descriptions for the 3D printer. Given that the 3D printer employed in this study can print three different materials simultaneously (or four - including the support material), it is possible to generate three to four 3D matrices at the native resolution of the printer. These material deposition descriptions can be used to achieve highly precise functionally graded materials (Figure 53). Here, ratios of locally proximal deposited material droplets dictate the functional properties of the printed material composites. As shown in Figure 53(a), by continuously varying the ratio of opaque (VeroRed) to transparent (VeroClear) material droplets, we can achieve high control over opacity gradients in the 3D printed part as shown in Figure 53(b) which effectively allows us to implement desired functional templating.

Additionally, this approach allows us to make use of high-resolution, highly precise Boolean-operations without modifying the actual geometry. We achieve this by specifying to use support-material over model-materials in areas, which are desired to be hollow in the final form. This allows us to create physically hollow channels, after the cleaning process, on arbitrary complex geometries without modifying the actual shape description as shown in Figure 53(c).

While the VeroClear materials are intrinsically transparent, the deposition of support material during the printing process results in a partial roughening of the VeroClear following support material removal, with the resulting part exhibiting partially diminished optical clarity. While this small reduction in optical clarity was adequate for our specific application; increased optical clarity can be achieved by polishing and or lacquering the 3D printed part to reduce this intrinsic surface roughness. While the build volume of the 3D printer employed in this study measures 50 cm x 40 cm x 20 cm; to achieve a wearable-scale object, we split the form into a five-piece assembly such that each piece could fit in the build volume of the printer. Each piece featured a single long channel and the combined five channels stretched 58 meters in total with diameters ranging from 1 mm to 25 mm.

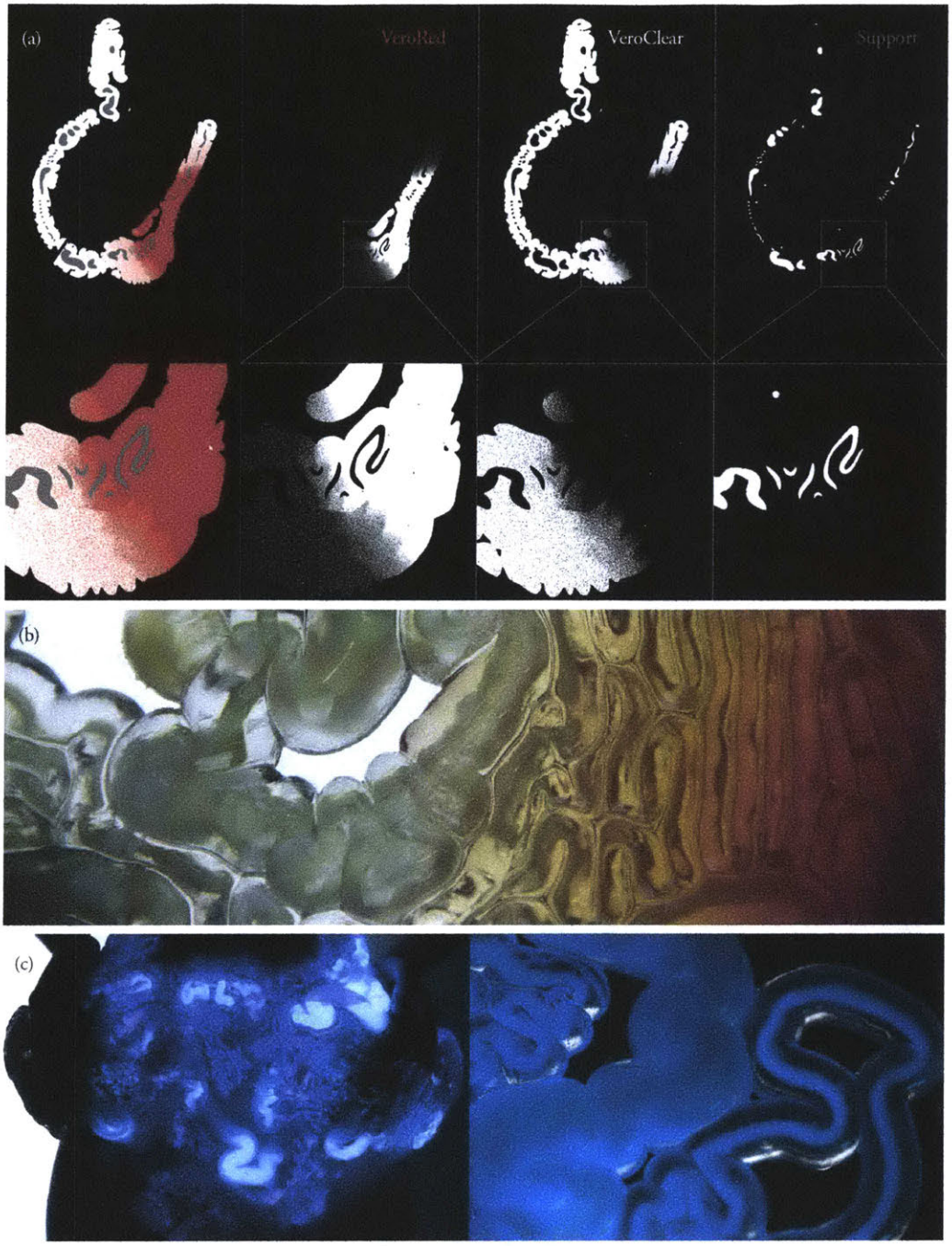


*Figure 53 – Fabrication of internal channels.* (a) A single layer of the 3D material deposition description (top), highlighting areas where optical gradients are modeled (bottom). (b) Actual fabricated optical gradients with filled internal channels. (c) Hollow channels filled with chemiluminescent liquid for the purpose of visualization.

### *Printing a Hollow Channel*

Multi-material 3D printers[13] use a separate support material to enable the printing of complex geometries with overhangs or internal structures. During the printing process, this gel-like support material (SUP705) is added to any internal structures, including the fluidic channel network. Once

the printing process is complete, the gel-like support material is abrasively removed using a high-pressure water jet that must come in direct contact with the support material. This process works well for large bulky geometries or those with short internal voids, but is not suitable for long fluidic channels due to the restricted channel access. To overcome this barrier, we investigated the use of two alternative support methods; an available soluble support (SUP707) and an experimentally developed liquid support. The soluble support material is a polymer material, which dissolves in water and can be substituted for the typical gel support in the normal 3D printing workflow. The liquid support method uses a material with similar pre-polymer material properties but cannot be polymerized by UV light. This liquid support can be printed into internal channels by assigning an STL mesh or a separate 3D voxel-matrix of the inner channel geometry to the liquid support material.

*Characterization and Evaluation of Support Methods*

Soluble support and liquid support present two potential options for creating internal fluidic channels within the wearable. To evaluate the two support methods, we designed test pieces that contained channels of 1 mm to 20 mm in diameter as is shown in Figure 54 (rightmost column). We printed the test piece using normal support (SUP 705), soluble support (SUP707), and liquid support. Cross sections of test pieces were examined using optical microscopy. Images were acquired using a Vividia 2.0 MP handheld USB Digital Endoscope as shown in Figure 54. The test pieces printed using liquid support in a horizontal orientation were the only test pieces that could be entirely cleared of support and liquid could easily pass through all channels (A-G) for each of the three sample replicates. In test pieces printed using soluble and liquid support in a vertical orientation, channels greater or equal to 1 mm in diameter (B-G) could be cleared. In test pieces printed with the traditional gel support, only channels greater than or equal to 3 mm (E-G) could be cleared. Three replicates were measured for each support type and three technical replicates were performed for each measurement. Table 1 summarizes the expected and measured dimensions of the test piece cross sections.

To test the suitability of each support material for the complex internal fluidic channels of the wearable, we designed a second test piece as shown in Figure 55 to reflect the geometry of the final wearable. The test piece featured five inlets and a channel diameter that ranged from 1.5 to 12 mm. First, the piece was printed with soluble support, which was unable to be cleared from the piece even after multiple attempts. We then printed the same patch using liquid support, which was cleared successfully, and demonstrated that liquid could easily flow through this piece from the inlet to the outlet. Even though the second test piece featured larger minimum diameter channels compared with the first test piece and contained multiple inlets, the soluble support still could not be cleared from

the second test piece. This finding suggests that the irregular geometry, including multiple branches, variable diameters, and small radii of curvature, factored into our inability to clear soluble support from the channels. Based on these two test pieces, we used the liquid support material for printing the wearable.

In summary, we found that both the soluble and liquid support materials can be used to fabricate fluidic channels using multi-material 3D printing. Liquid support can be successfully used to print channels with diameters as small as 300 microns but results in additional channel surface roughness. Soluble support has higher print quality, is more accurate, and creates less surface roughness than liquid support, but the soluble support could not be cleared from the smallest channels in the test pieces.

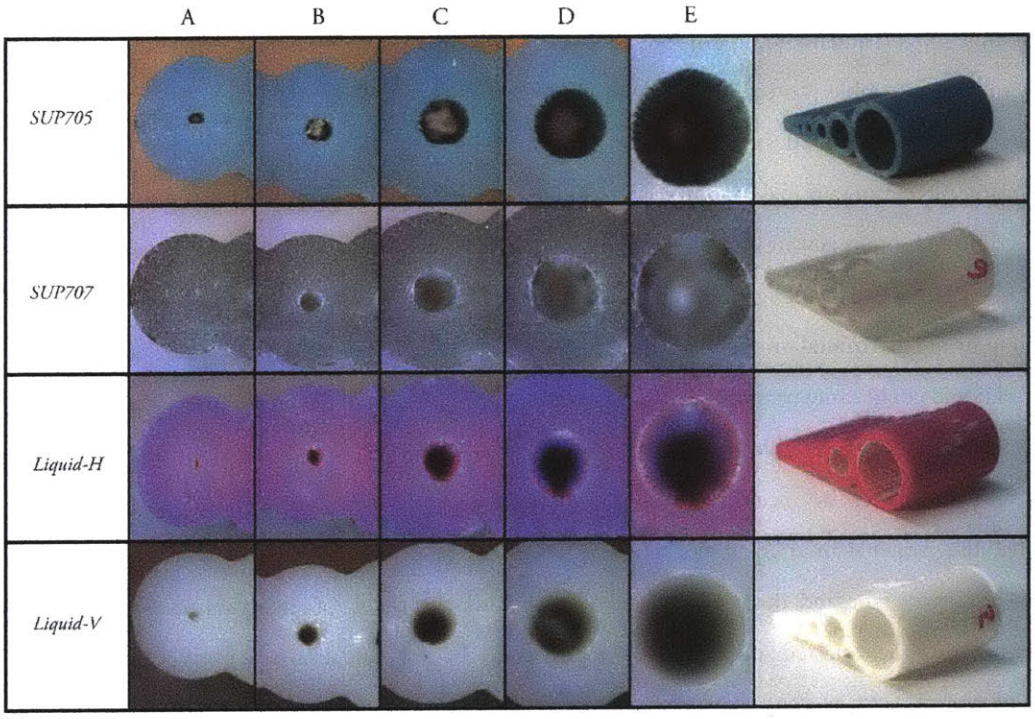


*Figure 54 – Representative optical images of test piece cross-sections* that were printed using the three support material methods.

| Diameter | Expected Value | Normal | Soluble | Liquid-H | Liquid-V |
|---|---|---|---|---|---|
| A | 0.5 | 0.46 ± 0.03 | 0.41 ± 0.03 | 0.3 ± 0.04 | 0.36 ± 0.04 |
| B | 1 | 0.97 ± 0.03 | 0.88 ± 0.05 | 0.73 ± 0.06 | 0.90 ± 0.05 |
| C | 2 | 2.02 ± 0.05 | 1.96 ± 0.05 | 1.76 ± 0.05 | 1.92 ± 0.06 |
| D | 3 | 3.10 ± 0.07 | 2.96 ± 0.08 | 2.82 ± 0.07 | 3.0 ± 0.1 |
| E | 5 | 5.2 ± 0.1 | 5.0 ± 0.1 | 4.9 ± 0.1 | 5.0 ± 0.1 |
| F | 10 | 10.0 ± 0.2 | 9.9 ± 0.2 | 9.8 ± 0.3 | 9.8 ± 0.2 |
| G | 20 | 20.0 ± 0.3 | 19.9 ± 0.3 | 19.0 ± 0.3 | 19.8 ± 0.3 |

*Table1: Mean and standard deviation of diameters A-G (mm) of the test pieces with various support materials.* The mean and standard deviation of each diameter per support type were calculated using 3 replicates printed and measured for each support type. Diameters were measured in the direction of the print orientation. Normal, soluble and Liquid-H were printed in the same horizontal orientation. Liquid-V was printed in a vertical orientation.


*Figure 55 – Visualization of smaller scale test-piece used.* The image on the left shows the actual shape of the printed piece. The image in the middle and on the right visualizes how the support material (blue) is distributed and printed inside the wearable to achieve a hollow channel.

### *Visualizing Mushtari's inner channels*

The final piece was printed with many 1.5 mm diameter inlets throughout the fluidic network, which were used for removing any remaining liquid support material and for filling the piece with test liquid. We next visualized the channels by filling *Mushtari* (Figure 53(b)). In addition to the clear media used for initial testing, *Mushtari* was also filled with a chemiluminescent liquid (Figure 53(c))

to better visualize the internal channel network. A 22-gauge needle was press-fit into the inlets, and after filling the piece; the inlets were capped with small plugs that were 3D printed from the same materials as the wearable to create a watertight seal.

While preliminary tests revealed that all channels in the five pieces were cleared of liquid support, we found that we were unable to manually flow liquid from inlet to outlet in the complete fluidic network. While in one piece, we were able to flow the injected liquid 3.5 meters through a channel section with diameters that ranged from 1.4 to 11 mm, as the path length increased, the pressure required for complete channel filling became insurmountable, likely due to accumulated resistance from variable channel diameter, channel length, and channel curvature. Information regarding these parameters is critical for future geometries that may be designed to culture bacterial communities for extended time periods, and which may be structurally optimized by fluid flow simulations during the initial design process. Under such culture conditions, flow will be important for the exchange of nutrients and channel diameter may be influenced by the growth of biofilms on the channel walls based on their diameter and curvature [96].

## Augmenting Mushtari

Synthetic biology is an interdisciplinary field that applies an engineering approach to biology[97]. As such, it alludes to practices that enable the engineering of molecules, cells and microorganisms to perform specific tasks[97]. In this vein, *Mushtari* was designed to act as a potential "host" environment for the co-culture of engineered microorganisms that make up a synthetic "community". Synthetic biologists use disparate bacteria in order to capitalize on each microbe's unique physiological specialties and evolved capabilities. *E. coli* is arguably the best-studied model bacterium[98] and has been modified to produce useful products including scents[84], colors[85], and fuels[86]. However, *E. coli* is not best suited for all applications. For instance, *B. subtilis,* a popular Gram-positive model bacterium found in soil, can secrete large quantities of proteins, making it an appealing option for the production of commercial enzymes and protein-based biopharmaceuticals[99].

Both *E. coli* and *B. subtilis* are heterotrophic, which means they must obtain their organic carbon from the external environment. In contrast, phototrophic microbes, including cyanobacteria and algae, can capture solar energy and use it to fix carbon dioxide. In nature, microbial communities are complex mixtures of different species that capitalize on different metabolic capabilities, allowing for an efficient division of labor. Synthetic biologists have begun to take advantage of this organization

by creating new systems that combine both phototrophic and heterotrophic assemblages[100]. *Mushtari* was engineered to provide an environment for such a consortium.

*Cytotoxicity Studies*

As one aim of the 3D printed wearable is to host microorganisms inside the hollow channels, the cytotoxicity of the 3D printed materials needed to be investigated. To investigate the potential cytotoxicity of the 3D printed pieces and their impacts on microbial growth, specialized tubes were printed to mimic the plastic labware used in standard microbial culture. The tubes had similar geometry to a standard 14 mL polypropylene culture tube (Falcon, Corning), while the 3D printed culture tubes were designed to be thicker in an attempt to minimize potential fissures and leakage. Before the 3D printed pieces could be used to culture microbes, they were pre-treated and sterilized. Pre-treatment involved removing support materials with a water jet (Powerblast High Pressure Water Cleaner, Balco, UK) followed by submersion in 2% sodium hydroxide for one hour. Another cleaning with the water jet followed. This process was then repeated, such that parts were exposed to the sodium hydroxide solution twice. The 3D printed parts were next boiled and rinsed in distilled water, then autoclaved to achieve sterility. Sterility was checked via the addition of rich media to tubes after sterilization. After overnight incubation at 37°C, no bacterial growth was visible. While many of the 3D printed tubes could be successfully used for cell culture, others proved not to be watertight. As this was most frequently seen in sterilized pieces as opposed to untreated test pieces, future studies will focus on optimizing the treatment and sterilization protocols to decrease harshness and, consequently, limit leakage.

For the microbial growth studies, two model bacterial species *E. Coli* and *B. subtilis* were used. *E. coli* (BW25113) and *B. subtilis* (168, ATCC #23857) were struck from frozen stocks onto Luria broth (LB) plates. Individual colonies were picked for biological replicates and grown in liquid LB. After growth either overnight or to a visually turbid state at 37°C, cultures were diluted to a low $OD_{600}$ (~0.05) as measured by cuvette in fresh liquid LB. These cultures were then split between three conditions: 1) polypropylene tubes as controls 2) VeroClear tubes with insoluble support (SUP705) material and 3) VeroClear tubes with soluble support (SUP707) material. Each uncapped culture tube was placed inside of a 50 mL polypropylene tube (Falcon, Corning), which was then capped. To prepare the negative controls 5mL of LB media was added to 3 VeroClear tubes, printed either with insoluble or soluble support material, and 3 polypropylene tubes. These tubes were also placed inside 50 mL BD Falcon polypropylene tubes. All tubes were cultured in a 37 C incubator shaking at 200 rpm. Measurements were taken every 30 minutes until the cells appeared to hit stationary

growth. $OD_{600}$ measurements were taken using a 96 well plate reader. Media blank readings were subtracted and these values are reported directly in the representative data shown in Figure 56(a) and (c). To calculate the doubling time, the log base 2 of each sample was calculated. The time series for each replicate was plotted with $\log_2$ ($OD_{600}$ value) vs. hours. For each condition, a line of best fit was determined for over each 1.5-hour period. The maximum growth rate with an $R^2$-value higher than >= 0.96 is reported. To quantify the variation between the biological samples for each condition, we then measured the doublings per hour for each biological sample and calculated the standard deviation. We found no statistically significant difference in the growth rates of *E. coli* or *B. subtilis* in the 3D printed tubes (+/- support material) in comparison to the standard control Falcon tubes. These results demonstrate that the microbial model organisms *E. coli* and *B. subtilis* can be grown within the 3D printed vessels with no measurable negative growth effects. Future work will explore the biocompatibility of these materials for the culture of other engineered heterotrophic and autotrophic microbes to add functionality to the consortia in complex fluidic systems.

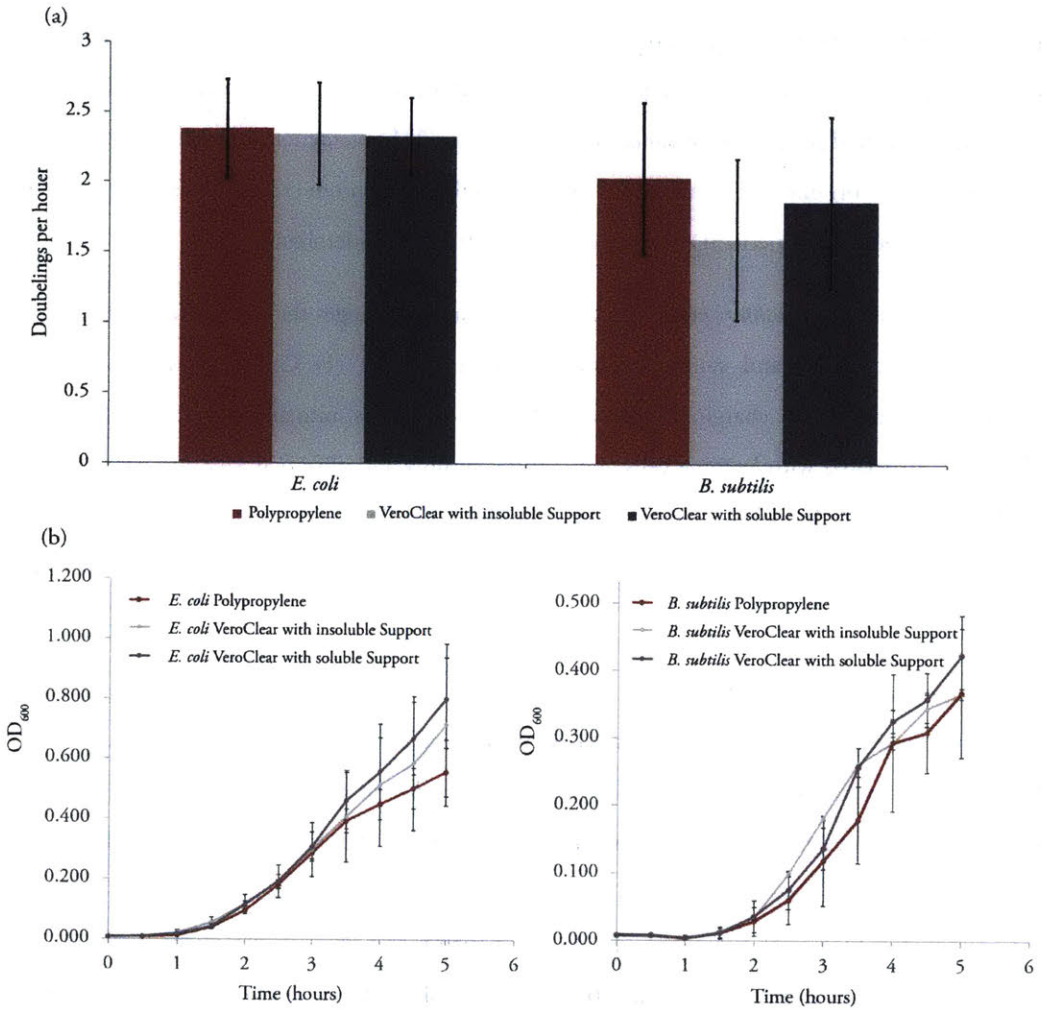


*Figure 56 – (a) Comparison of growth rates (doublings per hour) of Escherichia coli and Bacillus subtilis in various tube materials.* Error bars represent the standard deviation between at least six biological replicates. Representative growth of *E. coli* (b, left) and B. subtilis (b, right) in different tubes. Error bars represent the standard deviation among three biological replicates grown on the same day.

## Conclusion and Future Work

The fields of Synthetic Biology and 3D printing are developing rapidly, yet independently of each other. *Mushtari* – the wearable and its associated suite of tools, techniques and technologies – demonstrates and points towards design possibilities that lie at the intersection of these fields as well as the relevance of such intersection to applications in product design. We designed a fluidic wearable with the ultimate goal of mediating the functionality of microbial communities by "templating" their containing environments using multi-material 3D printing. As such, the experimental research presented herein, showcases a first of its kind fluidic wearable demonstrating *computational growth of 3D printable multi-material fluidic channels at product scale.*

The project accomplished three goals, relevant to three research domains, namely: computational design, additive manufacturing, and synthetic biology. Those include: (1) Development and implementation of a computational approach for generating product scale fluidics and heterogeneous modeling of material properties for functional templating; (2) Implementation, characterization and evaluation of support material formulations for creating fluidics at product scale, and; (3) cytotoxicity evaluations of photopolymeric 3D printed materials with model microbial species.

The current design of *Mushtari* embodies exciting research challenges that lie at the intersection of additive manufacturing and synthetic biology. Those include: (1) Challenges associated with charging the wearable, i.e. charging required media (cells or tissues) into and out of the product; (2) Challenges associated with keeping cells and cultures healthy and alive (e.g. sterility, gas exchange, and biocompatibility for other microbial species) and; (3) Challenges associated with extracting any "product" (e.g. sugar, fragrance, or biofuel) that has been generated by the microbes contained within the wearable.

In this paper, we demonstrated that using currently available multi-material 3D printers, it is possible to control the deposition of multiple materials at the printer's native resolution. In the context of *Mushtari*, we focused on the control of material opacity and fluid containment. Integrating flexible materials into the design process would enable us to also control the elastic modulus, which, in turn, could open up many new design possibilities. Such opportunities may include wearable skins that not only ***contain*** biological media but can also ***filter*** such media in a selective manner. Given that modern multi-material 3D printers can print in ca. 32-micron voxel resolution, we point out the possibility that, increasing the resolution of 3D printing systems would allow for the creation selectively permeable membranes and pores. This could enable the production of a more sophisticated and regulated transport and filtration systems inside the wearable, which exchanges and interacts with the wearer. In addition, therapeutic compounds created within the fluidic system could be stored in specific areas and locally administered to the skin. Finally, by combining advanced computational design strategies for digital growth with multi-material 3D printing in high spatial resolution as shown herein, *Mushtari* paves the way towards multi-functional objects with spatiotemporal property variation in high resolution. Single material systems such as *Mushtari* will in the future enable the design and production of "breathing" and "living" wearables that can interact with our bodies and our environment, forming a true material ecology across scales.

## Acknowledgements

The authors would like to thank Naomi Kaempfer, Director of Art, Fashion and Design at Stratasys, and related team members - Tal Ely and Yoav Bressler - for their insights and dedication in producing *Mushtari*. The company's support has enabled the use of the Objet500 Connex3 multi-material 3D printer. The authors also wish to acknowledge Yoram Reshef for his photographs of the final design; as well as Paula Aguilera and Jonathan Williams for their support on additional visual materials. This research was supported in part by the National Science Foundation Award DGE1144152, Department of Energy DE-SC0012658 'Systems Biology of Autotrophic-Heterotrophic Symbionts for Bioenergy', SynBERC, and the Wyss Institute for Biologically Inspired Engineering.

# Heterogeneous Hybrid Living Materials

Christoph Bader[1], Rachel Smith[1], Sunanda Sharma[1], Dominik Kolb[1], James C. Weaver[2] and Neri Oxman[1+].

*(in preparation)*

1. Mediated Matter Group, Media Lab, Massachusetts Institute of Technology, Cambridge, MA 02139, USA
2. Wyss Institute for Biologically Inspired Engineering, Harvard University, Cambridge, MA 02138, USA.

## Abstract

While materials engineering and computational methods move us closer to programmable material systems allowing to freely design with material properties, in the same manner synthetic biology thrives to develop programmable living systems to enable design with biological properties. Living materials integrating functional living components gain biological properties but often fall short on material sophistication and therefore miss out on the synergetic relationships between material and biological functionality. Here, we propose the integration of a programmable material systems and programmable living systems. We present the fabrication and application of heterogeneous living material hybrids as a merger of multi-material 3D printed parts with hydrogels containing functional living entities. By embedding small signaling molecules into hygroscopic swelling materials utilized in the printing processes, a relationship between a tunable material system and living organisms can be achieved through diffusion of the signals into the hydrogel. We point towards the emergent design space of heterogeneous hybrid living materials for biological templating, flexible biologically augmented devices and multi input arrays. Therefore, the presented design strategy to engineered living materials allows to transfer the capabilities and sophistication of a tunable material system to biological systems and enables tools for synthetic biology as well as techniques to customizable living wearables.

# Introduction

The level of geometric complexity [101] and material sophistications [95] in 3D printing pushes us ever closer to the proliferation of functional wearables for medical and consumer applications; not limited to optics, orthodontics, prosthetics, customized splints, eluting implants, and porous scaffolds. The praxis of useful biological augmentation and successful incorporation into functional wearables remains a destination for synthetic biologists and materials scientists in a biological age. Past research [102],[103] made evident that encapsulation of living systems is essential for living wearables. Yet, a material can be more than a static scaffold in which inhabiting organisms grow, rather it can act as an environment to spatially template how these organisms behave [82].

Therefore, building on this past work we introduce heterogeneous hybrid living materials as a scalable strategy that allows direct biointerfaceing to a living entity through a tunable material system, thereby fostering an ecology between the synthetic and the biological. Further, we present initial research towards a technology in which biologically augmented wearables are additively manufactured and capable of spatially differentiated signaling to the contained living biological components. Specifically, we introduce a method for establishing exogenous concentration gradients through multi-material 3D printing to biochemically control bacterial cells across the surface of complex 3D printed geometry, and present examples of novel applications.

Results contain (1) the process for the fabrication of heterogeneous hybrid living materials and structures; (2) the spatial control of biomolecular signals and associated templating of biological activity; (3) design processes and potentials enabled through heterogeneous templates, (4) development and validation of photopolymeric biosignaling resins for the multi-material 3D printing process; and (5) modeling and design of heterogeneous hybrid living materials. This new approach of fusing a synthetic material system with living materials – moving towards heterogeneous hybrid living wearables – enables to facilities synergetic advantages, thereby increasing flexibility and applicability of biologically augmented devices to a variety of domains.

## Results

### *Fabricating heterogeneous hybrid living materials*

In synthetic biology regulation of transcription is an essential element to enable controllable activity of protein synthesis. Any molecule, which will enhance the synthesis of a specific protein, is referred to as an inducer. Analogously any molecule, which will reduce the synthesis of a specific protein, is referred to as a repressor. Consequently, the process of enhancing or enabling synthesis of a specific product is usually called induction and the rate of induction is in general sensitive to the chemical concentration gradients activating the production. Engineered bacteria can be designed with promoter sensitive to specific small molecules allowing to activate the expression of a specified gene and thereby the production of a desired product.

Here we propose a strategy for the fabrication of hybrid living material structures through the incorporation of inducers in heterogeneous objects, which are merged with a hydrogel matrix containing bacterial cell. In short, by embedding small molecules into photopolymeric materials utilized in multi-material 3D printing processes, and growing engineered bacteria strains embedded in a hydrogel substrate on objects fabricated with endowed materials, a relationship between material and organisms can be achieved through diffusion of the chemical signal into the substrate.

Specifically, our approach consists of three parts Figure 57(a). First, the computational generation of multi-material 3D printing descriptions that relate to a defined diffusion gradient. Second, the fabrication of multi-material objects embedding small molecules in dedicated materials to enable the diffusion process. Lastly the application of a hydrogel containing a living systems which will receive signals from the additively manufactured part or the environment (*see Methods section for experimental details*).

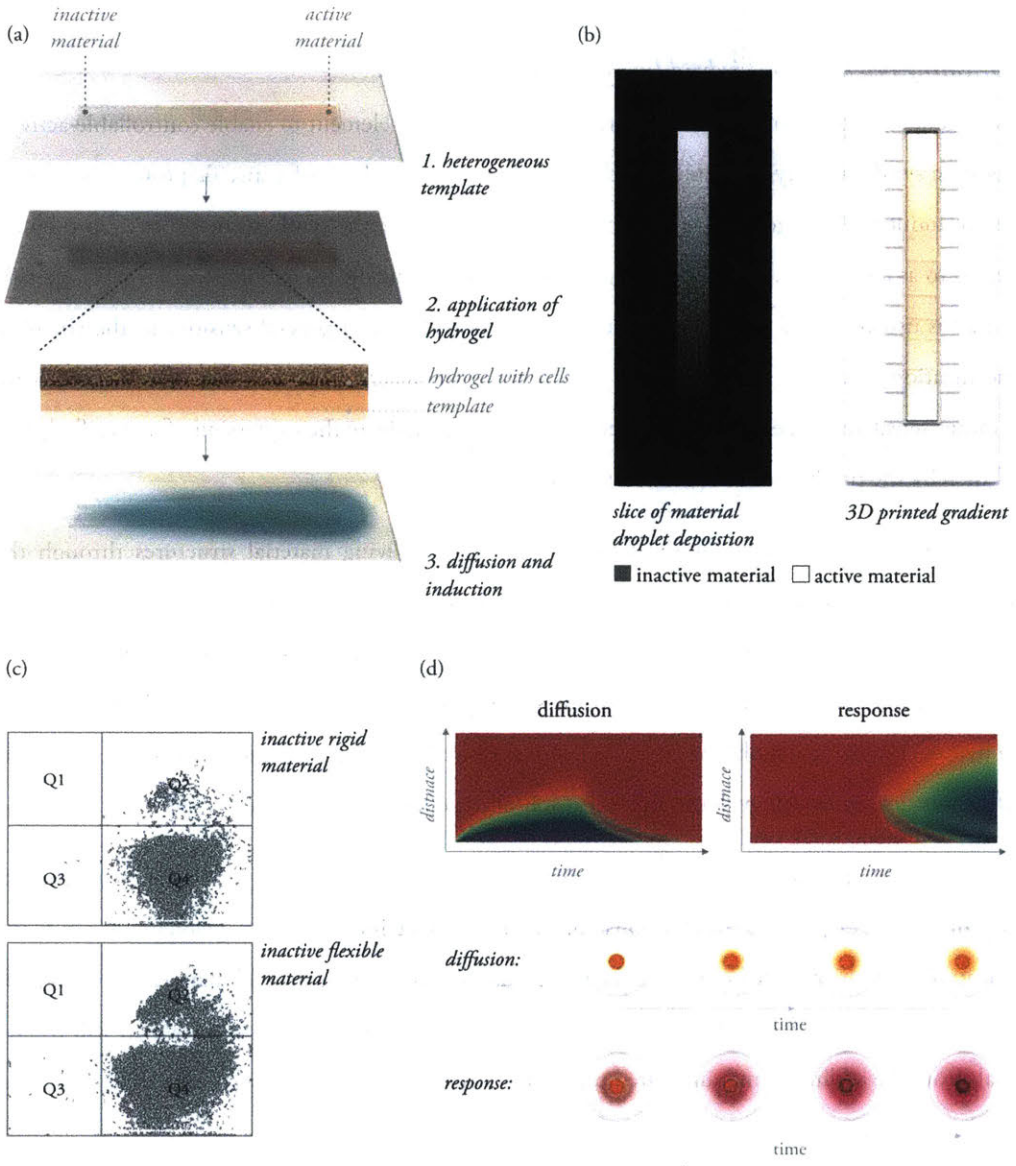


*Figure 57 – Process of fabricating heterogeneous hybrid living materials.* (a) Schematic illustration of the fabrication of a generic hybrid living material structure. First a heterogeneous template is additively manufactured utilizing two or more materials, where the active material is capable of releasing small molecules, whereas the inactive material does not exhibit this property. Next, the template is covered with a hydrogel embedding bacterial cells. Over time, areas with active material will signal through small molecules into the aqueous substrate where cells can response accordingly. (b) Illustration of the droplet deposition instruction in form of a raster file (left) needed in the fabrication process of the heterogeneous part with linear material gradient from inactive to active material (right). (c) BacLight LIVE/DEAD Assay results, quantified using FACS, showing cell viability of inactive rigid material and flexible material. (d) Colorimetric substrate CPRG used for visualization of small molecule diffusion (yellow) and bacterially produced enzymatic catalysis (magenta), measured over radial distance from central active material area and time.

We implement a voxel-based 3D printing technique [33] Figure 57 (b), which enables the digital fabrication of material property gradients. Multi-material 3D printers utilize an ink jet-like printing approach to construct parts by depositing UV-curable droplets of photopolymer resin in a layer-by-layer manner. By spatial varying material droplet density of materials with different characteristics, the deposited material concentration gradients allow to achieve material property variations in the 3D printed parts. These density values can be given at a higher level by a three dimensional volumetric description of material-distributions (relative mixtures of materials for each voxel) which can be decoded by volumetric dithering methods to material deposition descriptions. These material descriptions—for example given as set of layers in a raster file format—can be used to fabricate objects with highly precise functionally graded materials; examples include fabricated parts with continues gradients in transparency—from opaque to clear—or modulus—from stiff to soft.

We leverage this multi-material 3D printing process in our hybrid system by using materials which allow for the embedding of releasable small molecule inducers, incorporated either post-printing or in the resin utilized by the printer. Concretely, we use a hygroscopic swellable material as an active material and a non-hygroscopic swellable material as an inactive material. For the post-print incorporation, material-gradients of active to inactive material are fabricated in a 3D printed object, then—in a post-processing step—the 3D printed part is submerged in a chemical solution. In this process, the chemical solution will be absorbed and stored in the part where the absorption is depended on the concentration of hygroscopic swellable active material to non-swellable inactive material. In the second case, small molecules are incorporated into the hygroscopic swellable resin directly. This biosignaling resin can be used in the multi-material 3D printing process and the spatial droplet placement in combination with other non-hygroscopic materials will determine the concentration of small molecules diffused in specified areas. The advantage of method which includes a post-processing step, is that chemicals can be added at any given time after the digital fabrication process through absorption. The advantage of the method including the small molecule in the fabrication process is the ability to achieve a much greater degree of spatial control over their incorporation and to alleviate the need to post-process the parts in a chemical bath.

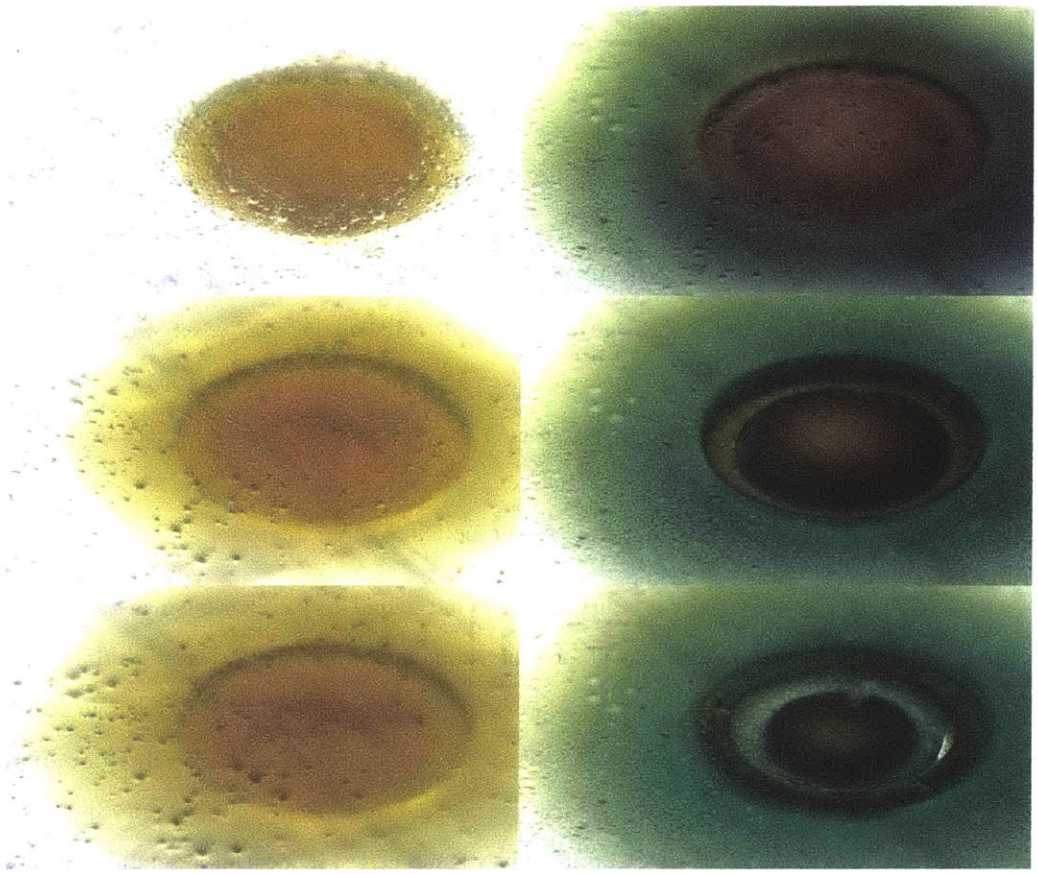

*Figure 58 – Close up of diffusion gradients visualized through CPRG (yellow) and bacterial response (green).*

Diffusion gradients can be established by applying a hydrogel with embedded bacterial cells on top of the heterogeneous part. The aqueous matrix of the hydrogel provides a viable layer for immobilization and growth of engineered cells, while facilitating the diffusive propagation of chemical signals across the surface of the print. Embedded cells of various types can act as programmable functional components receiving signals from the material, the environment or both. In order to evaluate the viability of cells in the hybrid environment, we used a live/dead bacterial viability kit (BacLight, ThermoFisher), and quantified staining using fluorescence activated cell sorting (FACS) Figure 57 (c). Most cells remain viable on the inactive flexible and rigid materials.

The applied hydrogel contains bacterial cells that are responsive to the previously endowed material. The hygroscopic swelling of the active material will ensure the release and diffusion of the small molecules into the hydrogel. To evaluate how printed material and the biological layer interact we visualize and measure diffusion and cellular response over time as shown in Figure 57 (d), with biochemical substrate CPRG.

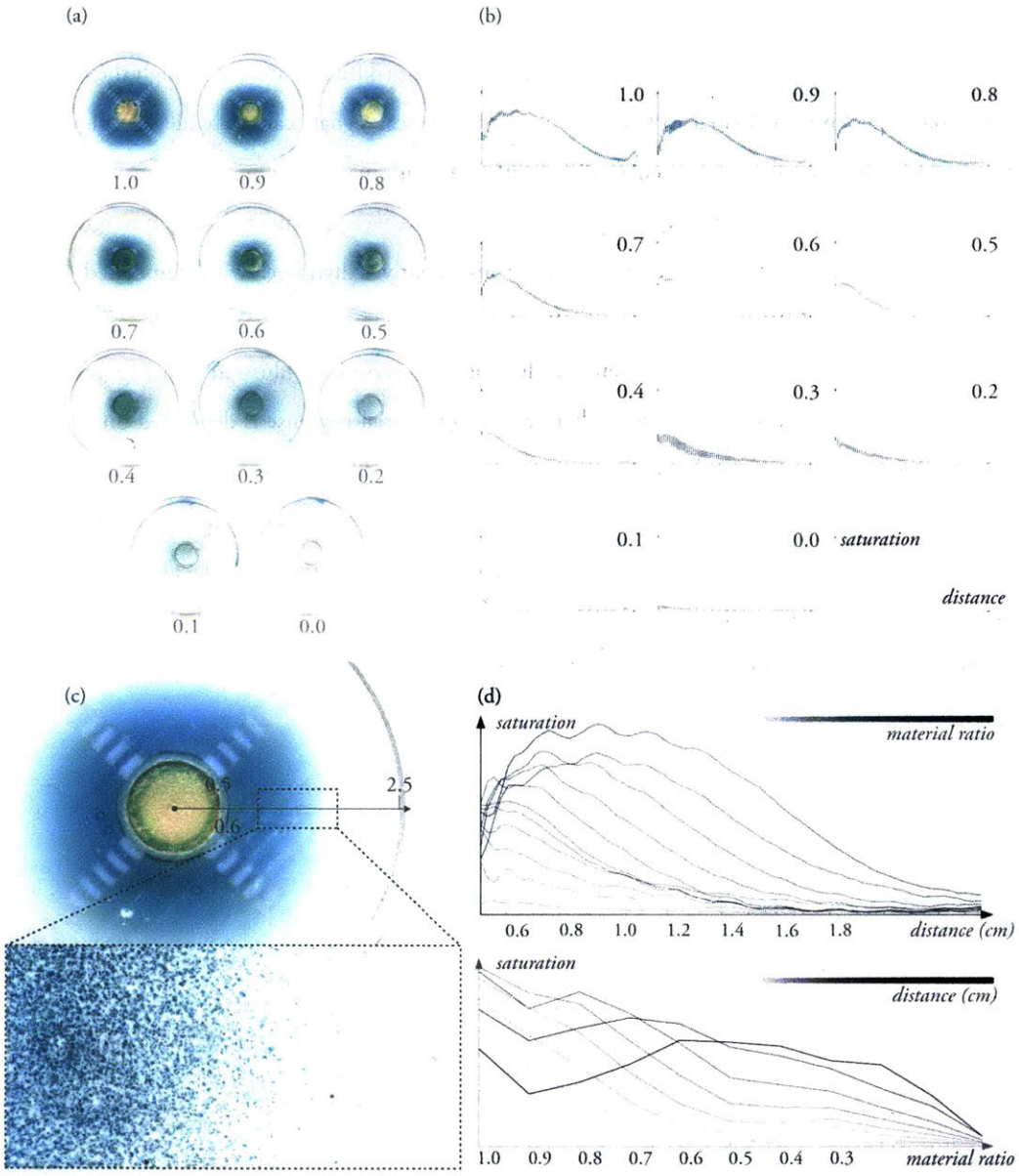


*Figure 59 – Templating of biological activity through material ratios.* (a) Circular disks with interior circular elements were additively manufactured and used for templating experiments. The interior elements are composed of material ratios between hygroscopic swellable material (active material) and rigid material (inactive material) while the exterior areas are made of rigid materials only. The ratios are given in parentheses and range from completely active material (1.0) to completely inactive material (0.0). Four samples per material ratio where used. (b) Here clear variation in degree of X-Gal cleavage through β-gal expression can be observed through pigment production. (c) Circular disks were fabricated with 5mm radius interior element, 2.5mm total radius, and spray-coated with a custom agar-media containing pUC19 *E. coli*. Small 1mm ridges were incorporated in order to reduce stresses during swelling caused by the hydrogel. A higher magnification view of the sample surface following induction is provided below. (d) High hygroscopic swellable material concentration (1.0 to 0.9) results in wider diffusion areas and higher pigment density, however peak density is achieved off center. Lowering hygroscopic swellable material concentrations (0.9-0.3) move the density maximum closer to the center, however, overall intensity is lost.

The introduced approach is utilized to spatially template bacterial response on multi-material additively manufactured parts. We show that the bacterial response to diffused signaling molecules is dependent on the material distribution of the part. Areas with high active material will cause large diffusion; while areas with low active material will cause smaller diffusion areas. Through the mixture of material types, precise spatial diffusion control of chemical signals can be achieved. Figure 59 shows additively manufactured circular disks with different material ratios between active and inactive materials used for the templating experiments. Parts were augmented by submerging in a solution of IPTG, X-Gal, Water and DMSO. Subsequently a hydrogel with embedded IPTG inducible *E. coli* pUC19 strain producing β-gal was applied to the surface of the part. After incubation for 30 hours at 37°C pigment production is observed, as illustrated in Figure 59(b). Evidently, physical diffusion transport of chemicals and bacterial response is depended on material mixing ratios between active and inactive material, where larger diffusion areas with off-center peaks are achieved by high active material concentrations, whereas controllably smaller and smaller diffusion gradients are achieved by introducing higher inactive material content. This allows clear characterization of biosignaling and therefore enables designable spatial templating of bacterial activity on additively manufactured geometries with multiple materials.

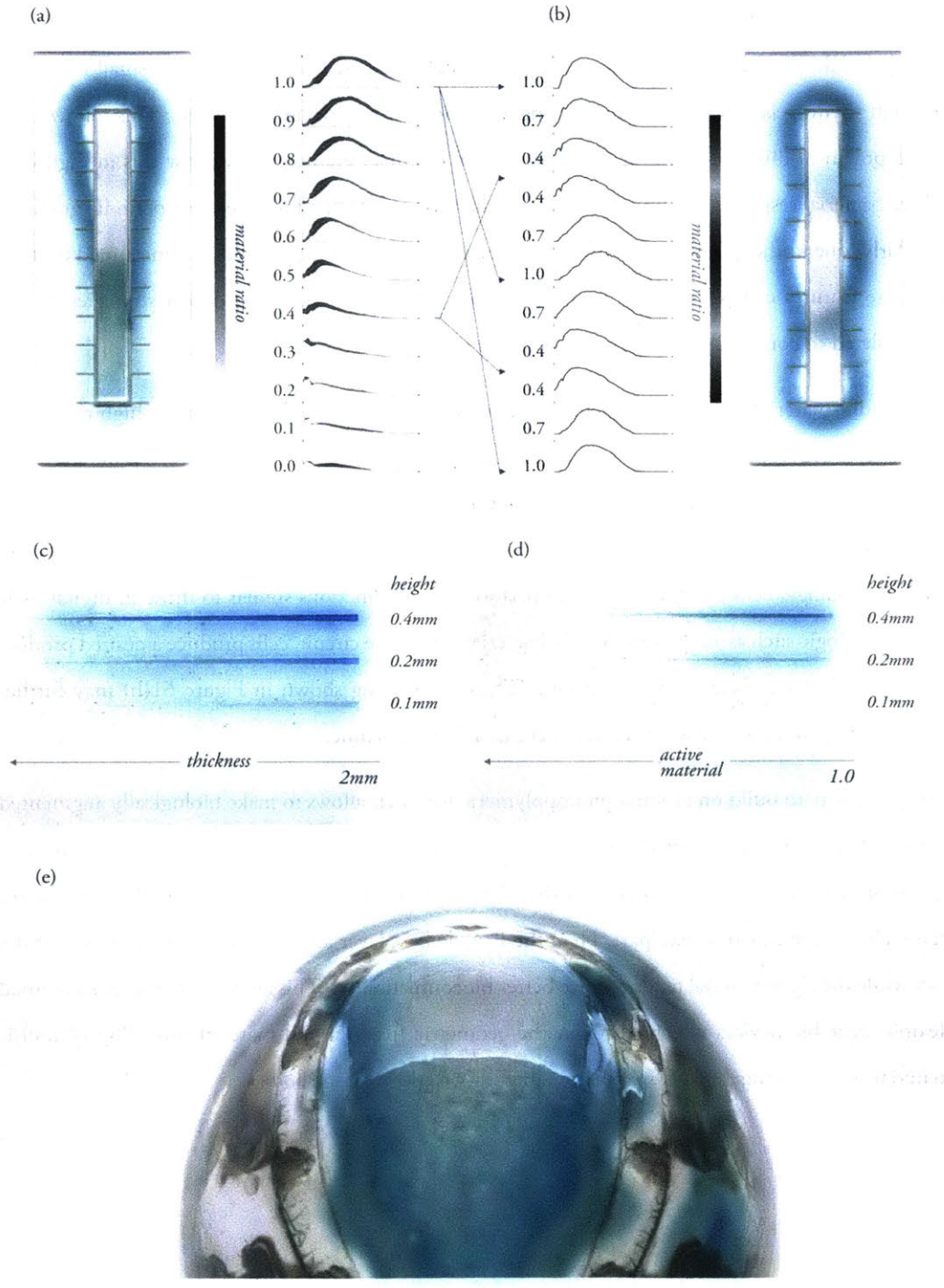


*Figure 60 – Rational design method through bacterial response characterization.* (a) Shows a part with linear material gradient from active to inactive material and corresponding bacterial response curves (n=3, standard deviation shown as graph thickness) associated with each material mixing ratio. These can be transferred to desired reposes curves (b) which then can be associated with material ratios to precisely design parts with the predicted bacterial response. Similarly, the geometry of the active material regions plays a significant role in the pattern formation processes. This is shown in (c) and (d) where height

and thickness of the active material regions are varied. Significantly, these design strategies carry over to more complex product scale objects as shown in (e).

Coupling volumetric description of material-distributions, the possibility to print these descriptions through multi-material 3D printing and experimentally obtained diffusion rates of small molecules through hydrogels, we can rationally design chemical diffusion gradients. This allows the development of diffusion patterns on surfaces from exemplar gradients. We show this in Figure 60 where bacterial response of a linear material gradient is recorded and mapped to a periodic gradient. Similarly, due to the geometric control in high resolution 3D printing processes, fine-tuned bacteria response features can be achieved as shown Figure 60 (c) and (d). These design strategies can be extrapolated to complex geometries as shown in Figure 60 (e).

Since multi-material voxel printing allows to place droplets of dissimilar materials at high resolution to fabricate heterogeneous parts, we can leverage this in our system. In Figure 61 we show the potential for multiple diffusion outputs in one fabricated part with mixing of adjacent diffusion gradients. This enables chemical interaction on the surface in predefined areas. Furthermore, in synthetic biology, cells can be designed to perform logical functions similar to those in digital logic or boolean logic such as an AND gate. In a bacterial AND gate circuit, cells produce a desired product if two signals are present at the same time. Thus, the mixing shown in Figure 61(b) may further increase the potential to spatially pattern cells in a desired manner.

The possibility to build on existing photopolymeric materials allows to make biologically augmented parts with a multitude of functionalities inherited from the fabrication technology. An example of this is shown in Figure 62, where inactive flexible materials, inactive rigid materials and active materials are combined in one part. Here the flexible base layer allows twisting and bending of the part while the rigid material tends to have better biocompatibility. This allows to fabricate functional flexible wearable devices which, through the geometric freedom and material tunability of multi-material voxel printing, enable seamless adaptability to the wearers' body.

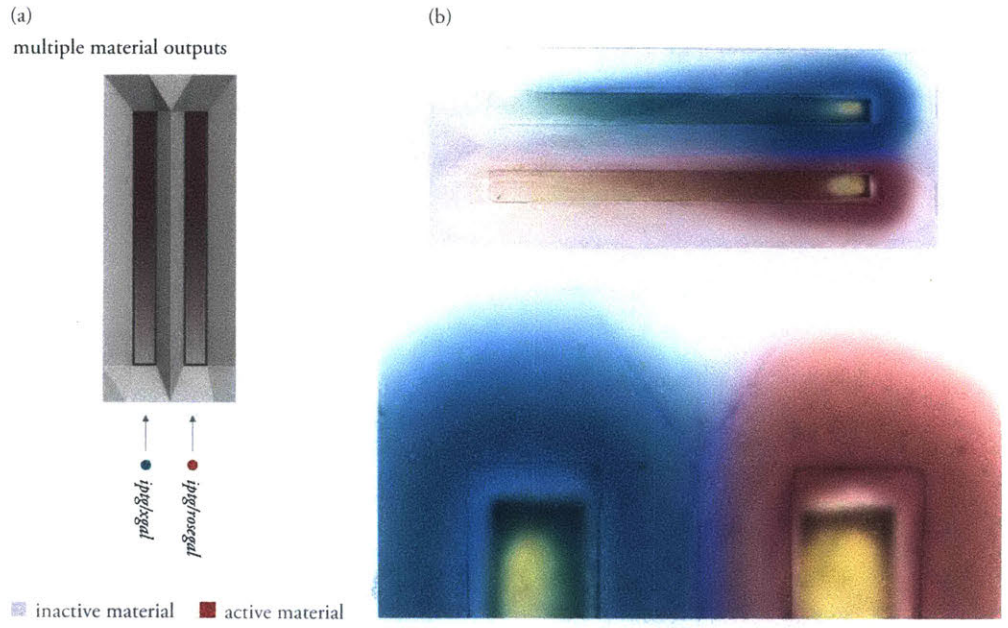


*Figure 61 – Part augmented with small molecules to allow multiple substrate outputs.* (a) Specification of part with two distinct active material gradients. (b) Part after incubation for 24 hours showing mixing of two outputs in areas with high active material concentrations and separation in areas with lower active material concentration.

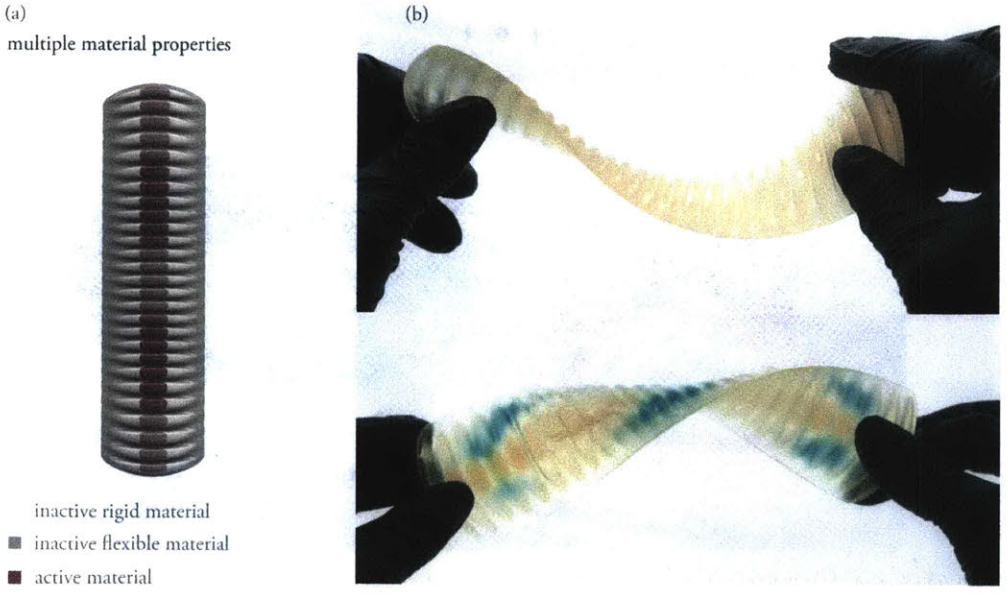


*Figure 62 – Heterogeneous additively manufactured part made out of flexible inactive, rigid inactive and active materials.* (a) Specification of material characteristics and continuous gradients between material properties for a flexible base layer with active periodic material gradient. (b) Fabricated flexible part before (upper) and after incubation (lower). The part stays flexible after incubation.

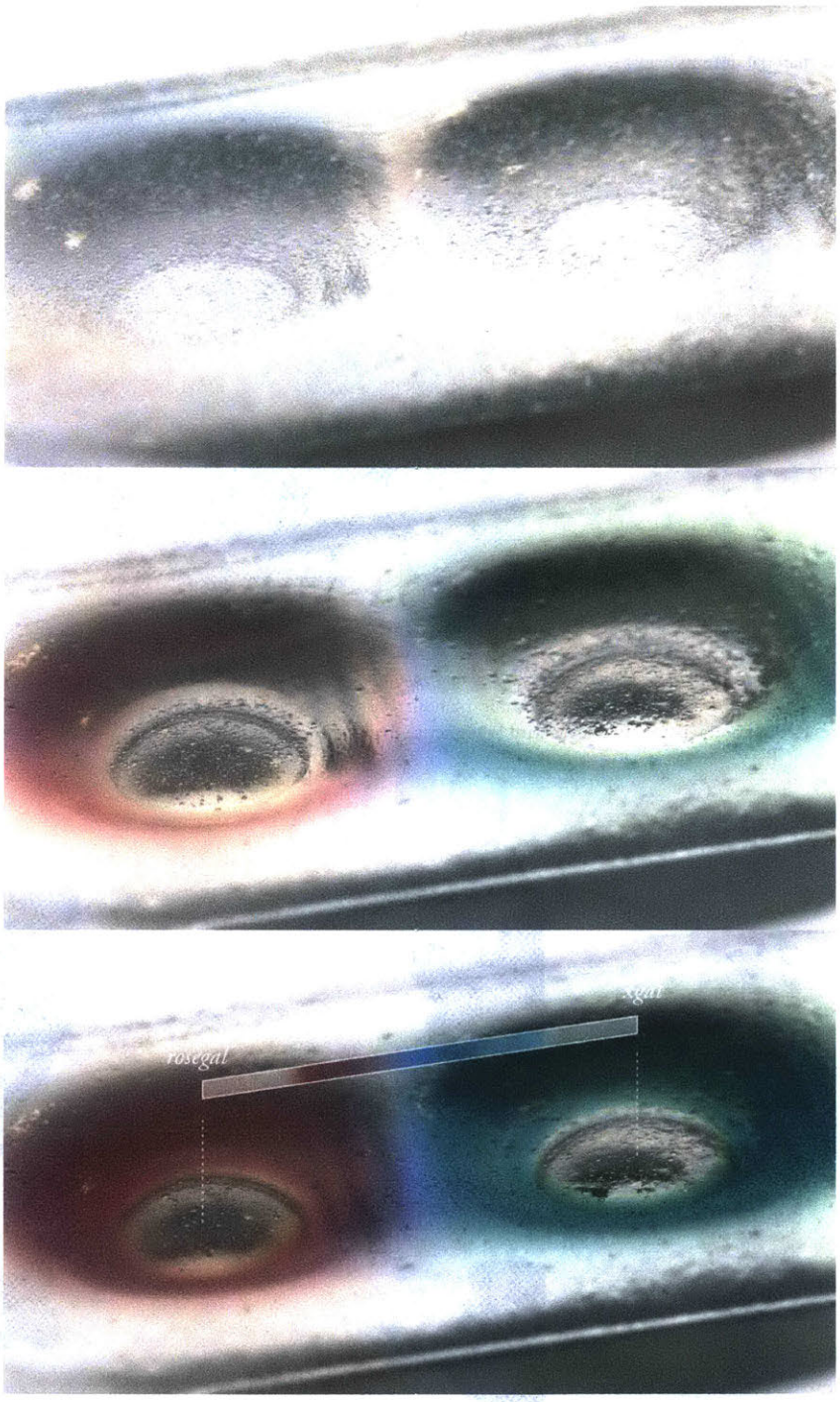


*Figure 63 Close up of the multiple output substrate mixing and bacterial response.* Here a clear gradient from magenta to cyan can be observed at the interface where the evolving chemicals meet.

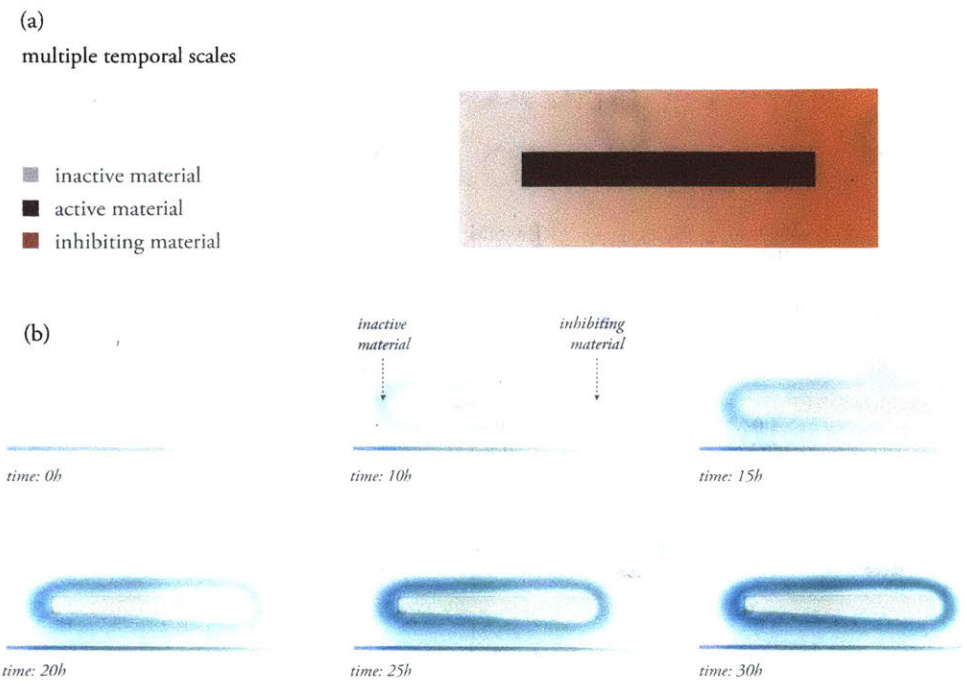


*Figure 64 – Multi-material fabricated part showcasing temporal control over bacterial activity.* (a) Specification of a part with active material and gradient between inactive and inhibiting materials. (b) The temporal response shows that regions with inactive material react faster than areas where growth is inhibited.

While the signaling process is time dependent by virtue of the diffusion and response mechanism, it is further possible to control the temporal response of the bacterial cells embedded in the hydrogel by material property variations. By using a material which is slightly cytotoxic, we can temporally inhibit growth and thereby control the bacterial response over time. An example of this potential response tuning is shown in Figure 64. While the temporal difference in this example is minimal, further research may allow for time guided release of bacterial products.

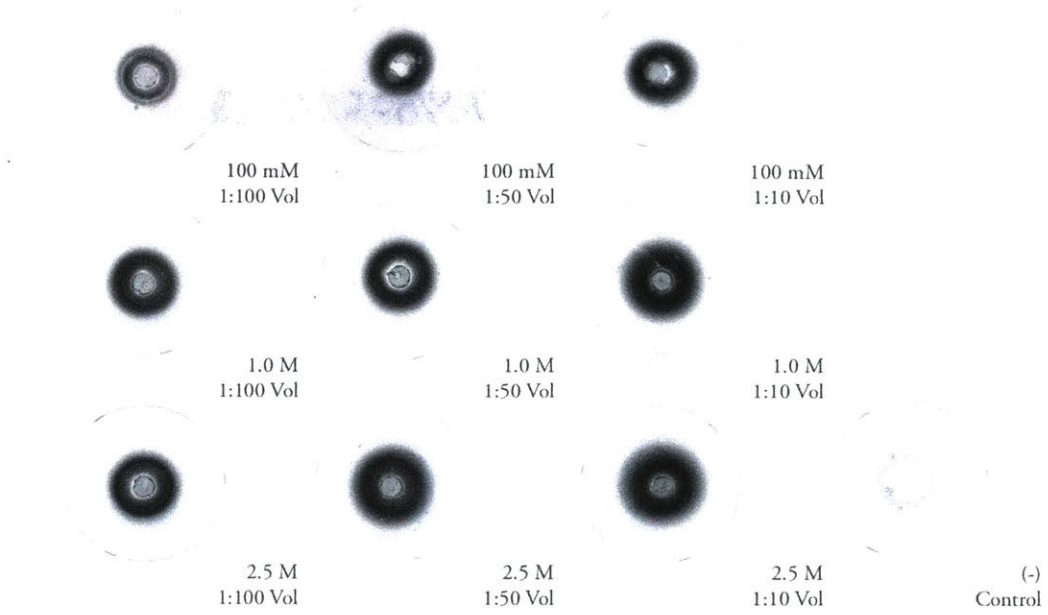


*Figure 65 – Inverted (to aid in visualization) transillumination photographs of GFP expression response to biosignaling resin test pieces.* IPTG was incorporated into the liquid resins pre-curing. Different test parts were then created adjusting inducer concentrations (rows) and volumetric ratios of inducer/DMSO (columns) and plated on LB Agar bed with IPTG/GFP strain. An appreciable fluorescence response can be observed even at low volumes and low inducer concentrations.

We can directly incorporate bioactive small molecules into pre-cured photopolymer resins, as opposed to embedding them post-print. This method allows spatial control of small molecule placement at the voxel level using volumetric material modeling methods. Furthermore, through the use of several resins with distinct small signaling molecules this enables the placement of multiple signals in parallel, and the tunable mixing of distinct signals natural to the multi-material printing process.

To understand the viability of this method, we prove the preservation of inducer functionality when solubilized in photopolymer resin and after undergoing curing conditions Figure 65. Small molecule IPTG in DMSO solution was mixed into photopolymer resin at a range of different volume ratios and chemical concentrations (1:100, 1:50, 1:10; 100mM, 1.0M, 2.5M). Each iterant resin mixture was UV-cured into a solid test piece, and plated onto LB-amp dishes with IPTG/GFP strains. Successful bacterial response to the biosignaling resins was measured as a GFP fluorescent signal, as compared to the bacterial response to the unmodified resin control test piece. This test shows that the photopolymer resin can maintain the biosignal functionality of IPTG, and release the

biomolecules from its solid state. Since, the modification to the resin is minimal, these types of custom resins can be used in the multi-material 3D printing process.

# Modeling

*Modeling of Living Hybrid Material Systems*

In this section we develop a model to quantitatively predict the behavior of the synthetic living material systems. The functionality for the heterogeneous template is reliant on two processes: Diffusion of previously endowed signaling chemicals over the surface of the 3D printed part and response of the adjacent cells to the signaling molecules. By virtue of the arbitrary complexity of the shapes producible by our method we are able to fabricate adaptive 3D printed wearable devices. Therefore, compared to previous models our model for diffusion transport needs to take such arbitrary configurations into account. We can approximate the transportation of inducer over a regular closed surface $\Gamma \subset \mathbb{R}^3$ by

$$\partial_t c(x,t) = \mathrm{D}\nabla_\Gamma^2 c(x,t)\ \forall x \in \Gamma \text{ and } \mathrm{t} > 0, \quad (1)$$

$$c(x,0) = c_0(x)\ \ \forall x \in \Gamma \quad (2)$$

Where $\nabla_\Gamma^2$ is the surface Laplace-Beltrami operator, $c(\cdot,t)\colon \Gamma \to \mathbb{R}$ is the concentration of diffused signaling chemicals, $t \geq 0$ is time, $D$ is a diffusion coefficient of the embedded chemicals, and $c_0\colon \Gamma \to \mathbb{R}$ is the initial concertation of chemicals endowed in the heterogeneous template dependent on the material gradients form active to inactive material. Here the diffusion coefficient for IPTG as an example can be estimated to be $D_{IPTG} = 3 \times 10^{-10}\frac{m^2}{s}$ [104]. Initial values for inducer are either known according to the developed bio signaling resins or can be estimated form weight and area expansion of the hygroscopic swelling process Figure 66(a). We note that there are no boundary conditions as it is assumes that the surface $\Gamma$ is closed otherwise the represented shape would not be 3D printable.

For spatial discretization we assume the regular surface $\Gamma$ is given as a simplicial mesh $M$ with vertices $V_M = \{v_1, \dots, v_n\}$ , edges $E_M = \{e_1, \dots, e_k\}$, $e_j \in V_M \times V_M$ and faces $F_M = \{f_1, \dots, f_m\}, f_k \in V_M \times V_M \times V_M$ and embedding $p_i = p(v_i)\colon V_M \to \mathbb{R}^3$. The concertation can be approximated by a piecewise linear function $c_i = c(v_i)\colon V_M \to \mathbb{R}$ on the mesh. The discrete laplace-beltrami operator of the concentration [28] then is given as

$$\nabla^2 c(v_i) = \frac{1}{2A_i}\sum_{v_j \in N(v_i)} (cot\alpha_{i,j} + cot\beta_{i,j})(c_j - c_i) \quad (3)$$

Where $A_i$ is one third the area of all triangles incident on $v_i$, $N(v_i)$ are the neighboring vertices connected by and edge, and $\alpha_{i,j}$ and $\beta_{i,j}$ are the angles opposing the corresponding edge. Since the laplacian is a linear operator this can be written as $Lc$, where $L \in \mathbb{R}^{|V|\times|V|}$ is the matrix of cotangent coefficients and $c \in \mathbb{R}^{|V|}$ is the piecewise linear approximation of concentrations over the surface. For temporal discretization we aim for large time steps essential for fast design iteration. Thus, for temporal discretization of (1) can we facilitate an implicit integration scheme such that $c(t+h) = c(t) + hDc(t+h) \Leftrightarrow (I - hDL)c(t+h) = c(t)$ [19].

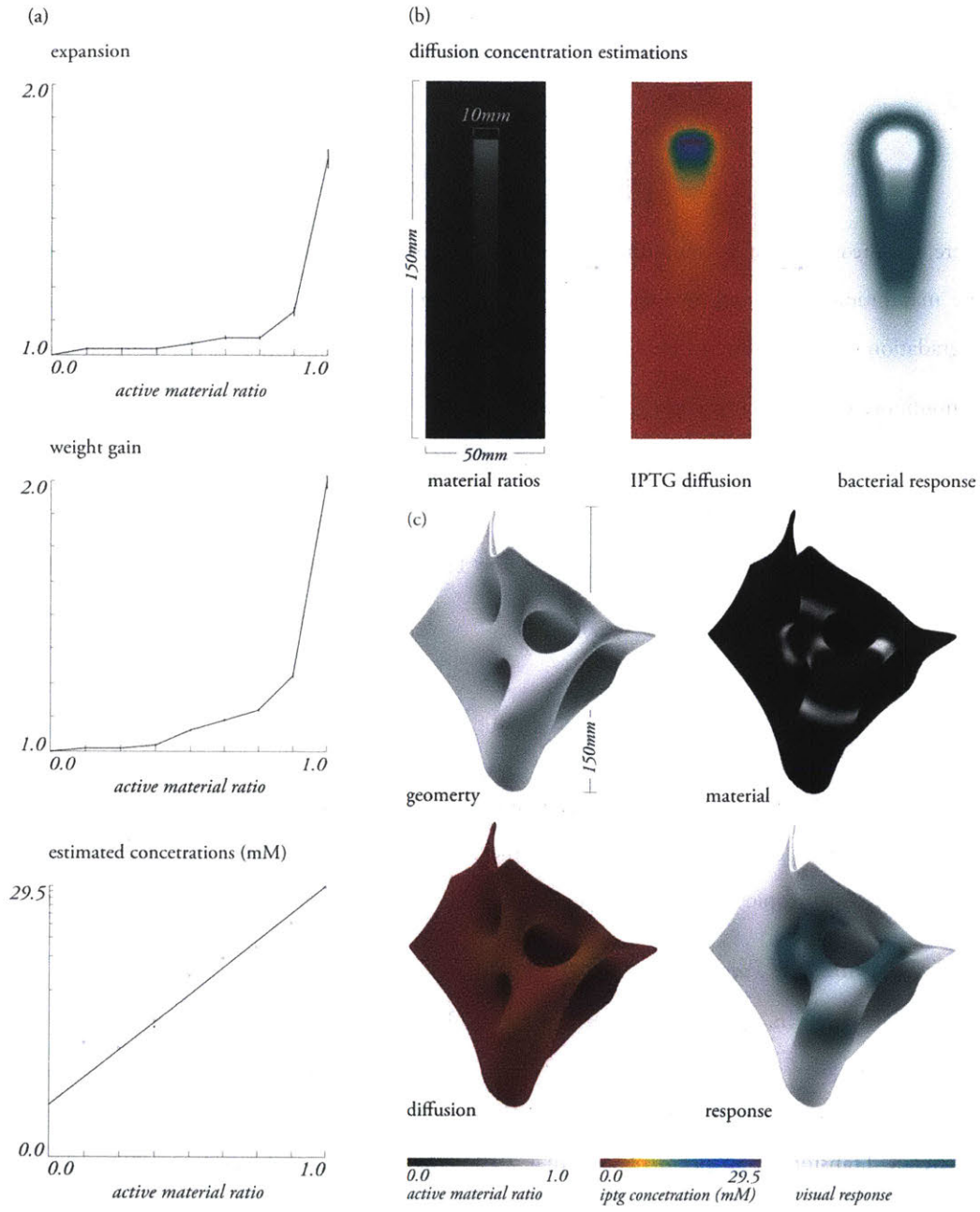


*Figure 66 – Modeling of IPTG diffusion and bacterial response.* (a) Shows the expansion and weight gain (upper and middle graph) of material mixtures between active material and inactive material after 24 hours (n=3). The lower part shows estimated IPTG concentrations ($R^2 = 0.9158$). We plot IPTG diffusion and bacterial response for a linear material gradient from active to inactive material in (b) which showcases remarkable resemblance to the material gradients in Figure 60(a). (c) Shows more sophisticated geometry and material logic. Here active material regions are assigned by member thickness of the scaffold. After induction more intense bacterial response can be observed around thinner members of the structure.

Bacterial response through GFP expression can be modelled through the coupled system of differential equations [105]:

$$\frac{\partial n}{\partial t} = P - m \cdot n - \mu \cdot n - D_n \quad (4)$$

and

$$\frac{\partial f}{\partial t} = m \cdot n - \mu \cdot f - D_f \quad (5)$$

Here, $n$ is the is the content of nonfluorescent GFP, $P$ is promoter activity, $m$ is a constant describing the maturation from nonfluorescent GFP to fluorescent GFP, q is the growth rate, $D_n$ is the degradation rate of nonfluorescent GFP, $f$ is the fluorescent GFP content, $D_f$ is the degradation rate of nonfluorescent GFP. Promoter activity can be estimated by the Hill function $P = \gamma \frac{C^h}{C^h + K^h}$, where $\gamma$ is the maximal expression level of the Promoter, $C$ is the concentration of IPTG form the previous diffusion, $K$ is the concentration of $C$ at which $P$ equals $\frac{1}{2}\gamma$ and $h$ is the Hill coefficient. From [105] again we can estimate these coefficients to be $\gamma = 1000s^{-1}$, $K = 0.3mM$, $h = 2$, $m = 1.16 \times 10^{-2}s^{-1}$ and $\mu = 1.20 \times 10^{-2}s^{-1}$.

## Materials & Methods

### *Template fabrication*

Models for templating experiments through soaking were fabricated using a Stratasys Objet Connex 500 multi-material 3D printer. Materials in the fabrication process were rigid, clear VeroClear (RGD810), hygroscopic swelling Support material (SUP705) and flexible Tango material (FLX 930).

### *Bacterial Strain and Plasmids*

An *Escherichia coli* (*E. coli*)K12 strain derivative (NEB Turbo, F' proA$^+$B$^+$ lacI$^q$ ΔlacZM15 / fhuA2 Δ(lac-proAB) glnV galK16 galE15 R(zgb-210:Tn10)Tet$^S$ endA1 thi-1 Δ(hsdS-mcrB)5) is used as the host strain in all templating experiments. Cells were cloned via New England Bio Labs High Efficiency Transformation protocol with pUC19 Vector (NEB), containing Ampicillin resistance and reporter gene lacZ for Isopropyl β-D-1-thiogalactopyranoside (IPTG) regulated beta-galactosidase (β-gal) production. Single colonies are selected and grown in an overnight culture of LB supplemented with 100 μg/mL ampicillin (LB-Amp), at 37.5°C.

### *Cell Viability Assay*

Cytotoxicity of the 3D printed substrate materials were assessed using a LIVE/DEAD BacLight Bacterial Viability Kit (Thermofisher). Quantification was done using fluorescence activated cell sorting (FACS).

*Template Diffusion Characterization*

A post-printing soak step is required to introduce small molecules to the printed plastics. 3D printed pieces are submerged in an aqueous mixture of inducer molecule, IPTG, and a histochemical substrate, 5-bromo-4-chloro-3-indolyl-β-D-galactoside (X-gal), for 12h at 4°C. The soaking solution is created by dissolving powder X-gal (VWR, 20mg/ml) and IPTG (VWR, 24mg/ml) in DMSO. The solution is then diluted with deionized $H_2O$, at a 1:1 ratio, on ice, for a resulting concentration of 50mM IPTG, 25mM X-gal. After soaking, the 3D printed templates are removed from their bath and spray-coated with a custom agar-media and pUC19 *E. coli*. This application of cells and media achieves even culturing, within a ~1-2mm thick agar layer, across the printed shapes. The growth media mixture is based on minimal media (Teknovo M9), that is supplemented with 0.8% Sucrose (VWR amresco), 0.1% Casamino acids (VWR amresco), 1% Agar (Bacto™ Agar) and 1% Agarose (VWR amresco). The minimal media mixture is brought to 100° C, to melt, and then cooled to 45° C, for the addition of pUC19 *E. coli* overnight stock (1:200) and Ampicillin. The mixture is stirred vigorously for even distribution before solidification, and transferred into a 50ml glass bottle with a fine mist sprayer (Vivaplex, 50ml amber glass bottle). Each piece is spray-coated with 15 spray strokes from the mist sprayer. After coating, the pieces are put into petri dishes, sealed with parafilm and incubated for 30h at 37° C.

*Preparation and Testing of 3D Printable Bio Signaling Resins*

Custom photopolymer resins integrated with biochemical signal molecules were created by mixing incremental concentrations and ratios of DMSO-solubilized inducer, IPTG, with uncured resin in low light. To rapidly manufacture material test pieces, a VeroClear tray was printed with 3x3 circular wells (10mm in diameter, 3mm in depth). Resin-IPTG mixtures generated for characterization tests were then pipetted into tray wells (180uL), cured under UV light for 2hrs, and removed from tray with a scalpel. Testing of preservation of biochemical functionality in cured photopolymer consisted of generating material test piece compositions with IPTG concentration (100mM, 1M, 2.5M) and ratio to resin (10%, 5%, 1% volume) variants. LB-Amp plates were prepared for each test piece by applying 100uL IPTG (50mM) in DMSO and 100uL of a IPTG/GFP overnight stock in a 1:10 LB dilution. Test pieces were placed in the center of the LB-Amp plate, and incubated at 37°C for 30hrs, and imaged for GFP response on a Blue Light Transilluminator (Invitrogen, Safe Imager 2.0).

*Characterization of Material Expansion and Weight Gain*

Material expansion in was measured by submerging 3D printed parts (disks with 30mm diameter and 3mm height) with different material ratios (0.0, 0.125, 0.25, 0.375, 0.5, 0.625, 0.75, 0.875, 1.0) between SUP705 and RGB810 in water and optically measuring the area scaling factor. Disks were submerged for 24 hours, when maximal expansion was achieved. Optical measurements were taken by an Epson Perfection V600 Flatbed Scanner and evaluated in Fiji. Weight gain was measured by submerging 3D printed parts with different material ratios between SUP705 and RGB810 (0.0, 0.125, 0.25, 0.375, 0.5, 0.625, 0.75, 0.875, 1.0) in water (cubes with 10mm side length) and weighing them after 24 hours.

# Conclusion

Herein we have shown the integration of programmable material systems with programmable biological components through the combination of multi-material 3D printed templates and hydrogels embedding living entities. Transferring capabilities of synthetic multi-material systems to programmable living materials was shown to be a promising strategy for engineered living materials with a multitude of potential applications. We have shown the potential to establish exogenous gradients through material property variation on arbitrary surface geometries, biological templating by material heterogeneity, flexible and bendable biologically augmented devices and multi input/output arrays. Finally, we propose a model utilizing state-of-the-art techniques from geometry processing to predetermine, visualize and design with signal diffusion in heterogeneous hybrid living materials. This works paves the way towards design at the intersection of advanced materials systems and programmable biological components. Potential applications may emerge as wearable healthcare products such as customizable cosmetic, as spatial templates for functional bacteria products or spatial and temporally differentiated bacterial sensing devices.

# Vespers – Series 3

*"What remains once life has been lived? Can the death mask drive the formation of new life? The third series revolves around death and rebirth, denoting both spiritual incarnation and biological recapitulation. In it, the masks become habitats for microorganisms and sites for the creation of new life.*

*Devoid of cultural expressions and nearly colorless, these masks are paradoxically the most alive of the three series. They 're-engineer' life by literally guiding living microorganisms through minute spatial features inside the artifacts of the dead. Transitioning from vessels of representative neuro-vasculature to actual biological urns, they mark a new cycle of life and the notion of continuation.*

*Their microorganisms are distributed according to the spatial logic provided by the second series. The microorganisms and/or their byproducts reinterpret the color palette of the first series, thereby biologically recreating their cultural precursors.*

*The faces are no longer preserved but have transformed into sites of and for new life."* [2]

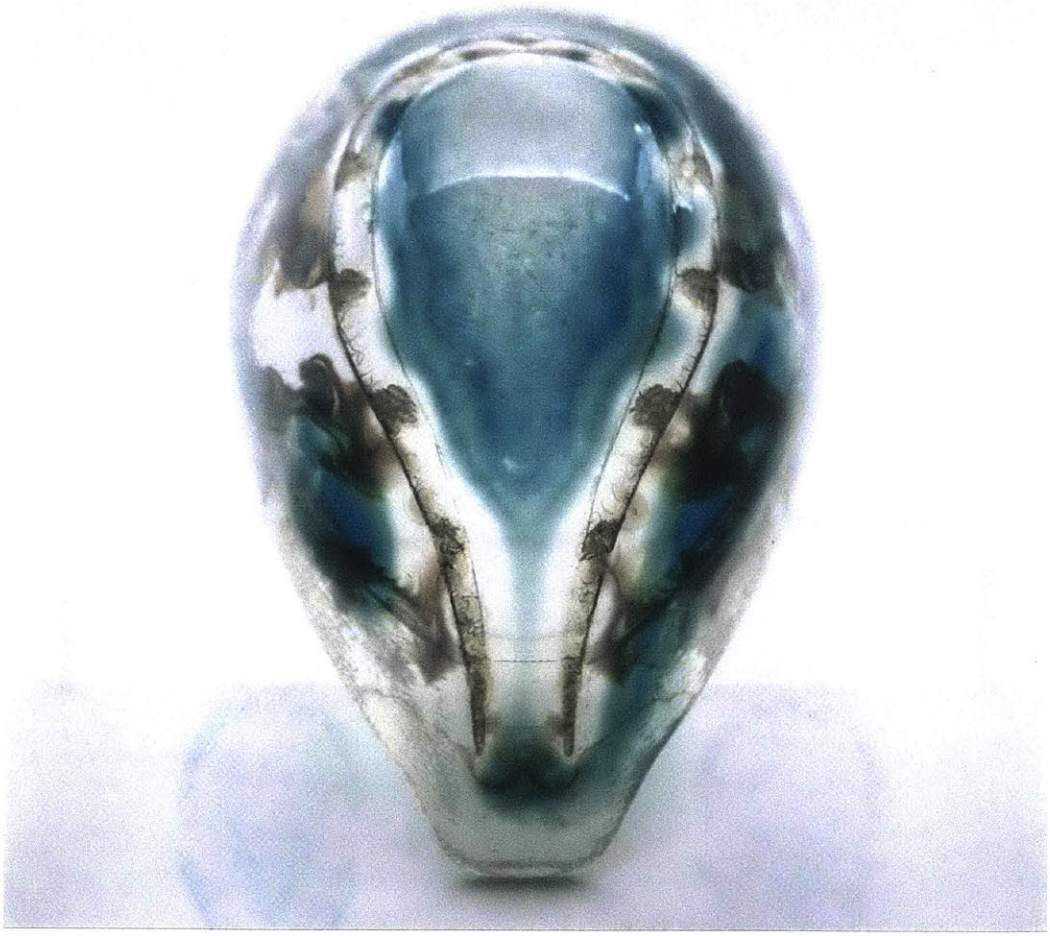

*Figure 67* – Vespers. *Series 3 Mask 2. Front view after incubation.* Designed by Neri Oxman and members of The Mediated Matter Group for The New Ancient Collection curated and 3D printed by Stratasys, 2016.

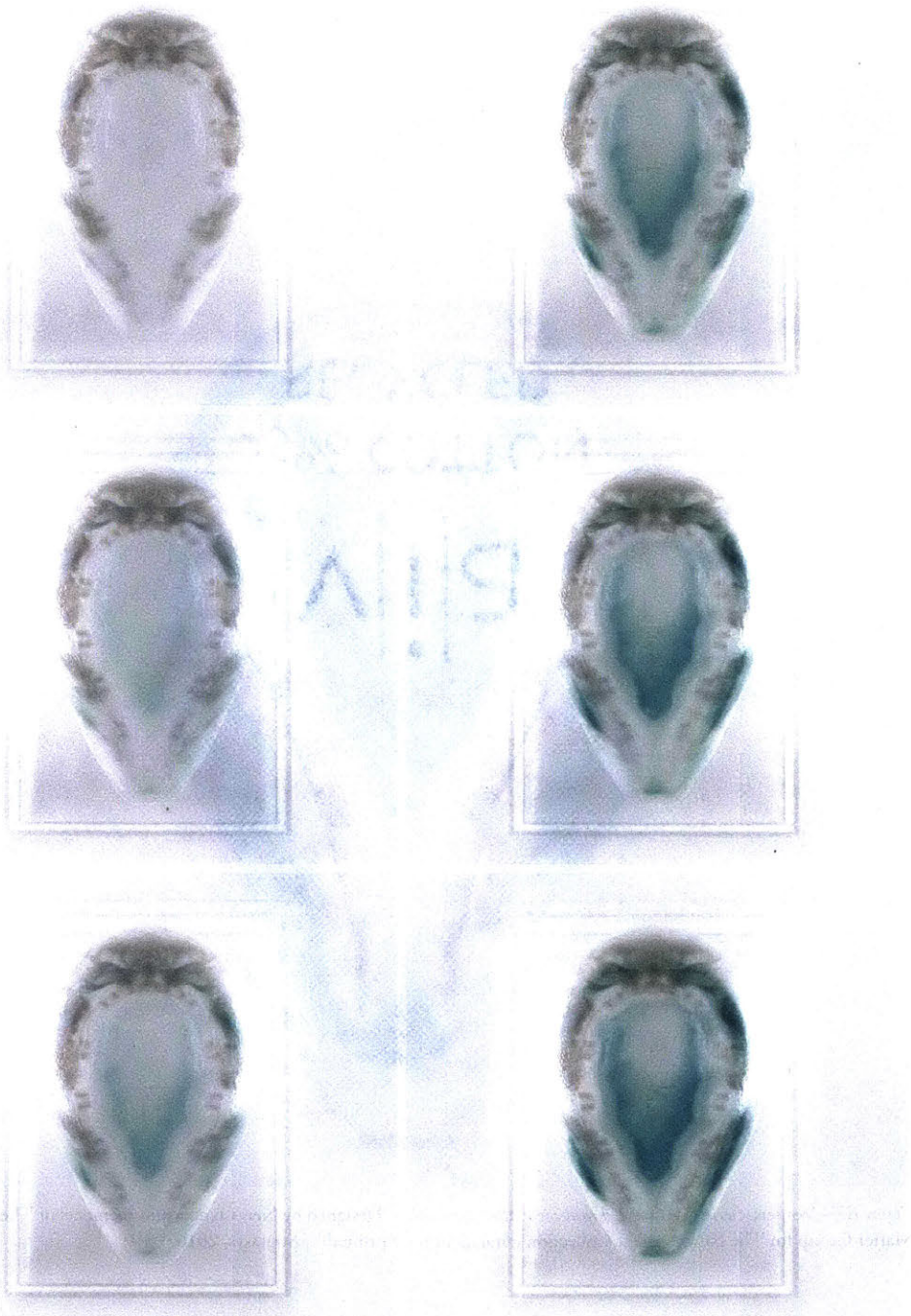

*Figure 68* – Vespers. *Series 3 Mask 2. Material induced pattern formation over time filmed during incubation.* Designed by Neri Oxman and members of the Mediated Matter Group for The New Ancient Collection curated and 3d printed by Stratasys, 2016.

*Figure 69* – Vespers. *Series 3 Mask 2. Side view after post processing.* Designed by Neri Oxman and members of The Mediated Matter Group for The New Ancient Collection curated and 3d printed by Stratasys, 2016.

*Figure 70* – Vespers. *Series 3 Mask 2. Front view after post processing.* Designed by Neri Oxman and members of The Mediated Matter Group for The New Ancient Collection curated and 3D printed by Stratasys, 2016.

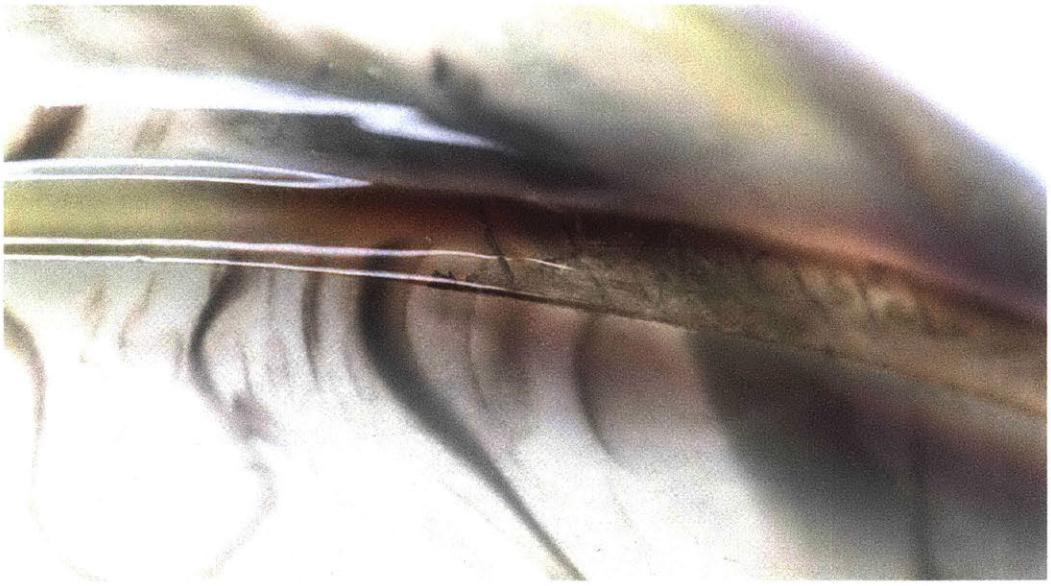

*Figure 71* – Vespers. *Series 3 Mask 1. Close up view.* Designed by Neri Oxman and members of The Mediated Matter Group for The New Ancient Collection curated and 3D printed by Stratasys, 2016.

*Figure 72* – Vespers. *Series 3 Mask 1. Close up view.* Designed by Neri Oxman and members of The Mediated Matter Group for The New Ancient Collection curated and 3D printed by Stratasys, 2016.

# Programmable Growth

To enable design with biological systems, the introduction of a template—be it a material, an exogenous gradient, or light—seems inevitable. Yet, biological pattern emergence can be self-sufficient starting from a single cell, through an interplay of growth and endogenous gradients, simple rules encoded in DNA drive the formation of matter from the embryonic to an almost arbitrary complexity. Recent advances in synthetic biology allow encoding rules for stochastic cell differentiation, endogenous establishment of small molecule gradients and the logic based repose to these chemical gradients by activation and repression of cellular behavior. Here, we will investigate how to computationally design with these 'biological primitives' and how this process can give rise to embryonic patterns that could lead to larger 2D skins of a living material or a complex structure.

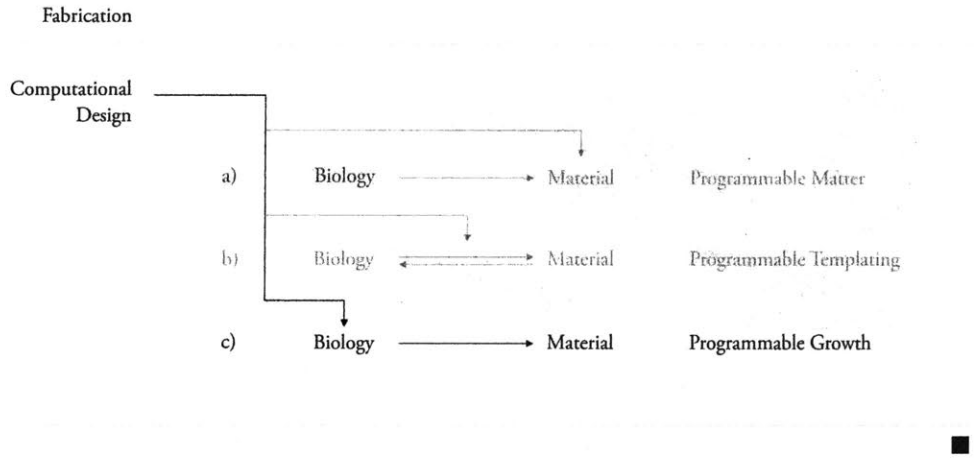


*Figure 73 – The programmable growth approach.* Applying computational design to biological systems to give rise to material architectures.

Designers often specify the final form of a material object prior to engaging with methods by which to fabricate or manufacture it. Indeed, computer-aided design tools—such as those encountered in mechanical engineering (e.g., AutoCAD, Solidworks etc.)—enable a user to specify a desired shape. The 3D design file can then be used to build the part to specification via additive or subtractive manufacturing. Here, first we propose a program to develop a framework with the ultimate objective to bring this capability to biology. In this proposed computational design environment, a final form or pattern-formation is specified, and then it is methodologically determined *how* to design a progenitor cell that can differentiate and grow into the desired form. This requires a radically different approach in two seemingly unrelated areas. First, in theoretical developmental biology, tools focusing on the bottom-up accurate simulation must allow the incorporation of top-down design elements

from synthetic biology. Secondly, in design, tools must enable top-down construction through bottom-up simulations of growing living organisms instead of static elements. Secondly, we present a prototypical implementation of a computational bottom-up approach for simulating the development of a single progenitor cell—or a collection thereof—over time. Thus, a simple framework will be established that describes the behavior of the generalized progenitor organism, including its representation, basic growth and division, differentiation, intercellular interaction, signaling and reaction to endogenous gradients.

# Engineering Living Materials – Programming seed cells to grow and differentiate into defined patterns

Christoph Bader[1], Sunanda Sharma[1], Rachel Smith[1], Neri Oxman[1]
In collaboration with Christopher A. Voigt[2] *et al.*, Timothy K. Lu[2] *et al.*, and Cullen R. Buie[3] *et al.*

1. MIT Media Lab, School of Architecture and Planning, Massachusetts Institute of Technology, 75 Amherst St. Cambridge, MA 02139, USA.
2. Department of Biological Engineering, Massachusetts Institute of Technology, 500 Technology Square, Cambridge, MA 02139, USA.
3. Department of Mechanical Engineering, Massachusetts Institute of Technology, 77 Massachusetts Ave, Cambridge, MA 02139, USA.

## Introduction

Computer-aided Design (CAD) tools, such as those used in architecture and mechanical engineering (*e.g.*, AutoCAD, or CATIA), enable the user to specify a desired geometrically defined shape. Here the ultimate objective is to bring this capability to biology in which a final form, texture or pattern is specified, after which it is determined *how* to design a seed cell that can differentiate and grow into the desired form. Achieving this objective requires a *radically* different approach in two seemingly unrelated areas. First, tools and techniques associated with the field of theoretical developmental biology, must be designed such that they focus on, and enable, *bottom-up* simulation of communicating engineered cells. Second, tools and techniques associated with the field of design (CAD-CAE-CAM) must be built such that they focus on, and enable, *top-down* construction of growing living organisms instead of static elements. Our aim is to lay the foundation for a design environment that allows a user to computationally grow a desired pattern and encode the growth process into a living system, thereby offering a bottom up and top down rule-based growth strategy to support the generation of a desired grown part (Figure 1).

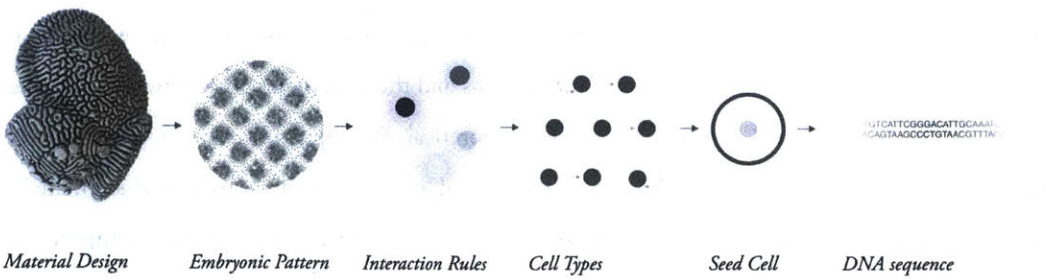


*Figure 74 – Design flow to create a single DNA sequence that controls the differentiation of a seed cell into a material.*

The shape formation process will be broken down into the design of a single seed cell programmed to grow and differentiate into a defined shape and pattern. The seed cell will contain a synthetic

DNA sequence that encodes all of the necessary regulation controlling these processes. As the seed cell grows, it will undergo two steps of differentiation. First, a stochastic switch will cause the seed cell to randomly differentiate into a set of cell types. These cell types are defined by the expression of a recombinase that permanently modifies the initial DNA sequence so that each cell type contains a different synthetic regulatory network. The networks encode cell-to-cell communication channels and simplified circuitry, gleaned from developmental biology, to drive pattern formation. This includes logic, feedback loops, and stable chemical gradients. The networks drive the formation of the final pattern as the cells continue to grow. After the cell population crosses a given threshold, a second differentiation circuit will be triggered, that (1) results in permanent excision of the developmental network; (2) causes expression of a cell type-specific transcription factor, and; (3) invokes the deletion of a gene required for growth.

We will experimentally create seed cells forming 2D arrangements of $10^3$-$10^8$ cells that serve as "embryonic patterns" that could lead larger 2D "skins" of a living material or a complex 3D structure. Advanced computer aided design tools and algorithms will be used to (1) computationally determine embryo patterns resulting from designed genetic circuits and; (2) investigate cell interaction rules that enable cells to grow into an embryo with a larger scale structure. *E. coli* has been chosen as the model system. However, the computational and imaging platforms will be generalized to include other environmental bacteria (*e.g.*, Bacilli) and fungi (*e.g.*, Mycocelium) due to their potential role in growing functional structural materials [106].

## Background

There are well-developed theories describing how cell signaling leads to patterns in biology. Most of these were developed around 50 years ago and have remained largely unchanged, including simple reaction-diffusion systems [107] (Turing patterns), positional information [108] (gradients), and logical rules [109] (cellular automata). In comparison, our approach is innovative in two ways. First, we are considerably expanding the classes of interactions and the underlying physics by which living systems form patterns and structures. Second, theoretical development only involves growth algorithms (i.e., the interactions between cells are defined and then the final pattern is simulated). Here, we attempt to develop tools to go the other way: define a final form and then compute the necessary cellular interactions.

Genetic circuit design has advanced significantly, but circuits that reproduce even simple developmental protocols (Turing patterns, gradients, or cellular automata) have not yet been

established. Recently, the Voigt Lab released the software Cello [110], which can be viewed as the state-of-the-art in genetic circuit design. However, it is yet impossible to incorporate memory, feedback loops, analogue computation, and communication between cells, all of which are required for the creation of developmental circuits.

A central capstone of such research will involve the creation of an advanced CAD software package where a user draws a desired pattern of cells and this pattern is then automatically compiled into a DNA sequence. The software will work with new genetic circuits that implement the fundamental units of computation required for cells to autonomously form patterns. The ability to program embryogenesis is a transformative step in biology, representing the first step to the growth of advanced biological forms, including materials. Seed cells will be constructed to demonstrate this capability.

## Methods

The elemental genetic circuits necessary for differentiation and the formation of patterns will be developed first. Imaging technology will be developed concurrently, with immediate applications relating to the quantification of cell-cell communication signals and embryonic patterns. Computer aided design tools will be further developed to simulate the growth of interacting cells and enable the top-down design of embryos and required cell types to build a defined pattern or structure.

The specific circuits and patterns that we propose to produce are shown in Figure 2. The first are recombinase state machines (RSM) that use nested recombinases that stochastically differentiate cells as they grow by inverting DNA [111]. By themselves, these can generate diverse patterns by paramter tuning, but they are expected to be unstable and stochastic (Figure 75(a)). These will be stabilized by incorporating cell-cell commution as a preliminary step towards reaction-difficusion models of embryogenesis (Figure 75(b)). We will focus on the controled production of "spokes" of a defined number and geometry in the colony. While simple, these spokes represent the initial assymetric division of cells that then can continue to grow into more complex patterns (e.g., drosophila embryogenesis). These embryos will be microscopic, therefore we will use a different system to generate pattern formation at the ~10cm length scale where chemical gradients can be controllably established in arbitrary geometries through mutli-material 3D printing. The established exogenous gradients are then used to give tise to patterns emergent from genetic logic systems (Figure 75(c)). Critical to this approach is that the chemicals were chosen such that they can be produced endogenously by cells as they grow. This system allows to construct and test logic circuits at a larger

scale. All three of these approaches will be integrated in the final phase of the project, where a seed cell is able to grow, differentiate, establish a stable gradient, and respond to this gradient to create a pattern.

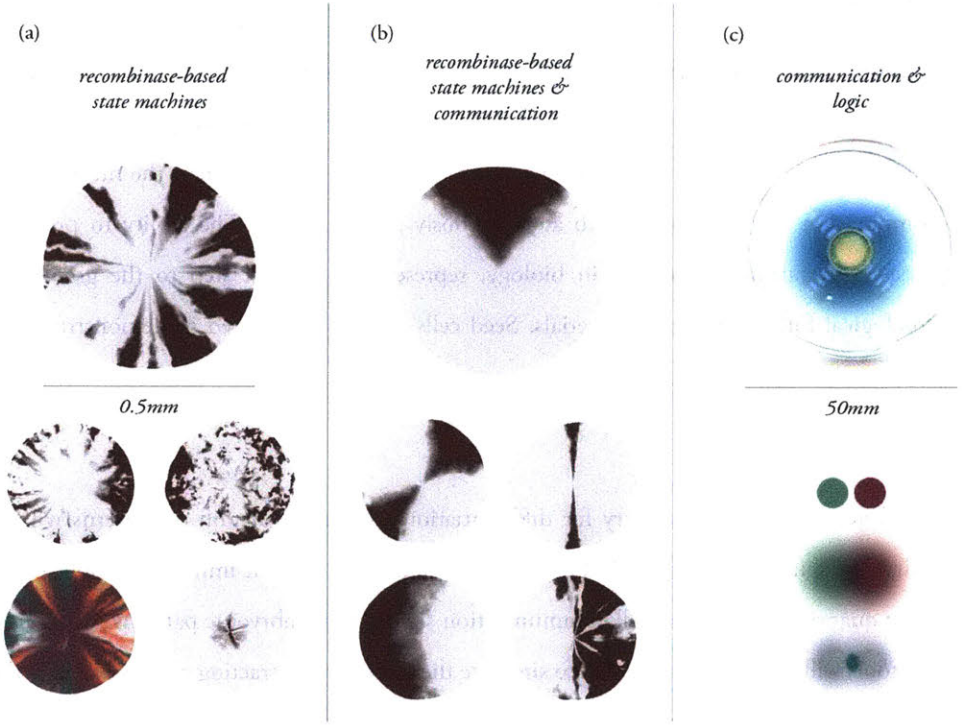


*Figure 75 – Exemplary target patterns to be produced.* An example pattern is shown along with potential patterns that can be achieved via parameter tuning. (a) Recombinase-based state machines with stochastic switching. Examples where the parameters are changed to (clockwise from upper left): 1. Slow irreversible switching, 2. Fast reversible switching, 3. Fast irreversible switching, and 4. Medium switching into four cell types. Cell-types are indicated by color. (b) The inclusion of quorum signaling to control the number and shape of spokes. A single spoke that divides the population in half represents polarization. (c) A plate is shown that establishes a small molecule gradient. The dot at center releases a small molecule to produce a signaling gradient from which engineering bacteria in an aqueous matrix on the surface are induced to produce a pigment. When two opposing gradients are released, cells can be 'programed' to react as a AND gate to turn on when both chemicals a represent (blue). This controlled establishment of exogenous gradients allows to prototype more complex logic based communication and response systems of cell.

### *Permanent differentiation of a seed cell into multiple cell types during growth*

Here the aim is to establish communities made up of self-organized cell-type niches starting from one seed cell. We approach this by encoding multiple genotypes in a cell, which are accessed by the expression of recombinases that modify the DNA. The recombinases are placed under the control of a stochastic switch so that the initial seed cell differentiates as it grows. The pattern of differentiation varies depending on the switching frequency and mechanism of the recombinase (irreversible versus reversible).

*Stochastic recombinase switches to program differentiation from a single seed cell during population expansion.* The recombinases will be constantly expressed at a low enough level that recombinase-mediated switching occurs at a rate slower than the rate at which cells reproduce. The stochastic recombinase switches will be used to enable the autonomous formation of communities with multiple cell-type niches starting from a single seed cell. The frequency of distinct niches should be proportional to the rate at which the progenitor cell switches to that cell-type. This can be tuned by controlling the level of recombinase expression. We will also incorporate a reversible recombinase switch to pattern nested niches.

*Differentiation cascades using recombinase-based state machines (RSMs).* Here we leverage stochastic RSMs. The state dependence of these RSMs will be based not on the history of input-driven recombination events, but rather on the history of stochastic recombination events. These stochastic RSMs will be designed similarly to those previously described [112], but instead of using inputs to drive recombinase expression, all recombinases will be expressed at constant, low levels for stochastic state switching. These stochastic RSMs will be used to enable autonomous formation of cascaded cell-type niches in an expanding population from a seed cell.

*Synthetic developmental circuits for the formation of "embryonic" patterns.*

Theories from developmental biology describe the classes of circuitry necessary for pattern formation. These require multiple cell types that communicate and differentially process this information in order to build a pattern. Relating this to biological primitives: Communication can be established by quorum sensing and signaling of endogenous gradients, disparate processing is archived through differentiation into distinct cell-types, and information processing is achieved by logic-based cell response Figure 76.

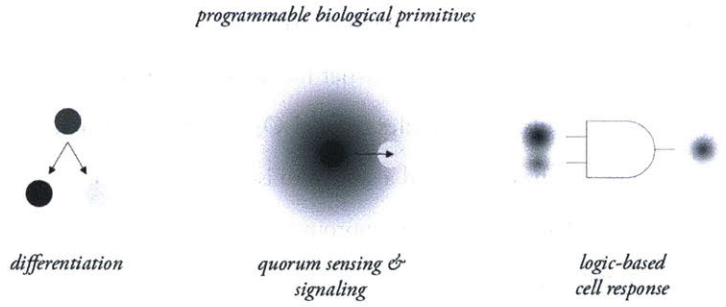


*Figure 76 – Programmable biological primitives.* Recent advances in synthetic biology give us biological primitives such as stochastic cell differentiation, endogenous establishment quorum signals and the repose to these chemical gradients by activation and repression of cellular behavior.

Here first, an approach to encode multiple regulatory networks for a set of cell types in a single DNA sequence that can be introduced to the seed cell will be developed. The expression of a recombinase will permanently modify the DNA to activate one network. As developmental networks also require cell-cell communication, quorum sensing will be utilized to program communication between cells at short and long range. Despite being ubiquitous in synthetic biology projects, quorum systems are poorly characterized from the perspective of using them for pattern generation, which will be addressed. This will be used as the basis for the design of logic gates and feedback loops to build arrangements similar to cellular automata and Turing patterns. Finally, after a pattern develops it is advantageous to remove the regulatory networks involved in the patterning to reduce the burden on the cells. Therefore, an approach is introduced where DNA is permanently deleted and a single transcription factor is turned on, which can be used to control cell type specific pathways. This project period is focused to building and integrating these circuits, but sufficient data will be gathered to enable fully automated genetic circuit design where a user defines patterns and circuit DNA design ought to be automated.

*Encode alternative regulatory networks in a single seed cell.* Pattern formation requires multiple interacting cell types that implement different sender-receiver functions for cell communication, logic operations, and establishment of gradients to project positional information. Here, an approach where all of these cell types can be encoded into a single cell and accessed via a process of permanent differentiation is developed. The approach introduces recombinase binding sites into genetic circuits to change the DNA when the recombinase is expressed. Inversion occurs when the binding sites have opposite orientations and additional complexity can be encoded by utilizing excision by aligning the sites.

*Quantitative characterization of the spatial control of quorum sensing.* It is necessary to develop a quantitative understanding of the ways in which quorum sensing can be modulated by the number of sender and receiver cells and the diffusive barrier for signal transport. In addition to the common AHL-based signals, faster diffusing molecules (*e.g.*, $H_2O_2$ and NO) and non-AHL metabolites will the quantified. The Buie Lab has developed a system to isolate a defined number of quorum sensing organisms into microscale chambers with nanoporous walls [113]. The diffusive flux of the molecule can be altered by modifying the pore size, porosity, and thickness of the walls. Wall thickness can be varied from 20 $\mu$m to 2 cm. This data will be essential for the computer aided design environment.

*Programmable patterning.* One mode of patterning in biology is via short-range interactions between growing cells. The cells communicate, this communication is processed according to a logic operation, and this is propagated to form the pattern. When there is no grid, this is referred to as "amorphous computing" [114]. Here, amorphous cellular automata will be implemented by combining cell-cell communication systems with the ability to implement arbitrary logic operations in cells. Cells will be built that can sense three or more diffusible signals, process this information using combinatorial and sequential logic, and then release additional signals in response. Simulation methods will be developed to predict different wiring leads to different patterns.

*Establishment of stable quorum sensing molecule gradients.* Turing patterns are a special class of periodic structures that arise spontaneously from interacting particles that spread through space at different rates. Turing patterns will be implemented using genetic circuits that connect two quorum sensing molecules- "Molecule 1" that spreads slowly and activates production of itself and "Molecule 2", and Molecule 2 that spreads fast and inhibits production of Molecule 1. Mathematical modeling has demonstrated that with the proper parameters (e.g., spreading rates and interaction strengths), the two molecules will spatially organize into Turing patterns. Several members of the AHL family exist with different sizes and chemistries from which a pair needs to be found that works best for establishing patterns. Alternatively, fast diffusing molecules will be utilized (e.g., $H_2O_2$ or NO) for which there are production enzymes that can serve as senders and transcription factors that can serve as receivers.

*Permanent differentiation and excision of developmental networks.* A circuit will be constructed that implements a terminal differentiation event after the complete pattern has been formed. A chemical signal will be released as the cells grow. Once a threshold has been passed, three events will be triggered by the expression of a recombinase. First, the regulatory networks involved in pattern formation will be excised by placing the recombination binding sites in the same orientation on either side of the circuit. This will eliminate the transcription factors whose continued expression would be burden on the cell. Second, it will flip a DNA in the genome that contains a promoter that leads to the low level expression of a transcription factor. Flipping can be performed by the same recombinase when the operators are oriented in opposite directions. This transcription factor will enable downstream processes to be linked to final differentiation state. Finally, a gene will be excised from the genome that stops cell division without metabolically killing cells.

*Flexible platform for high-throughput imaging of patterns.*

A high throughput platform of nanoporous microscale microbial incubators (NMMIs) to image the evolution of multicellular 'embryonic patterns' in real time will be developed. Here, lithographical patterning will be utilized which allows the platform to be configured in numerous designs. Additionally, the system will be fabricated such that flow channels can be incorporated in between independent 'embryos' in order to 1) deliver culture media to the system and 2) minimize cross-talk between growing 'embryos'. The fabrication technology is flexible and can facilitate the creation of nanoporous chambers from ~250 pL to 100s of nL.

*Long term incubation enabled with microfluidic nutrient delivery.* It will be critical to observe cell differentiation over many days in order to validate the patterns. Thus the system may require a fresh supply of nutrients (and removal of bacterial waste products) for long-term cultivation. This can be enabled using microscale flow channels integrated directly into the system and supplied with a low flow rate of fresh media. The typical system volume will be on the order 10 μL and thus a very small reservoir (e.g. 1 mL) could refresh the system hundreds of times for plenty for cultivation lasting over a week. Given the low flow rates required, the fresh media can be driven into the system using gravitational or capillary forces, which are easily controlled in microfluidic systems [115]. An advantage of the proposed system is that each incubation chamber is physically isolated from its neighbor and flow channels. Thus, media can be supplied to the system with minimal physical perturbation to cell growth patterns.

*Real time observation of cellular differentiation with variable levels of interaction.* The NMMI system is optically transparent, facilitating real time observation of cell cultivation. We will utilize fluorescence microscopy with high (e.g. 60X – 100X) magnification lenses to validate our synthetic circuits. The system can be modified to regulate the amount of interaction between incubation chambers, either by introducing flow channels or increasing the width of the wall between chambers (reducing permeability). This feature will allow us to examine the performance of circuits designed to sense and respond to stimuli from neighboring cellular communities.

*Development of a computer-aided design platform to simulate and design the growth of a seed cell into a final structure.*

Here the theoretical and technical groundwork for a rule-based computational design approach to pattern formation and emergence informed by cell behavior and differentiation will be established. A bottom up predictive simulation for growth will be built to align with the patterns resulting from

genetically engineered behavior and differentiation of model organisms. In addition to the predictability of stability and the reproducibility of emergent patterns, our goal is to ground simulations on biological 'primitives' established in previously, such as cell differentiation and signaling, and design within the constraints imposed by these to explore the available design space. Next, we will develop a general Computer Aided Design (CAD) environment, which enables further exploration of pattern formations and make predictions towards the rule-sets required to generate sophisticated patterns and shapes.

*Simulation of growth, signaling, differentiation, and physics of a cell into a final form.* We propose a computational bottom-up approach for simulating the development of a single progenitor cell—or a collection thereof—over time. This approach enables the design of rule-sets controlling the differentiation to cell types and specification of distinct cell behaviors following differentiation. Thus, a framework will be established that describes the behavior of the generalized progenitor organism, including its representation, basic growth and division, intercellular interaction and signaling. In comparison to simulations focusing on single cell interactions [116] or global modeling of substance interactions with partial differential equations [117], we leverage a hybrid approach supporting flexible and scalable simulation and design. We use simple geometric representations—such as polygonal meshes—to represent cell populations, where each vertex will represent a probabilistic set of cell-types, and, furthermore, physical cellular interactions will be resolved by position-based dynamics [118] methods recently introduced to graphics; thereby increasing speed and enabling scalability. Each cell type will have a specified program; each vertex will execute one of the cell types' programs based on the probabilistic estimation grounded in differentiation rules. Representation of global interactions—such as signaling—will be achieved by evolving fields, in grid-based schemes, where chemical processes such as diffusion flow can be resolved. Mesh and grid representations will interact with, and react to, system-based internal stimuli and—in combination with physical interactions—result in the formation of patterns. The initial target patterns that we will focus on are dots and rings. Furthermore, we will carry out the simulations to larger physical and longer time scales to demonstrate potential forms and constraints.

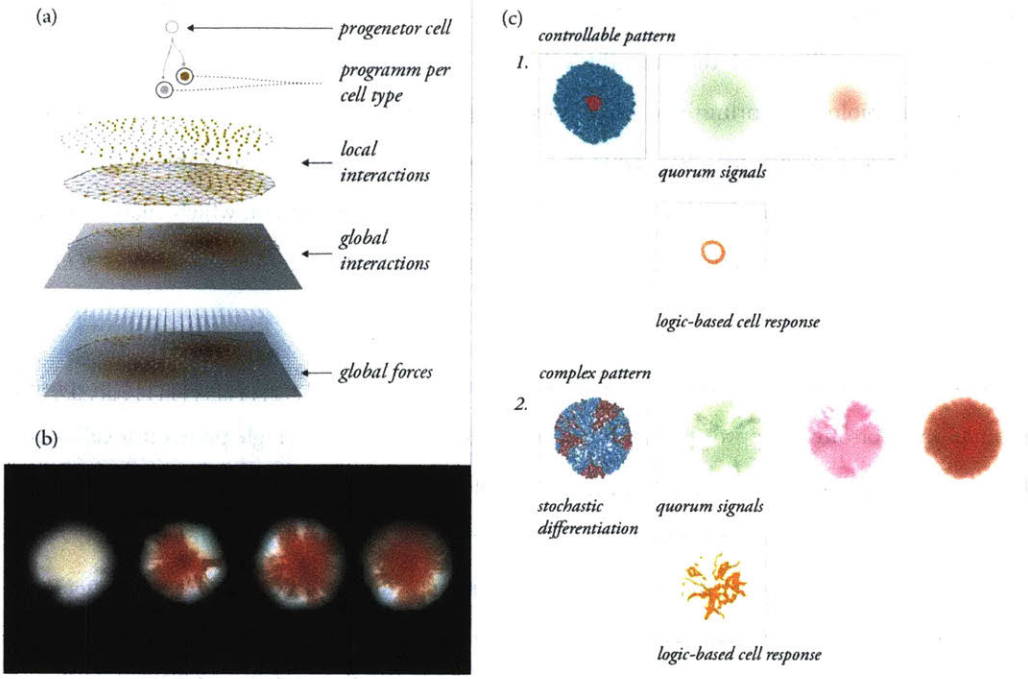


*Figure 77 – Bottom-up approach to simulation and design of cellular development and pattern formation.* Here a single progenitor cell will differentiate into two distinct cell types. These cells types will diffuse quorum signals for cell to cell communication enabling interaction between these. Finally, a logic-based cell response will result in the pattern formation. (b) Shows a red/white sectoring assay of *Saccharomyces cerevisiae* showcasing plasmid-loss [119]. This visualizes a similar process to stochastic differentiation and shows similarity to the simulated results. (c) Showcasing patterns possible through the system. ((c) 1.) The first pattern generates a simple circle and showcases the level of geometric control the system can give. Here stochastic differentiation is first inhibited and only activated after a certain time. Before the cells differentiate chemical A is released (red). When the cells differentiate, presents of this chemical inhibits differentiation into the blue cell type and absence allows to differentiate into the red cell type. The blue cell type releases chemical B (green) and where both chemicals A and B are presents the blue cell type activates reporter expression (bright yellow) ((c) 2.) The second pattern generates a more complex network-like shape and illustrates geometrical complexity (with less control over differentiation than is demonstrated in pattern (1.). In this example, reversible switching is controlled through a chemical gradient (red) that inhibits switching. Chemical A (green) and B (purple) are released through the two cell populations respectively. Both cell types can respond to the products of the chemicals by a logical AND operation releasing again a reporter (bright yellow).

*Top-Down Design: Exploration of evolving structures towards the mapping of digitally derived geometric evolution to regulatory networks.* Top down design refers to a user's ability to draw a pattern, based on a library of simulation templates, within our CAD environment. These drawn patterns are then used to generate rule sets and suggest potential circuit design specifications that allow for the development of the same pattern formations in vitro. To enable top-down design of evolving bacterial systems, simple patterns (e.g. rings, dots) will be chosen for which parameterizable simulations will be established (Figure 77). For each user specified pattern, a best fit simulation will be found; from here, the requirements for genetic circuit design will be delineated. Additionally, the previously adapted system will be moved beyond the constraints imposed by the initial assumptions made on the circuit design, to enable predictions towards new interactions and high-level behaviors required to evolve more complex patterns. For more intricate forms, we may utilize the experience of a

previously developed pattern formation tool for design applications [103]. A geometric input representation (e.g., a triangle mesh, a set of line segments, or a point cloud) is first transformed into an intermediate representation. Based on this intermediate representation, a coarse implicit representation is generated. Information generated from these three representations is then used to deform the initial geometric representation. Finally, the deformed initial representation is topologically modified to react to the deformation of the object. This is done iteratively, such that a given input representation is continuously deformed and refined. As the process repeats, the deformations aggregate into the growth of a coherent form. We have previously created a range of forms with associated growth models based on specific parameters related to transformation and expansion.

# Conclusions

## Review

In this thesis, we have discussed how computational design can act as a mediating language enabling design at the intersection of the material and the biological domain. This was validated by three proposed strategies: *Programmable Matter*, *Programmable Templating* and *Programmable Growth*. We have shown that the *Programmable Matter* approach allows to utilize computational design on synthetic material systems to enable biologically inspired design strategies. This was demonstrated first, through the introduction of a data-driven material modeling framework allowing to fabricate objects with continuous material distributions at high resolution and thereby mimicking visual complexities found in nature. Secondly, an extension to this approach allowing to model, preview and fabricate a range of functionally graded material systems was presented. We have shown that the *Programmable Templating* approach allows to utilize computational design at the intersection of synthetic and biological systems, facilitating synergetic relationships. This approach was showcased in two instances. First, a design approach to a macrofluidic habitat potentially hosting phototrophic and heterotrophic bacteria templated by continuous opacity gradients was introduced. Secondly, the spatio-temporal templating of programmable microorganism through exogenous inducer gradients established by a 3D printable heterogeneous template was investigated. Finally, we proposed *Programmable Growth* to show how computational design can be used on biological systems to give rise to material architectures. This approach was given in form of a proposal showcasing how CAD-based capabilities can be brought to biology by developing necessary biological primitives in synthetic biology and using these primitives in computational design applications to enable design. Therefore, —by all of the above, as shown herein—we allow to conclude that computational design can act as a translational unit between living and nonliving matter.

## Future Work

### Growth

The *Programmable Growth* approach was given as a proposal, considering that the biological primitives introduced have yet to be integrated into a single system. Similar to the primitives that can be found in design applications such as points, lines, triangles etc. the development of equivalent

'primitives' will enable design of bacterial pattern formation. This transfers a very literal interpretation of computational design, in the form of explicit top-down CAD modeling, to biological systems. However, a different view on design will be needed, as it may be a physical, biological and computational challenge to envision bacteria to grow into a predefined geometric shape in a controllable manner without any reference to a scaffold.

Computational design—in the form of generative design—may enable a more holistic view on the design of pattern formation processes. In generative design, rulesets are allowed to evolve into shapes and the designer is focused on the definition of these bottom-up procedures, rather than the sequential specification of actions. Similarly, the biological primitives themselves should be viewed as basic components of an evolution process and designers will have to progress their role to being designers of generators and reactions.

## Dynamics

We have shown how we can computationally design with a material system to influence the behavior of a living system. While some of the *Programmable Templating* systems introduced herein already represent a cascade and response system through events such as diffusion, induction and biosynthesis, here communication itself operates through a single channel. Introducing a loop into such systems is a challenge.

The heterogeneous hybrid living materials approach would be suitable for such a more symbiotic relationship. One example could be for the printed material to induce the production bacterial ethanol. The ethanol would then trigger swelling in certain material regions—as shown in the *Programmable Matter* section—to actuate in response to the bacteria signal. Another example is the production of spatially controllable Melanin. Melanin as a biosynthesized pigment has properties such as the ability to absorb, transduce and dissipate UV-light and radiation. However, purification from cells results in the loss of these features. Thus bacterial melanin can give heterogeneous templates additional properties which otherwise would not be possible.

As engineered bacterial systems become more predictable and easier to design, computational design must account for these feedback relationships in the modeling of integrated systems. Therefore—beyond the abundance of evaluation methods for physical processes—the biophysical dynamics of living systems will have to be integrated into design evaluation workflows as well.

## Unification

As digital fabrication attempts to give control over the physical domain and computational design peruses to give control over the digital domain both have shown to be of mutual benefit to each other. As shown in the *Programmable Matter* section, computational design can utilize recent advancements in additive manufacturing, enabling high resolution and high fidelity computational control of shape and material composition. This results in the ability to algorithmically create geometrical and materially customizable parts and structures. Synthetic Biology on the other hand utilizes recent advancements in genetic engineering, attempting to enable control in the biological domain. The *Programmable Templating* and *Programmable Growth* approach show how the fields can be made to integrate and how synergies may arise through a translational view on design computation. Ideally computational design environments can progress further to cast aside disciplinary boundaries for design and designers by providing unified platforms. While we have shown a pathway to a framework for the *Programmable Matter* approach that allows to design material distributions *and* predict their behavior, the unification of *Programmable Matter*, *Programmable Templating* and *Programmable Growth* in one design workflow, even for simple applications, remains a technological and conceptual challenge.

## Applications

While we have introduced translation design computation as a framework to shift across disciplines and scales in the intersection of materials engineering and biology, this thesis was focused on the validation of the practice much rather then the introduction of related applications. One particular utilization of the techniques introduced was given in form of the *Vespers* project. Here we briefly point towards pathways for future applications of the respective strategies.

The ability to finely tune material regions and material properties in specific geometries enables applications from reduction of interfacial failure through stiffness gradients to improved optics through refractive index gradients over self-assembling structures and data visualization. The *Programmable Matter* approach may provide a holistic framework to prototype biomimetic designs and the data driven material modeling workflow allows to transfer data from imaging sources to a wide range of material properties, thereby bridging the gap between digital and physical representations.

The interplay of a complex material system—going beyond an enclosing hydrogel which can support and maintain biological activity—allows functional biological components to be integrated into useful devices. Thus, the *Programmable Templating* approach is in particular interesting for biological augmented living wearables or engineered living materials. Wearables may manifest in producing an output in spatially templated regions filtered through selectively permeable hydrogels or customizable drug releasing devices interfacing with the human body.

Structural synthetic materials are usually expensive to produce, subject to damage due to environmental insults and ageing and have limited ability to response to changes in the immediate surroundings. The *Programmable Growth* approach may provide advantages over inert materials by virtue of the potential ability of engineered living materials to grow on-site, generate themselves autonomously, response to environmental cues and self-repair. However, all of these abilities have yet to be shown in future research.

# Conclusion

In summary, we can deduce that computational design itself can act as a mediating language between and across the physical, the digital and the biological domains. Thus we hope that the approaches presented herein will lead to an emergence of a translational view on design computation enabling synergetic relationships across the physical, the digital and the biological domains.

# References


[1] N. Oxman, "Mothering Nature - The shape of things to come," *The Economist*, 2015.

[2] N. Oxman, C. Bader, D. Kolb, S. Sharma, and R. Smith, *Fear & Love: Reactions to a Complex World: The Design Museum Opening Exhibition*. Phaidon Press, 2017.

[3] I. Stewart and M. Golubitsky, *Fearful Symmetry: Is God a Geometer*. Courier Corporation, 2010.

[4] D. K. Washburn, *Symmetry comes of age: the role of pattern in culture*. University of Washington Press, 2004.

[5] M. Enquist and A. Arak, "Symmetry, beauty and evolution.," *Nature*, vol. 372, no. 6502, pp. 169–72, 1994.

[6] a P. Moller and J. P. Swaddle, *Asymmetry, developmental stability, and evolution*. 1997.

[7] T. Jacobsen, R. I. Schubotz, L. Höfel, and D. Y. V Cramon, "Brain correlates of aesthetic judgment of beauty," *Neuroimage*, vol. 29, no. 1, pp. 276–285, 2006.

[8] J. McCormack, A. Dorin, and T. Innocent, "Generative design: a paradigm for design research," *Proc. Futur. Des. Res. Soc.*, pp. 1–8, 2004.

[9] H. Bohnacker, B. Gross, J. Laub, and C. Lazzeroni, *Generative design: visualize, program, and create with processing*. Princton Architectural Press, 2012.

[10] N. System, "Nervous Systems. Cell Cycle v 3.0," *2016*. [Online]. Available: https://n-e-r-v-o-u-s.com/cellCycle/. [Accessed: 08-Mar-2017].

[11] Autodesk, "Project Shapeshifter," 2016. [Online]. Available: http://shapeshifter.io/. [Accessed: 03-May-2016].

[12] J. Breuninger, R. Becker, A. Wolf, S. Rommel, and A. Verl, *Generative Fertigung mit Kunststoffen;Konzeption und Konstruktion für Selektives Lasersintern*. 2013.

[13] O. Sagi, "PolyJet Matrix™ Technology A New Direction in 3D Printing," Rehovot, Israel, 2009.

[14] N. Oxman, D. Dikovsky, B. Belocon, and W. C. Carter, "Gemini: Engaging Experiential and Feature Scales Through Multimaterial Digital Design and Hybrid Additive–Subtractive Fabrication," *J. 3D Print. Addit. Manuf.*, vol. 1, no. 3, pp. 108–114, 2014.

[15] G. Stiny, "Introduction to shape and shape grammars," *Environ. Plan. B*, vol. 7, no. 3, pp. 343–351, 1980.

[16] S.-W. Hsiao and C.-H. Chen, "A semantic and shape grammar based approach for product design," *Des. Stud.*, vol. 18, pp. 275–296, 1997.

[17] G. Stiny, "Ice-ray: a note on the generation of Chinese lattice designs," *Environ. Plan. B Plan. Des.*, vol. 4, pp. 89–98, 1977.

[18] J. A. Heisserman, "Generative Geometric Design," *IEEE Comput. Graph. Appl.*, vol. 14, no. 2, pp. 37–45, 1994.

[19] M. Botsch, L. Kobbelt, M. Pauly, P. Alliez, and L. Bruno, *Polygon Mesh Processing*. CRC Press, 2010.

[20] E. Catmull and J. Clark, "Recursively generated B-spline surfaces on arbitrary topological meshes," *Comput. Des.*, vol. 10, no. 6, pp. 350–355, 1978.

[21] J. A. Bærentzen, J. Gravesen, A. François, and A. Henrik, *Guide to Computional Geometry Processing*. Springer Science & Business Media, 2012.

[22] N. Ervinck, "Studio Nick Ervinck," 2016. [Online]. Available: http://www.nickervinck.com/. [Accessed: 03-May-2016].

[23] M. Hansmayer, "Projects." [Online]. Available: http://www.michael-hansmeyer.com/projects/projects.html?screenSize=1&color=1. [Accessed: 06-May-2016].

[24] N. Shaker, J. Togelius, and M. J. Nelson, *Procedural Content Generation in Games: A Textbook and an Overview of Current Research*. Springer, 2016.

[25] M. Botsch, S. Steinberg, S. Bischoff, and L. Kobbelt, "OpenMesh – a generic and efficient polygon mesh data structure," *OpenSG Symp.*, 2002.

[26] E. Konukoglu, B. Glocker, A. Criminisi, and K. M. Pohl, "WESD-Weighted spectral distance for measuring shape dissimilarity," *IEEE Trans. Pattern Anal. Mach. Intell.*, vol. 35, no. 9, pp. 2284–2297, 2013.

[27] M. Reuter, F. E. Wolter, and N. Peinecke, "Laplace-Beltrami spectra as 'Shape-DNA' of surfaces and solids," *CAD Comput. Aided Des.*, vol. 38, no. 4, pp. 342–366, 2006.

[28] M. Meyer, M. Desbrun, P. Schr, and A. H. Barr, "Discrete Differential-Geometry Operators for Triangulated 2-Manifolds," *Vis. Math. III*, pp. 113–134, 2002.

[29] K. F. Man, K. S. Tang, and S. Kwong, *Genetic algorithms: concepts and designs*. Springer Science and Business Media, 2012.

[30] J. Aron, "The mandelbulb: first 'true' 3D image of famous fractal," *New Sci.*, vol. 204, no. 2736, 2009.

[31] L. Kobbelt, M. Botsch, U. Schwanecke, and H.-P. Seidel, "Feature Sensitive Surface Extraction from Volume Data," *Siggraph*, vol. D, p. Pages: 57-66, 2001.

[32] W. Cho, E. M. Sachs, N. M. Patrikalakis, and D. E. Troxel, "A dithering algorithm for local composition control with three-dimensional printing," *CAD Comput. Aided Des.*, vol. 35, no. 9, pp. 851–867, 2003.

[33] C. Bader, D. Kolb, J. C. Weaver, and N. Oxman, "Data-Driven Material Modeling with Functional Advection for 3D Printing of Materially Heterogeneous Objects," *3D Print. Addit. Manuf.*, vol. 3, no. 2, pp. 71–79, 2016.

[34] R. W. Floyd and L. Steinberg, "An adaptive algorithm for spatial greyscale," *Proc. Soc. Inf. Disp.*, vol. 17, pp. 75–77, 1976.

[35] E. Zelzer, E. Blitz, M. L. Killian, and S. Thomopoulos, "Tendon-to-bone attachment: From development to maturity," *Birth Defects Res. Part C - Embryo Today Rev.*, vol. 102, no. 1, pp. 101–112, 2014.

[36] J. M. Gordon, "Spherical gradient-index lenses as perfect imaging and maximum power transfer devices.," *Appl. Opt.*, vol. 39, no. 22, pp. 3825–32, 2000.

[37] P. Fratzl and F. G. Barth, "Biomaterial systems for mechanosensing and actuation," *Nature*, vol. 462, no. 7272, pp. 442–448, 2009.

[38] M. Chen and J. V. Tucker, "Constructive volume geometry," *Comput. Graph. Forum*, vol. 19, no. 4, pp. 281–293, 2000.

[39] V. Chandru, S. Manohar, and C. E. Prakash, "Voxel-based modeling for layered manufacturing," *IEEE Comput. Graph. Appl.*, vol. 15, no. 6, pp. 42–47, 1995.

[40] R. Kempaiah and Z. Nie, "From nature to synthetic systems: shape transformation in soft materials," *J. Mater. Chem. B*, vol. 2, no. 17, p. 2357, 2014.

[41] N. Oxman, "Projects." [Online]. Available: http://materialecology.com/projects. [Accessed: 06-May-2016].

[42] E. L. Doubrovski, E. Y. Tsai, D. Dikovsky, J. M. P. Geraedts, H. Herr, and N. Oxman, "Voxel-based fabrication through material property mapping: A design method for bitmap printing," *CAD Comput. Aided Des.*, vol. 60, pp. 3–13, 2015.

[43] K. Vidim, S. Wang, and J. Ragan-kelley, "OpenFab: A Programmable Pipeline for Multi-Material Fabrication," in *ACM SIGGRAPH*, 2013, vol. 32, no. 4, pp. 1–11.

[44] W. K. Chiu and K. M. Yu, "Direct digital manufacturing of three-dimensional functionally graded material objects," *CAD Comput. Aided Des.*, vol. 40, no. 12, pp. 1080–1093, 2008.

[45] X. Y. Kou and S. T. Tan, "Heterogeneous object modeling: A review," *CAD Computer Aided Design*, vol. 39, no. 4. pp. 284–301, 2007.

[46] A. Biswas, V. Shapiro, and I. Tsukanov, "Heterogeneous material modeling with distance fields," *Comput. Aided Geom. Des.*, vol. 21, no. 3, pp. 215–242, 2004.

[47] Y. K. Siu and S. T. Tan, "Modeling the material grading and structures of heterogeneous objects for layered manufacturing," *CAD Comput. Aided Des.*, vol. 34, no. 10, pp. 705–716, 2002.

[48] N. Oxman, "Wanderers – An Astrobiological Exploration." [Online]. Available: http://materialecology.com/projects/details/zuhal. [Accessed: 06-May-2016].

[49] J. Stam, "Stable Fluids," *Proc. 26th Annu. Conf. Comput. Graph. Interact. Tech.*, pp. 121–128, 1999.

[50] S. W. Walker, *The Shape of Things: A Practical Guide to Differential Geometry and the Shape Derivative.* SIAM, 2015.

[51] M. W. Jones, J. A. Bærentzen, and M. Sramek, "3D distance fields: A survey of techniques and applications," in *IEEE Transactions on Visualization and Computer Graphics*, 2006, vol. 12, no. 4, pp. 581–599.

[52] S. Osher and R. Fedkiw, *Level Set Methods and Dynamic Implicit Surfaces*, vol. 57, no. 3. 2004.

[53] Stratasys, "OBJET500 CONNEX3." [Online]. Available: http://web.stratasys.com/rs/objet/images/SSYS-WP-Objet500 Connex3.pdf. [Accessed: 06-May-2016].

[54] M. Levoy, "Efficient Ray Tracing of Volume Data," *ACM Trans. Graph.*, vol. 9, no. 3, pp. 245–261, 1990.

[55] A. V. Srinivasan, G. K. Haritos, and F. L. Hedberg, "Biomimetics: Advancing Man-Made Materials Through Guidance From Nature," *Appl. Mech. Rev.*, vol. 44, no. 11, p. 463, 1991.

[56] B. Kieback, A. Neubrand, and H. Riedel, "Processing techniques for functionally graded materials," *Mater. Sci. Eng. A*, vol. 362, no. 1–2, pp. 81–105, 2003.

[57] O. Sagi, "Polyjet Matrix Technology: A New Direction in 3D Printing," 2009.

[58] C. Bader, W. G. Patrick, D. Kolb, S. G. Hays, S. Keating, S. Sharma, D. Dikovsky, B. Belocon, J. C. Weaver, P. A. Silver, and N. Oxman, "Grown, Printed, and Biologically Augmented: An Additively Manufactured Microfluidic Wearable, Functionally Templated for Synthetic Microbes," *3D Print.*

*Addit. Manuf.*, vol. 3, no. 2, pp. 79–89, 2016.

[59] E. L. Doubrovski, E. Y. Tsai, D. Dikovsky, J. M. P. Geraedts, H. Herr, and N. Oxman, "Voxel-based fabrication through material property mapping: A design method for bitmap printing," *CAD Comput. Aided Des.*, vol. 60, pp. 3–13, 2015.

[60] W. Cho, E. M. Sachs, N. M. Patrikalakis, and D. E. Troxel, "A dithering algorithm for local composition control with three-dimensional printing," *CAD Comput. Aided Des.*, vol. 35, no. 9, pp. 851–867, 2003.

[61] J. H. Waite, H. C. Lichtenegger, G. D. Stucky, and P. Hansma, "Exploring molecular and mechanical gradients in structural bioscaffolds," *Biochemistry*, vol. 43, no. 24. pp. 7653–7662, 2004.

[62] V. Imbeni, J. J. Kruzic, G. W. Marshall, S. J. Marshall, and R. O. Ritchie, "The dentin-enamel junction and the fracture of human teeth.," *Nat. Mater.*, vol. 4, no. 3, pp. 229–232, 2005.

[63] D. Raabe, C. Sachs, and P. Romano, "The crustacean exoskeleton as an example of a structurally and mechanically graded biological nanocomposite material," *Acta Mater.*, vol. 53, no. 15, pp. 4281–4292, 2005.

[64] A. Miserez, T. Schneberk, C. Sun, F. W. Zok, and J. H. Waite, "The transition from stiff to compliant materials in squid beaks.," *Science*, vol. 319, no. 5871, pp. 1816–1819, 2008.

[65] D. Raviv, W. Zhao, C. McKnelly, A. Papadopoulou, A. Kadambi, B. Shi, S. Hirsch, D. Dikovsky, M. Zyracki, C. Olguin, R. Raskar, and S. Tibbits, "Active printed materials for complex self-evolving deformations.," *Sci. Rep.*, vol. 4, p. 7422, 2014.

[66] Q. Ge, A. H. Sakhaei, H. Lee, C. K. Dunn, N. X. Fang, and M. L. Dunn, "Multimaterial 4D Printing with Tailorable Shape Memory Polymers," *Sci. Rep.*, vol. 6, no. April, p. 31110, 2016.

[67] A. R. Studart and R. M. Erb, "Bioinspired materials that self-shape through programmed microstructures," *Soft Matter*, vol. 10, no. 9, pp. 1284–94, 2014.

[68] C. Liu, H. Qin, and P. T. Mather, "Review of progress in shape-memory polymers," *J. Mater. Chem.*, vol. 17, no. February, p. 1543, 2007.

[69] I. Burgert and P. Fratzl, "Actuation systems in plants as prototypes for bioinspired devices.," *Philos. Trans. A. Math. Phys. Eng. Sci.*, vol. 367, no. 1893, pp. 1541–57, 2009.

[70] C. Dawson, J. F. V. Vincent, and A.-M. Rocca, "How pine cones open," *Nat.*, vol. 390, no. 6661, p. 668, 1997.

[71] Y. Forterre, J. M. Skotheim, J. Dumais, and L. Mahadevan, "How the Venus flytrap snaps.," *Nature*,

vol. 433, no. 7024, pp. 421–425, 2005.

[72] P. Fratzl, R. Elbaum, and I. Burgert, "Cellulose fibrils direct plant organ movements.," *Faraday Discuss.*, vol. 139, pp. 275-282-325, 419–420, 2008.

[73] A. Runions, M. Fuhrer, B. Lane, P. Federl, A.-G. Rolland-Lagan, and P. Prusinkiewicz, "Modeling and visualization of leaf venation patterns," *ACM Trans. Graph.*, vol. 24, no. 3, p. 702, 2005.

[74] Y. Zheng, H. Bai, Z. Huang, X. Tian, F.-Q. Nie, Y. Zhao, J. Zhai, and L. Jiang, "Directional water collection on wetted spider silk.," *Nature*, vol. 463, no. 7281, pp. 640–643, 2010.

[75] Y. Zheng, X. Gao, and L. Jiang, "Directional adhesion of superhydrophobic butterfly wings," *Soft Matter*, vol. 3, no. 2, p. 178, 2007.

[76] T. Nørgaard and M. Dacke, "Fog-basking behaviour and water collection efficiency in Namib Desert Darkling beetles.," *Front. Zool.*, vol. 7, no. 1, p. 23, 2010.

[77] W. Barthlott and C. Neinhuis, "Purity of the sacred lotus, or escape from contamination in biological surfaces," *Planta*, vol. 202, no. 1, pp. 1–8, 1997.

[78] D.-E. Nilsson, L. Gislén, M. M. Coates, C. Skogh, and A. Garm, "Advanced optics in a jellyfish eye.," *Nature*, vol. 435, no. 7039, pp. 201–5, 2005.

[79] A. M. Sweeney, D. L. Des Marais, Y.-E. A. Ban, and S. Johnsen, "Evolution of graded refractive index in squid lenses.," *J. R. Soc. Interface*, vol. 4, no. 15, pp. 685–98, 2007.

[80] A. R. Parker and N. Martini, "Structural colour in animals—simple to complex optics," *Opt. Laser Technol.*, vol. 38, no. 4, pp. 315–322, 2006.

[81] C. Bader, D. Kolb, and N. Oxman, "Mediated Matter - Rottlace," 2016. .

[82] N. Oxman, "Templating design for biology and biology for design," *Archit. Des.*, vol. 85, no. 5, pp. 100–107, 2015.

[83] S. G. Hays, W. G. Patrick, M. Ziesack, N. Oxman, and P. A. Silver, "Better together: Engineering and application of microbial symbioses," *Current Opinion in Biotechnology*, vol. 36. pp. 40–49, 2015.

[84] R. Thanasomboon, D. Waraho, S. Cheevadhanarak, and A. Meechai, "Construction of synthetic escherichia coli producing s-linalool," in *Procedia Computer Science*, 2012, vol. 11, pp. 88–95.

[85] P. R. August, T. H. Grossman, C. Minor, M. P. Draper, I. a MacNeil, J. M. Pemberton, K. M. Call, D. Holt, and M. S. Osburne, "Sequence analysis and functional characterization of the violacein biosynthetic pathway from Chromobacterium violaceum.," *J. Mol. Microbiol. Biotechnol.*, vol. 2, no. 4, pp. 513–519, 2000.

[86] S. K. Lee, H. Chou, T. S. Ham, T. S. Lee, and J. D. Keasling, "Metabolic engineering of microorganisms for biofuels production: from bugs to synthetic biology to fuels," *Current Opinion in Biotechnology*, vol. 19, no. 6. pp. 556–563, 2008.

[87] "Kinematics Dress - Nervous System." [Online]. Available: http://n-e-r-v-o-u-s.com/projects/sets/kinematics-dress/. [Accessed: 06-May-2016].

[88] C. M. B. Ho, S. H. Ng, K. H. H. Li, and Y.-J. Yoon, "3D printed microfluidics for biological applications," *Lab Chip*, vol. 15, no. 18, pp. 3627–3637, 2015.

[89] N. Oxman, C. Ortiz, F. Gramazio, and M. KohlerProf, "Material ecology," *CAD Computer Aided Design*, vol. 60, pp. 1–2, 2015.

[90] P. Prusinkiewicz, "Graphical Applications of L-Systems," *Graph. Interface*, pp. 247--253, 1986.

[91] A. M. Turing, "The Chemical Basis of Morphogenesis THE CHEMICAL BASIS OF MOKPHOGENESIS," *Society*, vol. 237, no. 641, pp. 37–72, 1952.

[92] A. Lomas, *Cellular Forms : an Artistic Exploration of Morphogenesis*. 2014.

[93] C. Bader and D. Kolb, "A unified approach to grown structures," 2014. [Online]. Available: https://www.youtube.com/watch?v=9HI8FerKr6Q.

[94] Y. K. Siu and S. T. Tan, "'Source-based' heterogeneous solid modeling," *CAD Comput. Aided Des.*, vol. 34, no. 1, pp. 41–55, 2002.

[95] C. Bader, D. Kolb, J. C. Weaver, and N. Oxman, "Data-Driven Material Modeling with Functional Advection for 3D Printing of Materially Heterogeneous Objects," *3D Print. Addit. Manuf.*, vol. 3, no. 2, pp. 71–79, 2016.

[96] R. Rusconi, S. Lecuyer, L. Guglielmini, and H. A. Stone, "Laminar flow around corners triggers the formation of biofilm streamers.," *J. R. Soc. Interface*, vol. 7, no. 50, pp. 1293–9, 2010.

[97] G. Baldwin, T. Bayer, R. Dickinson, T. Ellis, P. S. Freemont, R. I. Kitney, K. Polizzi, and G. B. Stan, *Synthetic Biology - A Primer*. 2012.

[98] G. M. Cooper and R. E. Hausman, "The Cell: A Molecular Approach 2nd Edition," *Sinauer Associates*. pp. 1–820, 2000.

[99] J. M. van Dijl and M. Hecker, "Bacillus subtilis: from soil bacterium to super-secreting cell factory.," *Microb. Cell Fact.*, vol. 12, p. 3, 2013.

[100] L. Goers, P. Freemont, and K. M. Polizzi, "Co-culture systems and technologies: taking synthetic biology to the next level.," *J. R. Soc. Interface*, vol. 11, no. 96, p. 20140065-, 2014.

[101] C. Bader and N. Oxman, "Recursive symmetries for geometrically complex and materially heterogeneous additive manufacturing," *CAD Comput. Aided Des.*, vol. 81, pp. 39–47, 2016.

[102] X. Liu, T.-C. Tang, E. Tham, H. Yuk, S. Lin, T. K. Lu, and X. Zhao, "Stretchable living materials and devices with hydrogel–elastomer hybrids hosting programmed cells," *Proc. Natl. Acad. Sci.*, vol. 114, no. 9, p. 201618307, 2017.

[103] C. Bader, W. G. Patrick, D. Kolb, S. G. Hays, S. Keating, S. Sharma, D. Dikovsky, B. Belocon, J. C. Weaver, P. A. Silver, and N. Oxman, "Grown, Printed, and Biologically Augmented: An Additively Manufactured Microfluidic Wearable, Functionally Templated for Synthetic Microbes," *3D Print. Addit. Manuf.*, vol. 3, no. 2, pp. 79–89, 2016.

[104] S. Lin, H. Yuk, T. Zhang, G. A. Parada, H. Koo, C. Yu, and X. Zhao, "Stretchable Hydrogel Electronics and Devices," *Adv. Mater.*, vol. 28, no. 22, pp. 4497–4505, 2016.

[105] J. H. J. Leveau and S. E. Lindow, "Predictive and interpretive simulation of green fluorescent protein expression in reporter bacteria," *J. Bacteriol.*, vol. 183, no. 23, pp. 6752–6762, 2001.

[106] E. Bayer and G. R. McIntyre, "Method for growing mycological materials," U.S. Patent No. 9,394,512., 2016.

[107] Britton, Nicholas. F, *Reaction-diffusion equations and their applications to biology*, vol. 18, no. 1. 1986.

[108] L. Wolpert, "Positional information and the spatial pattern of cellular differentiation," *J. Theor. Biol.*, vol. 25, no. 1, pp. 1–47, 1969.

[109] C. G. Langton, "Studying artificial life with cellular automata," *Phys. D Nonlinear Phenom.*, vol. 22, no. 1–3, pp. 120–149, 1986.

[110] A. a K. Nielsen, B. S. Der, J. Shin, P. Vaidyanathan, V. Paralanov, E. a Strychalski, D. Ross, D. Densmore, and C. a. Voigt, "Genetic circuit design automation.," *Science*, vol. 352, no. 6281, p. aac7341, 2016.

[111] P. Siuti, J. Yazbek, and T. K. Lu, "Synthetic circuits integrating logic and memory in living cells.," *Nat. Biotechnol.*, vol. 31, no. 5, pp. 448–52, 2013.

[112] N. Roquet, A. P. Soleimany, A. C. Ferris, S. Aaronson, and T. K. Lu, "Synthetic recombinase-based state machines in living cells," *Science (80-. ).*, vol. 353, no. 6297, p. aad8559, 2016.

[113] Z. Ge, P. R. Girguis, and C. R. Buie, "Nanoporous microscale microbial incubators," *Lab Chip*, vol. 16, pp. 480–488, 2015.

[114] H. Abelson, D. Allen, D. Coore, C. Hanson, E. Rauch, G. J. Sussman, R. Weiss, G. Homsy, T. F.

Knight Jr., and R. Nagpal, "Amorphous," *Commun. ACM*, vol. 43, no. 5, pp. 74–82, 2000.

[115] H. A. Stone, A. D. Stroock, and A. Ajdari, "Engineering flows in small devices: microfluidics toward a lab-on-a-chip," *Annu. Rev. Fluid Mech.*, vol. 36, no. 1, pp. 381–411, 2004.

[116] S. S. Jang, K. T. Oishi, R. G. Egbert, and E. Klavins, "Specification and simulation of synthetic multicelled behaviors," *ACS Synth. Biol.*, vol. 1, no. 8, pp. 365–374, 2012.

[117] R. E. Baker, E. A. Gaffney, and P. K. Maini, "Partial differential equations for self-organization in cellular and developmental biology," *Nonlinearity*, vol. 21, no. 11, pp. R251–R290, 2008.

[118] M. Muller, B. Heidelberger, M. Hennix, and J. Ratcliff, "Position based dynamics," *J. Vis. Commun. Image Represent.*, vol. 18, no. 2, pp. 109–118, 2007.

[119] A. R. Brannon, J. a Maresca, J. D. Boeke, M. a Basrai, and A. a McBride, "Reconstitution of papillomavirus E2-mediated plasmid maintenance in Saccharomyces cerevisiae by the Brd4 bromodomain protein.," *Proc. Natl. Acad. Sci. U. S. A.*, vol. 102, no. 8, pp. 2998–3003, 2005.